

25237305



LIBRARY
Michigan State
University

This is to certify that the

dissertation entitled

Preparation And Spectroscopic Characterization
Of Higher Oxidation States of Hemoprotein Models
presented by

Asaad Salehi

has been accepted towards fulfillment of the requirements for

Ph.D. degree in Chemistry

Chik. Chang Major professor

Date Oct 17, 1988

MSU is an Affirmative Action/Equal Opportunity Institution

0-12771

PLACE IN RETURN BOX to remove this checkout from your record.
TO AVOID FINES return on or before date due.

DATE DUE	DATE DUE	DATE DUE
	<u> </u>	

MSU Is An Affirmative Action/Equal Opportunity Institution choirclessedus.pm3-p.

PREPARATION AND SPECTROSCOPIC CHARACTERIZATION OF HIGHER OXIDATION STATES OF HEMOPROTEIN MODELS

Ву

Asaad Salehi

A DISSERTATION

Submitted to

Michigan State University in partial fulfillment of the requirements for the degree of

DOCTOR OF PHILOSOPHY

Department of Chemistry

1988

ABSTRACT

PREPARATION AND SPECTROSCOPIC CHARACTERIZATION OF HIGHER OXIDATION STATES OF HEMOPROTEIN MODELS

By

Asaad Salehi

This study utilizes synthetic octaethylporphyrin (OEP) complexes to establish vibrational, electronic and structural characteristics of hemoproteins' iron-porphyrin centers. The emphasis is primarily placed on the ring-centered π -cation radical state which may be involved in the reaction cycles of some hemoprotein enzymes and is also present in photosynthetic chlorophylls. A systematic study of these model radicals should aid detection and assignment of this particular mode of oxidation in the investigation of hemoprotein catalytic cycles by Resonance Raman spectroscopy.

Metalloporphyrins (MPs) were oxidized by chemical methods using oxidants such as AgClO₄, Fe(ClO₄)₃, Br₂ and pheno⁺·sbcl₆⁻ in dichloromethane. The progress of the reaction was followed spectrophotometrically until complete oxidation was achieved. The color changes associated with radical formation are diagnostic: typically the initial pink or orange color of the neutral MP changes to green or black upon oxidation. The 363.8 nm Ar ion laser is the principal excitation source in our RR investigation as this wavelength is in resonance with the near-UV absorption bands of the radicals and, consequently, it serves to minimize contributions from the neutral porphyrin contaminants which absorb at longer wavelengths. The vibrational modes mainly in the 1350-1700 cm⁻¹ region are

examined owing to their sensitivity to the metal oxidation, spin and coordination states, and most importantly, they feature a linear correlation to the macrocycle core-size.

Our RR data indicate that upon removal of an electron from the highest filled porphyrin π -bonding orbitals, a_{1u} or a_{2u} , the frequencies of vibrations which are predominantly C_bC_b character increase dramatically (20-30 cm⁻¹); whereas, those with C_aC_m and C_aN character decrease (3-10 cm⁻¹) in the RR spectra of OEP radical complexes relative to the neutral precursors. These vibrational trends seem to hold in all the OEP complexes and is consistent with $^2A_{1u}$ radical symmetry assignment. This observation, however, contradicts the previous classification of $Co^{III}OEP^{+}\cdot 2ClO_4^{-}$ as a $^2A_{2u}$ radical. Our data also suggest that the original classification of the radical optical spectra into two types, believed to arise from $^2A_{1u}$ and $^2A_{2u}$ ground states, may actually be caused by the planar vs. ruffled conformation of the macrocycle at the oxidized level.

Metallochlorin (MC) π -cation radicals, on the other hand, feature a more complex vibrational spectra in the high-frequency region owing to the macrocycle reduced symmetry and increased conformational flexibility which result in more RR-allowed bands and increased likelihood of changes in mode composition, relative to their MP analogs. This is demonstrated by a vibrational mode in the 1500 cm⁻¹ region which increases in frequency upon oxidation, in contrast with its MP counterpart. This characteristic is believed to result from both C_bC_b and C_aC_m contribution to this mode in MCs which differs from predominantly C_aC_m character of the corresponding mode in MPs.

TO MY PARENTS

ACKNOWLEDGEMENTS

I wish to express my deep appreciation to my advisors, Drs. Chris K. Chang and Gerald T. Babcock for their guidance, encouragement and friendship during the course of this work. I am also grateful to Drs. Michael Rathke and Alexander Popov for serving on my committee. Financial support provided by the Department of Chemistry at Michigan State University is gratefully acknowledged.

Many thanks go to my good friend and colleague Tony Oertling whose contribution to this study has been invaluable. I wish to thank all of the members of Dr. Chang's and Dr. Babcock's group for their help, friendship and support. I am especially grateful to Myoung S. Koo, Weishih Wu and Juan L.-Garriga whose friendship in and out of the lab will always be remembered. My special thanks go to a good friend, Mike Tornaritis, who has been like a brother to me during the past few years. I appreciate the help of Beverly Carnahan in typing my thesis and Ellen Rzepka for her sincerity and help in keeping my academic records accurate.

Finally, I wish to thank my parents for their faith in me, their continuous love, encouragement and support. I dedicate this work to them.

TABLE OF CONTENTS

	Page
LIST OF TABLES	i v
LIST OF FIGURES	vi
Chapter 1 - INTRODUCTION	
Research Objectives	4
Porphyrin π-cation Radicals	6
Metal-porphyrin Interactions	
Site-Selective Oxidation: Metal vs. Porphyrin	
Centered Oxidation Induction	11
Porphyrin Peripheral Substituents	
Metal Axial Ligand(s)	
Solvent (or Medium)	
Temperature	
Differention Between Metal vs. Porphyrin-	
Based Oxidation Reactions - Spectroscopic Methods	18
1. Optical Absorption Spectroscopy	
2. ESR Method	
3. Magnetic Susceptibility Measurement	26
4. Electrochemical Regularities	
Other Physicochemical Methods	
5. Proton NMR of Metalloporphyrin	
π-cation Radicals	29
6. IR of Metalloporphyrin π -Cation Radical	
7. Resonance Raman	
An Overview of this Thesis	
The Overview of this Thesis	
CHAPTER II - PREPARATION METHODS AND SPECTROSCOPIC PROPERTIES OF OXIDIZED COBALT PORPHYRINS	
1. Preparative Methods	44
Instrumentation	
2. Electronic Absorption Spectra	47
3. ESR And Magnetic Susceptibility	55
Infrared Diagnostic Band of the Cation Radicals	58

rage
RR Vibrational Analysis of Co ^{II} OEP and its Oxidized Products-Spectral Characteristics of the Cation Radicals in the High-Frequency Region
CHAPTER III - IRON PROPHYRIN II-CATION RADICALS: SOLUTION RESONANCE RAMAN SPECTRA OF OEP+·Fe(X)(X')
Experimental Section
CHAPTER IV - RESONANCE RAMAN SPECTRA OF THE II-CATION RADICALS OF COPPER, COBALT, AND NICKEL METHYLOCTAETHYLCHLORINS: VIBRATIONAL CHARACTERISTICS OF CHLOROPHYLL MODELS
Materials and Methods
as octaethylporphyrin-d ₂ using acid-catalyzed exchange reaction
trans-octaethylchlorin- $d_2(\gamma, \delta)$
trans-octaethylchlorin-d ₄ 110
trans-octaethylchlorin- $d_2(\alpha,\beta)$
Conclusion
CHAPTER V - NOVEL B-PYRROLIC SUBSTITUTION REACTIONS OF TETRAPERFLUOROPHENYL PORPHYRIN
General Characteristics a. Reduced Affinity to Metal Ions

	Page
c. Reduced Proton Affinity	115
d. Optical Absorption Properties	116
e. 'H-NMR	118
f. Reversible Oxidation Reactions of MTFPP	
Derivatives	119
Experimental	120
Results	
Cu(II) and Ni(II) Adducts	
Ag(II) Adducts	
Zn (II) Adducts	
Discussion	
CHAPTER VI - METAL-AXIAL LIGAND VIBRATIONS IN	
METALLOPORPHYRINS, THEIR Π-CATION RADICALS	
AND OTHER RELATED SYSTEMS	
Experimental	142
Results and Discussion	142

LIST OF TABLES

	Page
1-1	Spin Densities in Porphyrin Cation Radical8
1-2	The Nature of Axial Ligand(s) in Some Hemoproteins14
1-3	Proton and Deuteron NMR Chemical Shifts for Copper and Silver Porphyrins and Their One-Electron Oxidation Products
1-4	Proton NMR Spectra of Monomeric Iron Porphyrins32
1-5	Proton NMR Resonances for Bis(imidazole)iron(III) Porphyrin Radicals
2-1	Resonance Raman Frequencies (cm ⁻¹) for the Parent CoOEP and its Oxidation Products67
3-1	RR Frequencies (cm ⁻¹) of Selected Iron OEP Species86
3-2	Vibrational Assignments (1450-1700 cm ⁻¹) for Ferric Porphyrins and their π -Cation Radicals86
4-1	Resonance Raman Frequencies (cm ⁻¹) and Optical Absorption Maxima (nm) for Parent MOEP and MMeOEC and their Corresponding π -Cation Radicals
4-2	Estimated K(cm ⁻¹ /Å) and A(Å) Values for the υ and υ Vibrations of the Parent MOEP, MMeOEC and their π -Cation Radicals
5-1	Absorption Spectra (nm) of Dicationic Salt of H ₂ TFPP in CH ₂ Cl ₂
5-2	Comparison of H ₂ TFPP Absorption Maxima (nm) in CH ₂ Cl ₂ with Those of H ₂ TPP and H ₂ OEP117

•		Page
5-3	Solvent-induced Absorption Maxima Shifts (nm) of TFPP Adducts	118
5-4	Changes in the Optical Absorption (nm) in CH ₂ Cl ₂ of the Ag ^{II} and Co ^{II} Complexes of TFPP Upon One-Electron Metal-Centered Oxidation	119
5-5	Absorption Maxima (nm) of TFPP and TPP Adducts in CH ₂ Cl ₂	129
5-6	Absorption maxima and FAB-MS Data on AgTFPP Adducts	130
5-7	Absorption Maxima (nm), FAB-MS m/z and ¹ H-NMR β-proton Multiplicity Number (MN) of ZnTFPP Adducts	134
6-1	Stretching Frequencies (cm ⁻¹) of (Fe-Cl) and (FeOFe) Vibrations in Several Different Ferric Porphyrin (P) Complexes	141

LIST OF FIGURES

	. P	age
1-1a	Oxidation of hemoproteins porphyrin-iron centers in biological systems.	2
1-1b	Oxidation mode of photosynthetic chlorophyll a	2
1-2	Chemical structures of: (a) protoporphyrin IX and its synthetic analogues; (b) meso-tetraphenyl-porphyrin and (c) octaethylporphyrin.	5
1-3	The atomic orbital (AO) structure of two HOMOs of porphine. The AO coefficients are proportional to the size of the circles; solid lines indicate positive values, dashed lines negative. The view is from the positive z axis. The straight dashed lines indicate the nodes of the a_{1u} (π) orbital.	8
1-4	Shape and nodal characteristics of the four essential porphyrin π -molecular orbitals ("Frontier" orbitals; a_{2u} and a_{1u} are filled, e_g are unoccupied).	10
1-5	Typical π -electron energy level scheme of a closed-shell metalloporphyrin: (A) one-electgron energies of highest occupied and lowest unoccupied π -molecular orbitals; (B) configuration energies for the lowest π -excitations before (left) and after (right) configuration interaction. (From Wang et al., J. Am. Chem. Soc., 1984, 106, 4235.)	20
1-6	Visible absorption spectrum of octaethylporphyrinatonickel(II), Ni(OEP), in CH ₂ Cl ₂ . (From Kitagawa et al., Struct. Bonding (Berlin), 1987 , 64, 75.)	20

		Page
1-7	Oxidation of MgOEP in CH ₂ Cl ₂ . The solid line is the absorption spectrum of Mg(II)OEP, the broken line that of [Mg(II)OEP]+·ClO ₄ (From Ref. 16a.)	22
1-8	Oxidation of MgTPP in CH ₂ Cl ₂ . The solid line is the absorption spectrum of Mg(II)TPP, the broken line that of [Mg(II)TPP]+·ClO ₄ (From Ref. 16a.)	
1-9	Upper spectra are those of [Co(III)OEP] ²⁺ ·2ClO ₄ ⁻ (solid line) and [Co(III)OEP] ²⁺ ·2Br ⁻ (dotted line). The lower spectra are those of the primary complexes of horseradish peroxidase (solid line) and catalase (dotted line). (From Ref. 16a.)	24
1-10	RR spectra of (a) CuOEP; (b) CuOEP+·ClO ₄ CH ₂ Cl ₂ bands are marked with an *. CW laser power 20-35 mW	36
2-1	Visible absorption spectra of CoOEP (Soret = 391 nm) and Co ^{III} (MeOH) ₂ OEPBr ⁻ (Soret = 411 nm) in dichloromethane.	49
2-2	Electronic absorption spectra of Co ^{II} OEP derivatives: (a) Co ^{II} OEP(); (b) Co ^{II} OEP+·ClO ₄ ⁻ (); (c) Co ^{III} OEP+·2ClO ₄ ⁻ (), in CH ₂ Cl ₂ ; (d) spectral changes on addition of methanol to a methylene chloride solution of (b) producing Co ^{III} (CH ₃ OH) ₂ OEPClO ₄ ⁻ , total methanol content < 0.01%.	50
2-3	Electronic absorption spectra showing the conversion of Co ^{II} OEP+•ClO4 ⁻ to Co ^{III} (H ₂ O) ₂ OEPClO4 ⁻ as the temperature is lowered. Solvent, "dry" CH ₂ Cl ₂ ; path length ~ 2mm (EPR tube).	52
2-4	Electronic absorption spectra of oxidation products of CoOEP. (a) Co ^{III} (MeOH) ₂ OEPBr ⁻ (); (b) Co ^{III} OEPBr ⁻ (); (c) Co ^{III} OEP+·2Br ⁻ (···), the small feature at 401 nm is due to 1% H ₄ OEP ² +2Br ⁻ contamination as discussed in the text. Solvent, dry CH ₂ Cl ₂ , except for (a) which contains ~ 5% methanol (MeOH)	54

	Page
2-5	250-MHZ proton NMR spectrum of Co ^{III} OEPBr ⁻ in CDCl ₃ at 25°C. Impurity peaks labeled X54
2-6	Spectral changes on addition of methanol to a dichloromethane solution of Co ^{III} OEP+·2ClO ₄ ⁻ in the visible region producing Co ^{III} (CH ₃ OH) ₂ OEPClO ₄ ⁻ , total methanol content ~ 2%
2-7	Infrared spectra (in KBr) of Co ^{II} OEP and its oxidized products. The porphyrin cation radical diagnostic band is labeled with an asterisk
2-8	RR spectra of cobaltous octaethylporphyrin in CH ₂ Cl ₂ 61
2-9	RR spectra excited at 363.8 nm (~ 35 mW) of CoOEP and its oxidation products. (a) CoOEP; (b) Co ^{III} (MeOH) ₂ OEPClO ₄ ⁻ ; (c) Co ^{III} OEP+·ClO ₄ ⁻ ; (d) Co ^{III} OEP+·2ClO ₄ ⁻ ; (e) Co ^{III} (MeOH) ₂ OEPBr ⁻ ; (f) Co ^{III} OEPBr ⁻ ; (g) Co ^{III} OEP+·2Br ⁻ . Solvent, dry CH ₂ Cl ₂ except (b) and (e) which contain ~ 5% methanol. Solvent bands are marked with an *
2-10	Electronic absorption spectra of oxidation products of CoOEP.(a) Co ^{III} (MeOH) ₂ OEPBr ⁻ (-); (b) Co ^{III} OEPBr ⁻ (); (c) Co ^{III} OEP+·2Br ⁻ (···), the small feature at 401 nm is due to 1% H ₄ OEP ² +2Br ⁻ contamination as discussed in the text. Solvent, dry CH ₂ Cl ₂ , except for (a) which contains ~5% methanol (MeOH).
2-11	RR spectra of cobaltic octaethylporphyrin π cation radicals in CH ₂ Cl ₂ 66
3-1	Absorption spectrum of Fe ^{III} OEP+·(Cl ⁻)(SbCl ₆ ⁻) in CH ₂ Cl ₂
3-2	Near-UV RR spectra of OEP+·Fe ^{III} (X)(X') complexes. The laser power was 35-40 mW. The solvent (CH ₂ Cl ₂) band at 1423 cm ⁻¹ is labeled with an asterisk (*)79

	l'age
3-3	RR spectra of ferric chloride porphyrins in CH ₂ Cl ₂ 81
3-4	RR spectra of ferric chloride porphyrin π cation radicals in CH ₂ Cl ₂ .
3-5	RR spectra of model compounds in CH ₂ Cl ₂ . Conditions: 25-30 mW incident on the sample in a spinning cell at 25°C
4-1	Chemical structures of copper(II) derivatives: (a) transoctaethylchlroin (t-OEC); (b) methyloctaethylchlorin (MeOEC)
4-2	Optical absorption spectra of CuMeOEC(-) and its one- electron oxidation product, CuMeOEC+•ClO4 ⁻ () in CH ₂ Cl ₂ 93
4-3	Near-uv RR spectra of t-CuOEC (a), Cu (b), Co (c), Ni (d) complexes of MeOEC. The laser power was 20-30 mw. The solvent (CH ₂ Cl ₂) band at 1423 cm ⁻¹ is labeled with an asterisk (*)
4-4	RR spectra of (a) t-CuOEC++, (b) CuMeOEC++, (c) CoMeOEC++, (d) NiMeOEC++. The laser power was 20-30 mw. The solvent (CH ₂ Cl ₂) band at 1423 cm ⁻¹ is labeled with an asterisk (*)
4-5	Chemical Structures
4-6	250-MHZ proton NMR spectra of t-OEC and its deuterium labeled derivatives in CDCl ₃ . S indicates residual undeuteriated solvent and X represents other impurities
4-7	The electron impact mass spectra (EI-MS) of trans-octaethyl-chlorin and its deutero derivatives at 70 ev
5-1	Absorption spectra of tetrakis(perfluorophenyl) porphyrin complexes taken in CH ₂ Cl ₂ at room temperature: (A) free base; (B) Zn complex, (C) Cu complex; (D) Pd complex. (From Ref. 7.)

		Page
5-2	Solvent-dependent absorption spectra of zinc tetrakis (perfluoro-phenyl)porphyrin in visible region: (A) dry toluene; (B) toluene shaken with H ₂ O;(C) 75% toluene and 25% CH ₃ CN; (D) 75% toluene and 25% ethanol; (E) 75% toluene and 25% pyridine; (F) 75% toluene and 25% triethylamine. (From Ref. 7.)	123
5-3	Electronic absorption spectra of CuTFPP() and Cu(2-B) in CH ₂ Cl ₂	124
5-4	Absorption spectrum of HAg(4-B) in CH2Cl2	•••••
5-5a	Expanded β-pyrrolic region of ¹ H-NMR spectrum of Zn(2-B), fraction 2, in CDCl ₃	127
5-5b	Expanded β-pyrrolic region of ¹ H-NMR spectrum of Zn(2-B), fraction 4, in CDCl ₃	128
5-6a	Electron absorption spectrum of H2TFPP/AgNO3/HOAC reaction products; t<1 h. *The 593 nm band is due to the β -pyrrolic adducts. **Gouterman reports AgTFPP λ_{m} at 416, 536 and 570 nm in ϕ CH3	133
5-6b	Partial FAB mass spectrum of AgTFPP prepared by AgNO ₃ /HOAC method in < 1 hour. The m/z at 1081 (M+,AgTPP) is not shown	134
6-1	UV-vis spectra of CoOEPX in CH ₂ Cl ₂	143
6-2	Absorption spectrum of $Co^{III}OEP^{+}\cdot 2X^{-}$ (where $X = FeCl_4^{-}$ or Cl^{-}) in CH_2Cl_2	145
6-3	UV-vis spectra of FeOEPX in CH ₂ Cl ₂	146
6-4.	Absorption spectrum of Fe ^{III} OEP+•(Cl ⁻)(SbCl ₆ ⁻) in CH ₂ Cl ₂	147
6-5	RR spectra of CoOEPX in CH ₂ Cl ₂ excited at 363.8 nm. The solvent bands at 1422, 703 and 283 cm ⁻¹ are labeled with an asterisk.	148

		Page
6-6	RR spectra of FeOEPX in CH ₂ Cl ₂ excited at 363.8 nmm	150
6-7	(a) RR spectra of $54/56$ FeOEPF in CH ₂ Cl ₂ excited at	
	363.8 nm; b) RR spectra of ^{54/56} FeOEPCl in fH excited at 413.1 nm.	152
6-8	RR spectra of FeOEPX in benzene excited at 406.7 nm. The solvent bands are marked with an asterisk	153
6-9	RR spectra of Co ^{III} OEP+·2X ⁻ in CH ₂ Cl ₂ excited at	
	363.8 nm: (a) $X^- = \text{FeCl}_4^- \sim \text{Cl-}$; (b) $X^- = \text{Br}^-$	155

CHAPTER I

INTRODUCTION

The diversified functions of hemoproteins in biological systems include roles such as the transport of electrons (e.g., cytochrome b₅), the transport of oxygen (e.g., hemoglobin) and the catalysis of redox reactions (e.g., horseradish peroxidase and cytochrome P-450). 1-3 These proteins contain an iron (III) protoporphyrin-IX as their prosthetic group. Other related systems, containing a saturated porphyrin ring macrocycle, mediate the rapid flow of electrons in photosynthetic reaction centers (e.g., chlorophyll a, a magnesium chlorin) and catalyze the reduction of nitrite and sulfite (e.g., siroheme, an iron isobacteriochlorin).⁴⁻⁵ Intuitively, it may be recognized that the widespread use of heme family prosthetic group arises from the presence of a macrocyclic unit, which contains an extensive delocalized π -system (e.g., 18 pi electrons) as well as an iron atom coordinated in the central cavity and, that both the iron and the π -system are capable of rich electron-transfer chemistry and reversible redox reactions, Figure 1.6 The system is tuned for a particular function by means of specific macrocycle peripheral substituent(s), metal axial ligand(s), and the structural influence of the surrounding protein pocket which imposes both conformational and axial coordination restrictions on the encapsulated heme center. For example, horseradish peroxidase (HRP) and catalase (CAT) are two distinct enzymes that react with hydrogen

Figure 1a. Oxidation of hemoproteins porphyrin-iron centers in biological systems.

Figure 1b. Oxidation mode of photosynthetic chlorophyll a.

peroxide to produce transient oxidized intermediates referred to as HRP I and CAT I, respectively, which possess two additional oxidizing equivalents relative to the resting ferric state. 7 Compound I in both species has been assigned to a ferryl porphyrin π -cation radical in which one oxidizing equivalent is stored in the form of a tetravalent iron stabilized by oxygen (Fe^{IV}=O) and the second equivalent resides in a porphyrin π -cation. In the HRP case, the fifth proximal ligand to iron is a neutral histidyl imidazole, whereas the iron atom in CAT bears a tyrosine phenolate. This distinction in the nature of the heme-iron axial ligand is presumably the principal factor in the functional differentiation of these hemoproteins.⁸ The macrocyclic π cation radical species has also been observed in the chlorophyll photochemical reaction for the primary products generated by the photooxidation of the chlorins in the photosystem I and II and, possibly in the cytochrome P-450 reaction cycle. In order to account for the contribution that each structural parameter makes to the overall reactivity, synthetic analogs of hemoproteins are invaluable in this regard because they provide the chemist with an opportunity to introduce a composite of several different structural parameters in a stepwise fashion and, consequently, clarify the details of biological redox mechanisms that involve hemoproteins iron-porphyrin centers. Additionally, the protein-free heme model complexes are more frequently responsive to detailed scrutiny than the hemoproteins themselves.

While use of specific peripheral substitution pattern of protoporphyrin is essential for the elucidation of biological function, its chemical reactivity and asymmetric distribution make this porphyrin a poor substrate for in vitro model studies. Instead, we utilize two synthetic porphyrins, octaethylporphyrin (OEP) and meso-tetraphenylporphyrin (TPP), which,

owing to their high solubility, chemical stability and relative ease of preparation, have proved to be exceptionally useful for model studies. The OEP complexes, however, will be the main focus of this study owing to their biologically-relevant substitution pattern, analogous to that of protoporphyrin species, Figure 2. Focusing on these structurally-related porphyrins will demonstrate systematically how the model compound reactivity may be tuned to obtain a desired potential (E^O), a desired number(s) of electrons transferred in the reaction sequence, or a specific ultimate product (e.g., change in the valance of the central metal or generation of a π -cation radical).

Research Objectives

This study aims to utilize synthetic porphyrins and their derivatives to establish vibrational, electronic and structural characteristics of the oxidized states of hemoproteins iron-porphyrin centers. The emphasis will primarily be placed on the porphyrin-based π -cation radical state which serves as one of the two oxidizing equivalents in the reaction cycle of peroxidases, catalases and photosynthetic chlorophylls. At the time that the present work began, the redox behavior of metalloporphyrins had been widely investigated and there were already numerous reports available on the visible absorption, ESR, magnetic susceptibility and NMR properties of these radicals; $^{10-13}$ however, their vibrational characteristics had not been studied in any detail. This may partially result from the limited stability of these radicals, their preparation under conditions (e.g., solvent, co-solvent and concentration)

Figure 2. Chemical structures of: (a) protoporphyrin IX and its synthetic analogues; (b) meso-tetraphenylporphyrin and (c) octaethylporphyrin.

that may not be suitable for vibrational studies, and the time required to scan a spectrum when a conventional spectrometer is used.

Resonance Raman (RR) spectroscopy has been utilized as a powerful probe, in the last few decades, to study hemoproteins structures, functions, and mechanisms. A major advantage of RR is its selectivity for individual chromophoric species in a multicomponent hemoprotein system. Since the interpretation of RR vibrational frequencies relies heavily upon previous studies of model compounds that were designed to mimic the structure of molecular species thought to exist in the more complicated protein sample, this prompted us to investigate vibrational characteristics of synthetic metalloporphyrin π -cation radicals. A systematic study of these radicals will demonstrate the sensitivity of RR frequencies to the vibrational, electronic and structural changes accompanied by removal of an electron from the porphyrin-based π -system. This will, in turn, aid detection and assignment of this particular mode of oxidation in the catalytic cycles of hemoproteins currently under investigation. The RR data obtained in this study are intimately supported by other spectroscopic methods, in particular, optical absorption, ESR, magnetic susceptibility and IR data.

It is the objective of this chapter to present a general background of the structural parameters involved and the methods commonly used in the study of metalloporphyrin redox reactions.

Porphyrin π -Cation Radicals

The striking feature of the porphyrin ring is its ability to undergo facile oxidation under chemical or electrochemical conditions to form a π -cation

radical. Probably the first direct evidence for the existence of porphyrin π -cation radicals was Commoner's observation of a rapidly decaying, sharp ESR signal at g=2.00 in photosynthetic material. Another early report on signals that were similar but of high stability was made for solutions of TPP. Easy access to stable cation radical as well as their detailed analysis, was achieved when ESR spectra, absorption spectra and redox potentials were quantitatively related to the oxidative formation of these radicals and crystalline material was obtained. 16

Gouterman¹⁷ has shown that in a metalloporphyrin (MP), the highest filled orbitals, a_{1u} and a_{2u} , are nearly degenerate, Figure 3. Removal of an electron from these orbital produces a π -cation radical and the remaining unpaired electron occupies either an a_{1u} or a_{2u} orbital with $^2A_{1u}$ or $^2A_{2u}$ ground state (D_{4h} symmetry), respectively. Based on recent calculation by Zerner, ¹⁸ the two ground states differ in energy by about 4 kcal/mole; thus, small perturbation such as changes in peripheral groups, axial ligand(s) or the central metal could determine the symmetry of the ground state. Moreover, MO calculation as well as ESR data showed that in the $^2A_{2u}$ state, high spin density appears at both the meso-carbon and nitrogen atoms, while in the $^2A_{1u}$ state, spin density is primarily localized on the α carbons, Table 1.¹⁹ For example, the ESR evidence confirms that, indeed, the π -cation radical of MgOEP occupies a $^2A_{1u}$ and that of MgTPP a $^2A_{2u}$ state.²⁰

As a rule, the a_{2u} orbital is found to be higher than the a_{1u} orbital. Taking into account the fact that a_{2u} orbital has its maximum electron density on the nitrogen and meso-carbon atoms, we can assume that addition of meso-substituents (e.g., phenyl groups in TPP) will lead to an increase in the

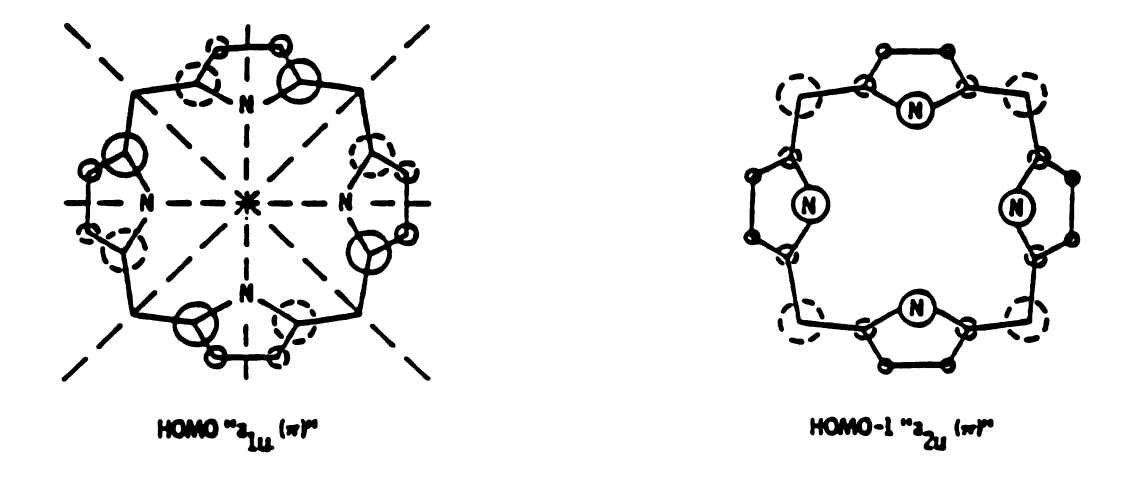
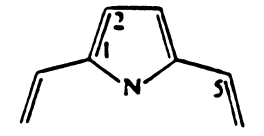


Figure 3. The atomic orbital (AO) structure of two HOMOs of porphine. The AO coefficients are proportional to the size of the circles; solid lines indicate positive values, dashed lines negative. The view is from the positive z axis. The straight dashed lines indicate the nodes of the a_{1u} (π) orbital.

Table 1.

Spin Densities in Porphyrin
Cation Radicals



Atom	² A ₂ , (calculated)	² A ₁ , (calculated)
C-1	-0.0094	0.0981
C-2	0.0134	0.0262
C-S	0.1932	0.0012
N	0.049	0.000

(From Ref. 19.)

energy of this orbital to an extent that it becomes higher than the energy of the a_{1u} orbital. In this case, the electron abstraction will take place from this orbital to form a ${}^2A_{2u}$ π -cation radical. Indeed, almost all metallotetraphenylporphyrin cation radical display a ${}^2A_{2u}$ ground state. In the OEP case, the introduction of alkyl substituents in the pyrrole rings probably results in the a_{1u} orbital being higher than the a_{2u} level. The electron density will therefore be removed from the orbital with a_{1u} symmetry to form a ${}^2A_{1u}$ cation radical. However, several investigations have demonstrated that the OEP-type system is more responsive to the change in the ground-state symmetry as a result of perturbation caused by metal or axial ligand, than the corresponding TPP complexes.²¹

Metal-Porphyrin Interactions

The role of the centrally coordinated iron in hemoprotein catalysis is to hold the reacting species in conformations favorable for reaction and act as a source of, or sink for, electrons. Calculations on model compounds have shown that metal interacts with the porphyrin ring in two ways, which are referred to as inductive and conjugative effects.²²

1. Inductive Effect: This mode of interaction results from the change of electron density at the nitrogen atoms as the result of substituting different metals in the central cavity. This perturbation affects the energies of the doubly degenerate LUMO $e_g(\pi^*)$ and HOMO $a_{2u}(\pi)$ but not $a_{1u}(\pi)$ orbital because the latter has nodes through the central nitrogen atoms, Figure 4. As the central metal becomes less electronegative, the sigma electron shell shifts from the metal towards the ring which raises the e_g and a_{2u} orbitals by inductive effect.

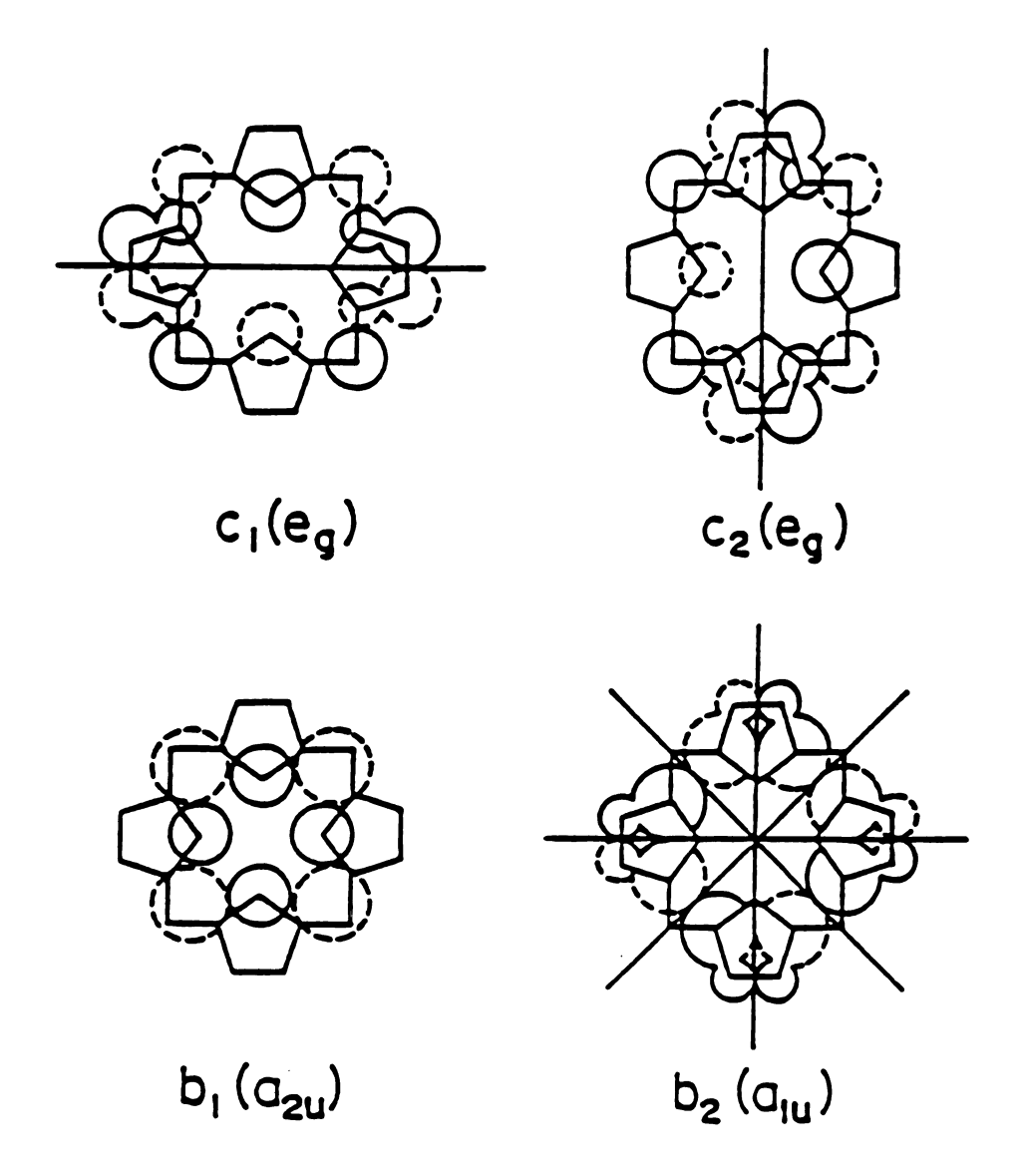


Figure 4. Shape and nodal characteristics of the four essential porphyrin π -molecular orbitals ("Frontier" orbitals; a_{2u} and a_{1u} are filled, e_g are unoccupied).

2. Conjugative Effect: This effect results from the interaction of metal P_{π} orbitals with those of porphyrin π -electron system (e.g., e_g and a_{2u}). For example, as the central metal becomes less electronegative, that part of the pi electron density located in the metal $4P_Z$ orbital can move back into the ring causing an increase in the energy of the a_{2u} orbital at the expense of a decrease in conjugation between metal and porphyrin pi orbitals.

Site-Selective Oxidation: Metal- vs. Porphyrin-centered Oxidation Induction

Metalloporphyrin redox reactions may be classified into three categories:

- 1. Reversible changes in the formal oxidation number of the metal ("inorganic redox reactions"),
- 2. Reversible changes of the oxidation state of the porphyrin ("organic reversible redox reactions") and
- 3. Both metal and the porphyrin ligands undergo reversible redox reactions.

As was previously noted, several structural parameters contribute to the selective oxidation reactions of the metal and porphyrin centers. These are:

- 1. the nature of the central metal,
- 2. macrocycle peripheral substituent(s),
- 3. metal axial ligand(s),
- 4. solvent (or medium) and
- 5. temperature.

The role of these parameters will be discussed individually in the following section and examples will be given.

- 1. Effect of the Central Metal: The redox chemistry of metalloporphyrins is dominated by strong σ-electron donation from the nitrogens to the metal ion. Metals of low electronegativity and low oxidation number activate the porphyrin ring with respect to oxidation and deactivate it with respect to reduction. The opposite is true for metals of high electronegativity and/or oxidation number. Such reversible reactions of the macrocyclic ring are of importance in biological systems containing magnesium metal; namely, photosynthetic chlorophyll a. On the other hand, electron-rich transition metal ions (e.g., iron) with formally high oxidation numbers are stable in the porphyrin cavity and tend to transfer some electrons to the axial ligand. This effect is of biological importance in hemoproteins, which function in electron transfers and oxygen activation.
- 2. Porphyrin Peripheral Substituent(s): The one-electron oxidation products of the MP's are highly reactive species having redox potentials between those of I₂ and Br₂ (~ 0.5 1.2 volts). Experimentally, it is found that oxidative titration in organic solvents with a stoichiometric amount of oxidant are only possible for complexes with midpoint potential below 0.3 volts (e.g., magnesium octaethylchlorin, MgOEC; ZnOEC and BChl a) and iodine as an oxidant. In all other cases, an excess of oxidant is needed to complete the oxidation of MP probably because the organic solvents, or reducing impurities contained in them consume oxidant above 0.5 volts. A range of oxidants may be used to produce π-cation radicals including I₂, Br₂, CuBr₂, NBS, DDQ, Fe(ClO₄)₃, FeCl₃, pheno+• SbCl₆-, φ₃N+X-, Ce^{IV} salt, XeF₂²³. In special cases, stable cation radicals

of porphyrin itself may be used to induce oxidation in another porphyrin system such as $ZnTPP^+ \cdot ClO_4^-(\epsilon_{1/2} = 0.77 \text{ volts vs. SCE})$ and $(FeTPP)_2O^+ \cdot ClO_4^-(\epsilon_{1/2} = 0.84 \text{ volts vs. SCE}).^{24}$

Recent findings concerning the role of the propionate and vinyl groups of iron (III) protoporphyrin-IX in cytochrome b5 highlights the significance of macrocycle peripheral substitution pattern. This study, reported by Reid et al, 25 indicated that heme proteins modulate the reduction potentials of their heme redox centers by constraining the position of the vinyl groups with respect to the plane of the heme and thereby affecting the electron-withdrawing ability of the vinyls. By forcing the vinyl substituents into the plane of the heme prosthetic group, their electron-withdrawing ability is enhanced, and the reduction potential of the heme center is increased. In another study, they also suggested distinctly different roles for heme propionate groups, one partially responsible for determining the reduction potential of the iron center, and the other group is involved in recognition of and interaction with heme proteins that are physiological redox partners of cytochrome b5. As demonstrated by model studies, in general, the presence of electron-donating or electron-withdrawing substituents modify the electron density at the central metal and lead to shifts in redox potentials, the magnitude of which are dependent on the substituents and their orientation with respect to the macrocycle ring plane. For example, metallochlorins are oxidized by as much as 0.3 volts lower than metalloporphyrins, and bacteriochlorins are again 0.3 volts lower. This trend can be rationalized by noting that in the β-hydrogenated

porphyrins, one or two of the electron-withdrawing pyrrole units, which can be formulated as pyrrole anions (pk~16), are replaced by pyrroline units, which function as aza bridges (pk~2) in the inner conjugation path. Therefore the ligand becomes less basic and the oxidation potential of the central metal increases; therefore, it becomes easier to remove an electron from the porphyrin ligand itself.²⁶

3. **Metal Axial Ligand(s):** Metalloporphyrins can bind one or two ligands at the axial coordination sites and these ligands can potentially dictate the chemistry of the heme group. The heme in the electron carrier hemoproteins is exceptional in that it has two strong axial ligands and generally does not bind molecular oxygen or peroxides. The heme in all other hemoproteins has one accessible coordination site which allows it to react with peroxides and other ligands (Table 2).

Table 2. The Nature of Axial Ligand(s) in Some Hemoproteins

Axial Ligand(s)
Cystein thiolate (1)
Histidine Imidazole (1)
Tyrosine Phenolate (1)
Histidine Imidazole (1)
Histidine Imidazole (2)
Histidine Imidazole (1)
Methionine Methylthioether(1)

The number in parenthesis indicates the number of axial ligand(s) coordinated to the heme-iron center.

The nature of the axial ligand can trigger metal vs. porphyrin-based oxidation, influence the ground state symmetry of the porphyrin radical $({}^{2}A_{2u}$ or ${}^{2}A_{1u})$, alter the spin state of the central metal and disturb the conformation of the macrocycle.

For example, the site of oxidation of ruthenium(II) porphyrins (metal or porphyrin) is dependent on the nature of the axial ligand. When pyridine occupies the extraplanar sites, oxidation occurs at the ruthenium ion. If CO is one of the extraplanar ligand, the site of oxidation is at the porphyrin ring. This change has been attributed to stronger ruthenium back-bonding to CO compared to pyridine, which stabilizes metal d_{π} orbitals relative to the porphyrin π levels; the latter then becomes the valance MOs of the system.^{27a}

It has also been shown that in iron(III) tetramesitylporphyrin, TMPFe^{III}(L), strongly basic ligands such as $L = \phi^-,OH^-,OCH_3^-,F^-$ and = O favor the formation of iron (IV) species, whereas weakly basic anions such as $L = ClO_4^-$, Cl^- and imidazole cause porphyrin cation radical formation.^{27b}

As discussed earlier, the species $CO^{III}OEP^{+}\cdot 2X^{-}$ can be made to occupy either of the two ground states $(^{2}A_{1u} \text{ vs } ^{2}A_{2u})$ as a function of its axial ligands. When the dibromide $(^{2}A_{1u} \text{ state})$ is treated with AgClO₄, the bromide ligands are removed and the resultant diperchlorate salt now shows characteristics of the $^{2}A_{2u}$ state. 16a

The variation of the axial ligand can result in a change in spin state, particularly of iron porphyrins, and concomitant structural changes. High-spin hemes (S = 5/2) are five-coordinated and exist in

square-pyramidal conformation. The iron atom is displaced from the porphyrin plane toward the axial ligand (e.g., $X^- = Cl^-, N_3^-$) which makes the binding of further ligands unlikely. On the other hand, the formation of two strong axial bonds (e.g., bis imidazole derivative) involves an in-plane position of iron and a low-spin state (S = 1/2). Thus, the obligatory structural changes that accompany the low-spin to high-spin transition is an expansion of the porphyrin core size (e.g., $PFe^{III}(Im)_2^+ \rightarrow PFe^{III}(DMSO)_2^+$). High-spin Fe(II) and Fe(III) porphyrins are both too large to fit into the central cavity of the porphyrin ring and they are forced out of the porphyrin ring by ~ 0.4 and 0.5 Å, respectively. These out-of-plane structures exhibit significant doming and ruffling of the porphyrin ring.²⁹

4. **Solvent (or Medium):** Protic solvents (e.g., CH₃OH) slowly destroy the cation radical and may only be used as co-solvents in oxidation reactions, when the electron transfer is very rapid. Although, the stabilizing effect of nucleophilic solvents on the oxidation of certain metalloporphyrins (e.g., MgOEP) favors the use of solvent mixture such as CHCl₃-CH₃OH(4:1);¹⁰ however, the electrophilic nature of the porphyrin cation radicals may cause nucleophilic addition of the solvent to the bridged meso carbon of the cation radical and the subsequent formation of an isoporphyrin complex.³⁰ Thus, care must be taken to avoid occurrence of this side reaction.

Solvent effects on the porphyrin redox potentials are small. However, solvent effects on metal redox potentials can be extraordinarily

large. For example, the Co^{III}/Co^{II} redox couple involves low-spin d^6/d^7 configurations. Strongly binding axial ligands (solvent molecules) destabilize the d_Z^2 electron (in d^7) and favor oxidation to low-spin d^6 species. Thus, in this case, the potential shifts negatively with increasing donor strength of the solvent (e.g. DMA = DMF< DMSO < pyridine).³¹

Solvent may also play a role in the selective formation of metal-or porphyrin- centered oxidation product. The first oxidation of CoOEP in dry CH₂Cl₂, for example, involves formation of a Co(II) porphyrin cation radical while the second and third oxidations involve abstraction of electrons first from the Co(II) center and then from the porphyrin π -system. This ordering in the sites of oxidation is reversed in coordinating solvents or in the presence of nucleophiles. In the latter solutions, the first oxidation of CoOEP invariably involves the Co(II)/Co(III) transition.³²

5. **Temperature.** Oxidation of NiTPP at room temperature results in the abstraction of an electron from a porphyrin-centered π orbital to form a π -cation radical. This species, NiTPP+; displays an exceptional thermal behavior. As the temperature is lowered, an internal electron transfer occurs, with the hole moving from the periphery to the metal to generate a Ni(III) species.³

Although the structure of protein determines the heme-iron spin equilibrium in hemoproteins through control of axial ligation,³⁴ a thermal spin-state equilibrium can be observed in a model heme system whose axial ligation is characteristic of these proteins.^{35a},^b Several studies have indicated that the nature of the axial ligand is an important

factor in determining the high-spin or low-spin character of the iron center. Weak field ligands such as F- form high-spin, six-coordinate iron (III) complexes; strong field ligand such as CN- and imidazole form low-spin hexacoordinate iron (III) complexes, and ligands such as N₃- having intermediate field strength form complexes that exhibit temperature-dependent, spin-state equilibrium.³⁶ The position of the equilibrium at a given temperature is sensitive to the immediate environment of the iron(III) porphyrin cation. For example, OEPFe^{III}(py)₂+ C1O₄- show a magnetic moment at 77°K corresponding to an almost pure low-spin state (S = 1/2) and a moment at room temperature appropriate for 1:1 mixture of the low-spin and high-spin (S = 5/2) states.^{35b}

Differentiation Between Metal vs. Porphyrin-based Oxidation Reactions - Spectroscopic Methods

1. **Optical Absorption Spectroscopy:** The oxidation reactions of metalloporphyrins usually can be followed visually: a neutral metalloporphyrin gives a reddish color solution; oxidation most often changes this color to dark brown or green if the reaction is porphyrin-centered, whereas the red color maintains if the reaction proceeds at the central metal. 10, 32

Since MPs and their oxidized products display characteristic electronic absorption spectra, the following section will briefly address the optical properties of these species.

A typical absorption spectrum of the metal complex of the biological-type (=pyrrole-substituted) porphyrin (e.g., OEP) features two visible bands (α or $Q_{0.0}$ and β or $Q_{0.1}$ bands) of moderate intensity ($\epsilon \approx$

 10^2 - 10^3 M⁻¹Cm⁻¹) in the 500 - 600 nm region and a very strong ($\varepsilon \approx 10^4$ - $10^5 \,\mathrm{M^{-1}Cm^{-1}}$) band, called the Soret (also δ or B) band near 400 nm, Figure 6. The visible and near-uv spectra of MPs can be interpreted within the context of the four-orbital model proposed by Gouterman and coworkers.³⁷ The electronic transitions that give rise to the characteristic spectra of MPs arise by excitation from the two highest filled orbitals (HOMO's), the nearly-degenerate $a_{1u}(\pi)$ and $a_{2u}(\pi)$ levels, into the doubly-degenerate lowest unfilled orbitals (LUMO's), eg(π^*) levels, (D_{4h} symmetry). For the porphyrin ring, the lowest singlet excited configurations, $1(a_{2u},e_g)$ and $1(a_{1u},e_g)$, are of the same symmetry (E_u) and of similar energy, Figure 5. These transitions have strong electronic interaction between them and are mixed by configuration interaction to yield the relatively weak visible $Q_{0,0}$ band in which the transition dipoles nearly cancel, and the intense near-uv Soret band, in which the transition dipoles of the two configurations add. The closer the degeneracy of the configurations (a_{2u},e_g) and (a_{1u},e_g) , the weaker is the In some instances (e.g., CoTPP), the $Q_{0,0}$ band essentially disappears. In addition, the $Q_{0,1}$ vibronic overtone is also active and appears as an additional peak on the high-energy side of $Q_{0,0}$ transition. The $Q_{0,1}$ band arises from vibronic mixing of the $Q_{0,0}$ state with the B state and is constant among porphyrins.³⁸ The assignment of this band is based on the constancy of its energy separation from the $Q_{0,0}$ band and its nearly constant intensity.

Comparison of the optical spectra of a number of π -cation radicals 16a reveals that they fall in two categories typified by either

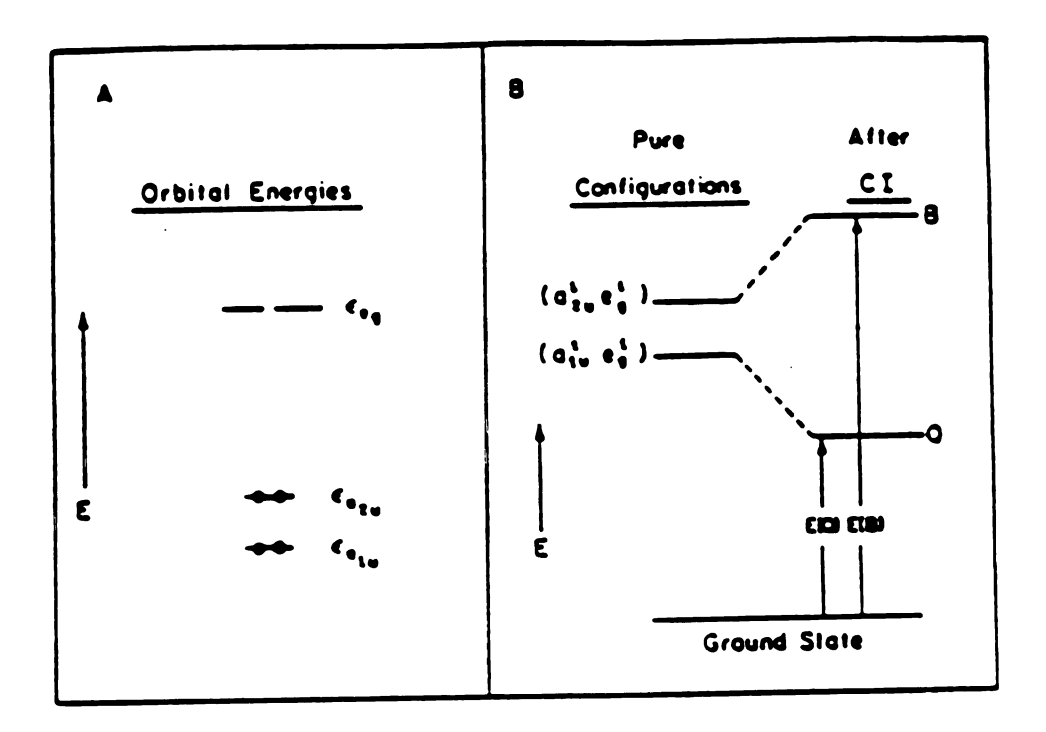


Figure 5. Typical π -electron energy level scheme of a closed-shell metalloporphyrin: (A) one-electgron energies of highest occupied and lowest unoccupied π -molecular orbitals; (B) configuration energies for the lowest π -excitations before (left) and after (right) configuration interaction. (From Wang et al., J. Am. Chem. Soc., 1984, 106, 4235.)

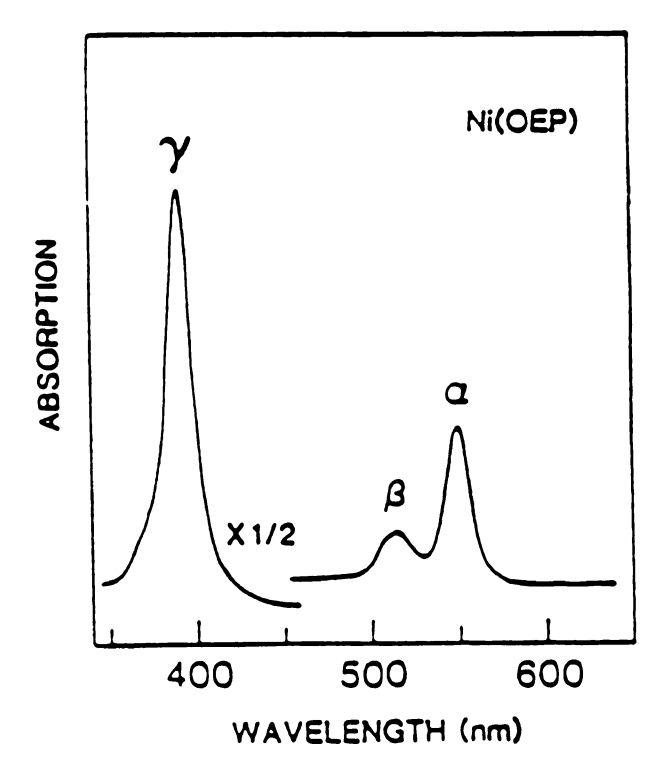


Figure 6. Visible absorption spectrum of octaethylporphyrinatonickel(II), Ni(OEP), in CH₂Cl₂. (From Kitagawa et al., Struct. Bonding (Berlin), 1987, 64, 75.)

MgOEP, Figure 7, and MgTPP π -cation radicals, Figure 8. The MgOEP radical has a visible spectrum that is characterized by a major absorption peak near 700 nm with a high-energy shoulder, while the MgTPP radical exhibits a broad, near featureless absorption in the region 500-700 nm. These differences have been ascribed to two close-lying ground states of the radicals: ${}^{2}A_{1u}$ (class 1) for MgOEP+• and ${}^{2}A_{2u}$ (class 2) for MgTPP+•

The preceding interpretation has been utilized for some time as the optical criterion by which to distinguish between the two possible ground states. Qualitatively perhaps, it is still useful, however exceptions have been found and caution must be used in making any definite assignments that are based on the optical characteristics. For example, Godziela et al. recently showed that CuOEP++, previously taken as an example of ²A_{2u} ground state, ^{16a} exhibits NMR chemical shifts characteristic of a ²A_{1u} radical.³⁹ A recent study by Zerner and coworkers has provided a firm foundation for a quantitative interpretation of MP π -cation radicals. This work demonstrates that ²A_{1u} cations lie lower in energy than the ²A_{2u} cations by only 4 kcal/mole, consistent with the findings that both radicals are found depending upon substituents and solvent. The visible region of the spectrum of the ²A_{1u} species is predicted to consist of three separate bands decreasing in intensity with increasing energy, while that of the ²A_{2u} species is calculated to consist of three allowed transitions of nearly equal intensity, in accord with the experimental findings. The Soret region of the ²A_{1u} ions is dominated by at least four allowed transitions spread over 100 nm, while that of the $^2\mathrm{A}_{2\mathrm{u}}$ radicals contains at least

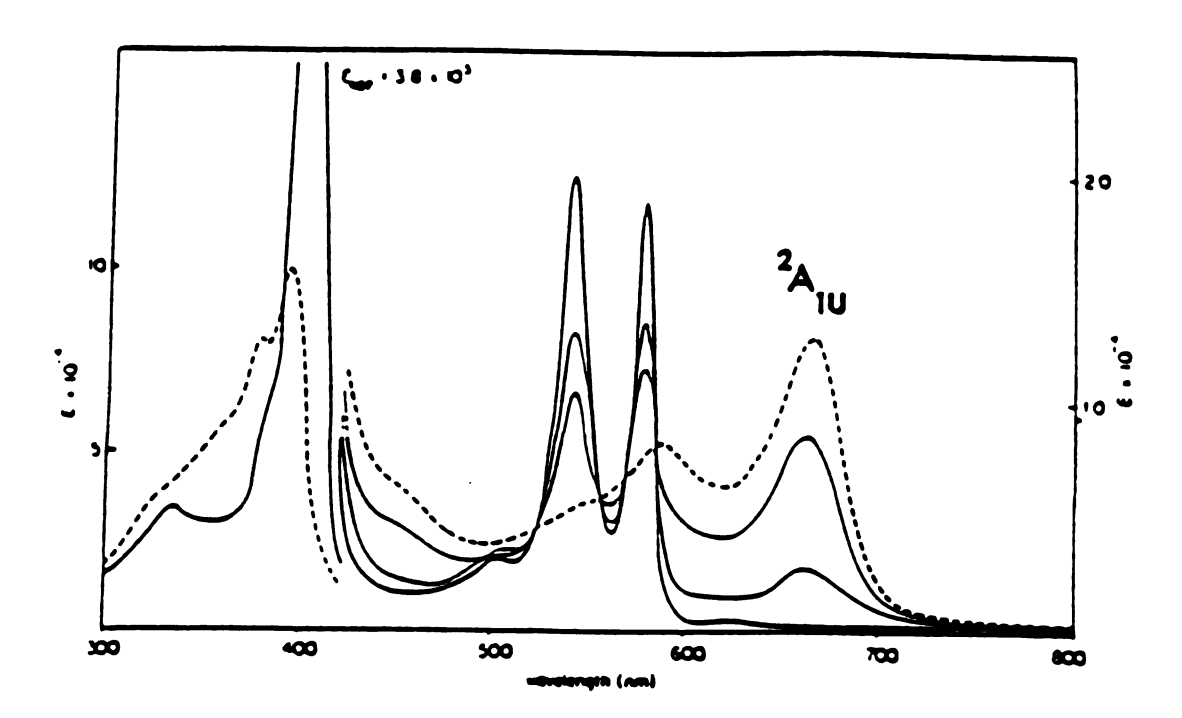


Figure 7. Oxidation of MgOEP in CH₂Cl₂. The solid line is the absorption spectrum of Mg(II)OEP, the broken line that of [Mg(II)OEP]+-ClO₄*. (From Ref. 16a.)

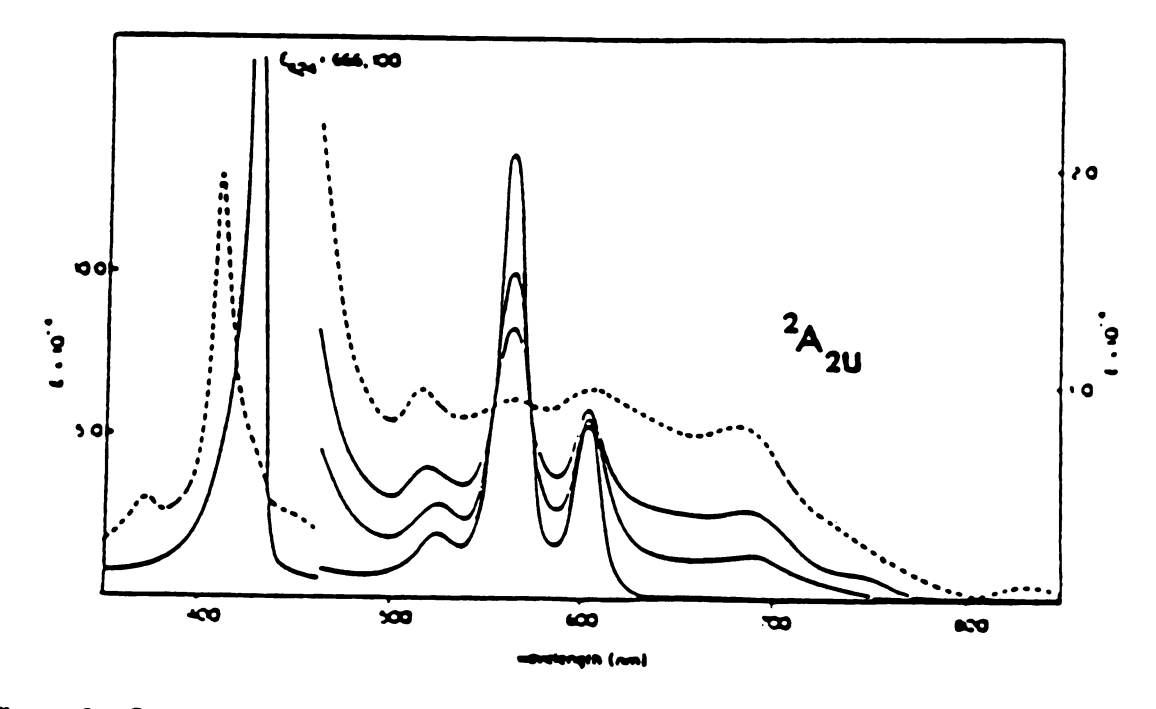


Figure 8. Oxidation of MgTPP in CH₂Cl₂. The solid line is the absorption spectrum of Mg(II)TPP, the broken line that of $[Mg(II)TPP]^+$ -ClO₄*. (From Ref. 16a.)

three allowed bands, but the intensity in this region is dominated by only one of them.

Thus, an absorption spectrum with two sharp bands in the visible region and a narrow Soret band indicates a pyrrole-substituted MP with the porphyrin ring in its zero oxidation state. If this spectrum is found in an oxidation product from a MP, then oxidation has occurred at the metal (e.g., $Ag^{II}OEP \rightarrow Ag^{III}OEP$). If, however, the electronic spectrum broadens considerably after oxidation, then the porphyrin ligand might have reacted (e.g., $Cu^{II}OEP \rightarrow Cu^{II}OEP^{+}$). 16a As a matter of fact, similarity between the optical spectra of catalase and horseradish peroxidase compound I with those of Co^{III}OEP+ · 2Br- and Co^{III}OEP+ · 2ClO₄, respectively, led to the notion that these complexes may be characterized as porphyrin π -cation radicals and that, CAT I exists in the ²A_{1u} ground state, whereas HRP I exists in the ²A_{2u} state. It was also speculated that differences in reactivity between the two enzymes are the result of differences in the ground states, which may, in turn, be caused by minor changes in the axial ligation, as demonstrated by the optical characteristics of the two cobalt octaethylporphyrin cation radicals, Figure 9.16a

- 2. **ESR Method.** If only one unpaired electron is found in the product, then its location is easily determined by examination of line width, g-values and hyperfine structure in the ESR spectrum. Typically, the ESR experiments yields two possible results:
 - 1. An isotropic signal characteristic of an organic free radical around g = 2.00 and of line width less than 12 G (e.g., ZnTPP+•). 19

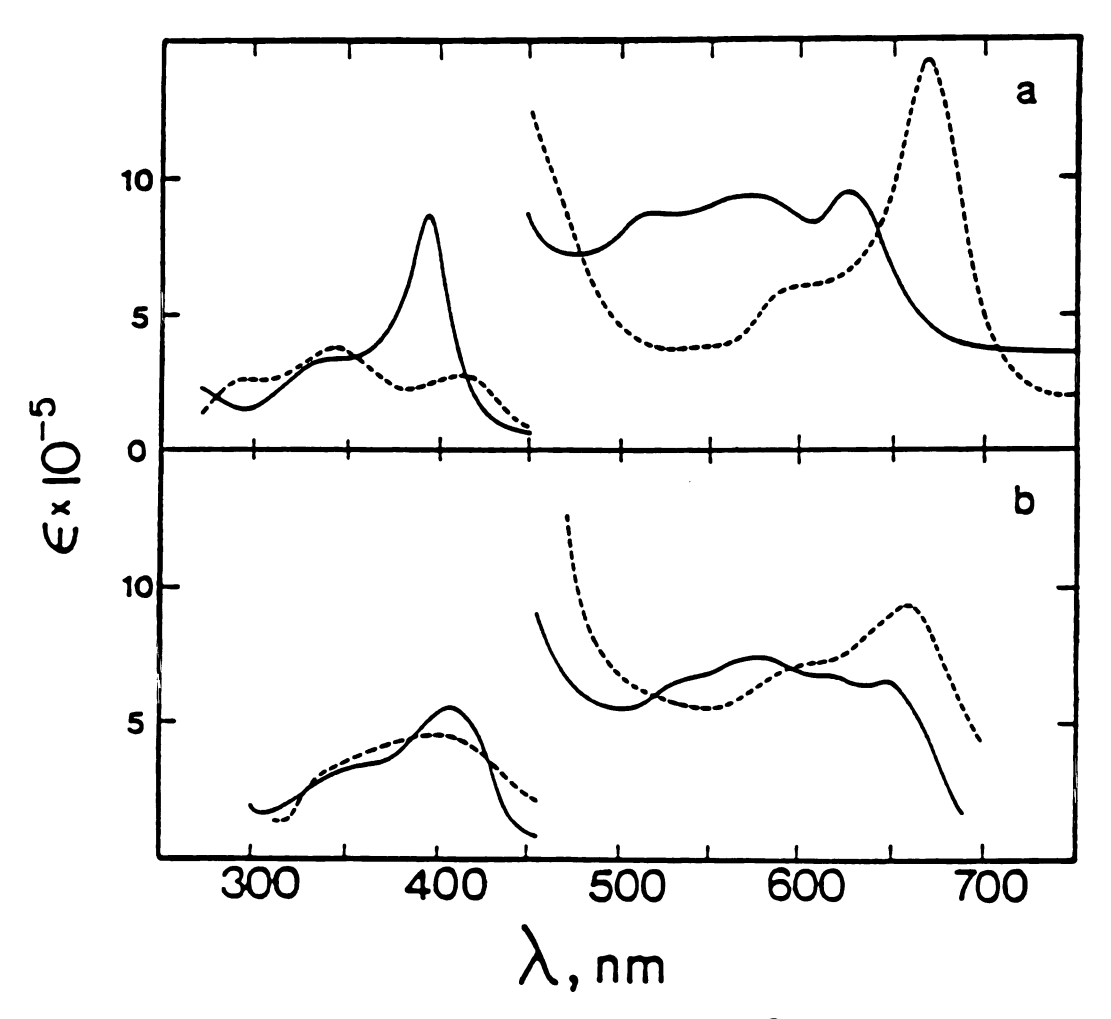


Figure 9. Upper spectra are those of [Co(III)OEP]^{2+.}2ClO₄⁻ (solid line) and [Co(III)OEP]^{2+.}2Br⁻(dotted line). The lower spectra are those of the primary complexes of horseradish peroxidase (solid line) and catalase (dotted line). (From Ref. 16a.)

2. An anisotropic signal of line width > 50 G with various g values typical of transition metal ions (e.g., $Co^{III}TPP+\cdot$).⁴¹

Copper porphyrin cation radicals, on the other hand, are more complex owing to the presence of one odd electron on the central metal $(3d_{x^2-y^2})$ orbital) and the other on the porphyrin ring. Therefore, their spin state is either singlet or triplet depending on which is lower in energy. Since no triplet ESR spectrum had been detected for some time for any copper porphyrin radicals, it was speculated as being due to a singlet ground state or to line broadening of triplet spectra. However, Konishi and coworkers recently reported the first detection of a triplet spectrum of a copper porphyrin cation radical produced in tetrachlorethane matrix at 77°K by δ radiolysis. 42

The ESR spectra obtained for MP+ \cdot can be classified into two types, exemplified by $^2A_{2u}$ and $^2A_{1u}$ ground states. The ESR analysis of the $^2A_{2u}$ state reveals:

- 1. Large spin density at the meso carbons which can be transmitted to the meso substituents (e.g., phenyl group).
- 2. Enough spin density at pyrrole nitrogens to cause nitrogen hyperfine splitting (1-2G).
- 3. Zero spin density at β -pyrrole positions.
- 4. Enough spin density at the metal to cause metal hyperfine splitting (e.g., $a_{ZR} = 1G$).
- 5. Charge density transmission to the counterion (e.g., ZnTPP+•(Py)ClO₄-).

In the ${}^2A_{1u}$ state, on the other hand, small hyperfine splittings from the meso protons are observed (e.g., $a_H = 1.48G$ for MgOEP+•ClO₄-). This

ground state also does not display any splitting due to the nitrogens, central metal, or counterion and the electron density is mostly localized on the α carbons.

3. Magnetic Susceptibility Measurement: When both the metal and the porphyrin ring contain unpaired electrons, magnetic susceptibility measurements by using a SQUID susceptometer in the solid state⁴³ or Evan's NMR shift method in solution⁴⁴ help to locate the site of a The theory of spin state in these MP+ is based on the occupations and symmetries of the so-called magnetic orbitals, i.e., those orbitals on the metal and the ligand that contain an unpaired electron. MP+ complexes whose half-occupied d orbitals are strictly orthogonal to the porphyrin π -radical orbital are expected to show ferromagnetic coupling (like Hund's rule). Thus, the spin state of higher multiplicity will be lower in energy. For example, in a strictly planar environment of D_{4h} symmetry as well as in the absence of any complication from aggregation, $CuTMP^+\cdot SbCl_6^-$ features orthogonal copper $d_{\chi^2-\chi^2}$ and porphyrin a_{1u} or a_{2u} orbitals and shows an S = 1 (i.e., triplet), μ_{eff} = 2.9µB, ground state.⁴⁵ On the other hand, complexes whose metal and ligand magnetic orbitals are not strictly forbidden by symmetry to overlap are expected to show antiferromagnetic coupling (or bond formation). The spin state of lower multiplicity will be lower in energy. This is exemplified by the CuTPP+ \cdot SbCl₆- crystal which shows an S = 0 (i.e., singlet) ground state. This crystal exhibits a saddle-shaped conformation in which nearly planar pyrrole rings tilt up and down and the phenyl groups become nearly coplanar. 46 Although this

conformation allows the appearance of tightly associated pairs of cations, the face-to-face structure of the dimer lacks any recognizable specific HOMO-LUMO interaction or the popular but unproven intermolecular metal-nitrogen interaction. The large Cu-Cu separation (5.43 Å) also makes it unlikely for the trivial d-d coupling between cofacial $d_{x^2-v^2}$ orbitals. For similar reason, the intermolecular $d-\pi$ coupling is also considered unlikely. This leaves an intramolecular $d-\pi$ coupling within each CuTPP+ molecule as the likely source of complete diamagnetism. Thus, Reed and coworkers⁴⁶ suggested that intramolecular metalporphyrin spin coupling occurs as a result of the lowering of the local symmetry from D_{4h} to C_s which destroys the orthogonality of magnetic orbitals. Under C_s symmetry, the $d_{\chi^2-y^2}$ and the a_{2u} orbital overlap become symmetry allowed and the resultant spin pairing may be viewed as copper porphyrin bond formation with the two electrons spin paired in the bonding molecular orbital. In solution, however, the monomeric CuTPP+ is planar and strict orthogonality of the magnetic orbitals gives rise to the paramagnetic state.

A yet alternative mode of coupling is demonstrated by CuOEP+· whose nearly planar conformation is prone to the formation of tightly-spaced dimers (Cu-Cu separation of ~ 4Å) at low temperatures or in solid state and at high concentration in solution. This can reduce the moment of the monomeric CuOEP+· triplet ground state (μ_{eff} = 2.9 μ_{B}) as a function of the extent of association into dimeric units or higher order aggregates. The driving force for dimerization is probably best

viewed as a case of weak π - π bond formation between two half-occupied porphyrin HOMOs. Indeed, NiOEP+• is diamagnetic from presumed π - π coupling.⁴⁶

- 4. Electrochemical Regularities: A systematic voltammetric investigation of the redox potential of metal complexes of octaethylporphyrin including all members of the first transition series has yielded some useful electrochemical regularities that provide additional support for the site of oxidation in metalloporphyrins.⁴⁷
 - 1. The differences in potential between the first oxidation and reduction of the porphyrin ring are, with two exceptions (Mn, Mo), constant:

$$E_{ox}$$
 - E_{red} = 2.25 ± 0.15V

2. The differences in potential between the removal of the first and second electron are also constant:

$$E^{2}_{OX}$$
 - E^{1}_{OX} = 0.29 ± 0.05V

These empirical rules together with chemical and spectroscopic data may be used to correlate various redox steps of a metalloporphyrin system with metal vs. porphyrin-centered reactions. The more interesting of these two electrochemical rules is certainly the first one: regardless of any intermediate change in the oxidation states of the central metals, the difference between the highest occupied and lowest unoccupied orbitals is a constant 2.2 eV in the ground state. With stable divalent metals, linear correlations between redox potentials and metal electronegativities have been demonstrated. The fact that a rise in oxidation potential is accompanied by a lowering of the reduction potential clearly points to the inductive effects of the metals on the porphyrin π -system.

Voltammetric waves corresponding to potentials which are far away from these patterns are expected to be associated with reactions of the central metal ions.

Other Physicochemical Methods: In addition to the more conventional methods of investigation described above, metalloporphyrin redox reactions have recently been studied by other techniques including NMR, IR, and resonance Raman (RR) spectroscopy. The utility of these methods will be briefly discussed in the following sections; however, RR vibrational analysis of macrocycle-based oxidized hemoprotein models represents the main subject of this dissertation and will be covered in detail in the following chapters.

5. Proton NMR of the Metalloporphyrin π-cation Radicals: The salient features of ${}^2A_{2u}$ porphyrin π-cation radical are distribution of a substantial amount of positive spin density at the meso carbons and the pyrrole nitrogens, while the radical orbital in ${}^2A_{1u}$ cations has a node at these atoms (D_{4h} symmetry). Since the isotopic shift of the meso proton is proportional to the meso carbon spin density according to the McConnell equation, the typical ${}^2A_{2u}$ radical is expected to induce a large upfield contact shift for the meso proton whereas the ${}^2A_{1u}$ radical should exhibit a downfield bias. In the TPP complexes, the π-cation radical character, described as an a_{2u} radical type, is strongly implicated by a large upfield and downfield spread of the phenyl proton signal, Table 3. The most striking difference between high-spin and low-spin iron(III) TPP radical is the fact that the signs of phenyl resonances are

reversed for the two species. Thus, phenyl ortho- and para-proton signals are far downfield for the high-spin chloroiron(III) species, Table 4; but, shifts of the same magnitude, but upfield, are seen for the bisimidazole complex, Table 5. No description is offered for this reversal phenomenon; however, it is suggested that the phenyl shift pattern of the high-spin iron(III) porphyrin radical is the exceptional case and that the pattern for the low-spin iron(III) radical parallels the shift pattern of several other recently identified MP+• (e.g., CuTPP+•, Table 3). A shift of the OEPFeCl methine protons upon oxidation, Table 4, is consistent with the expected shift direction of known a_{1u} radicals, also demonstrated by CuOEP+• ClO₄-, Table 3.

Another interesting observation made by Morishima and coworkers is concerned with the non-Curie law behavior of the temperature dependence of meso-D resonance shift in $Co^{III}OEP+\cdot 2X^-$ (where $X = Br^-,ClO_4^-$). They interpreted this behavior in terms of thermal equilibrium between $^2A_{1u}$ and $^2A_{2u}$ states. If we assume as they suggested, that the a_{1u} orbital possess slightly higher energy than the a_{2u} orbital in biological-type porphyrins, the thermal mixing of the $^2A_{2u}$ state increases with increasing temperature to afford more positive spin density at the meso positions, and eventually inducing more upfield isotropic shift.

6. IR of Metalloporphyrin π -cation Radicals. This method provides a diagnostic tool for detecting porphyrin π -cation radical character, as was first reported by Shimomura and Goff.⁵² For the TPP radical complexes, an intense new band appears in the 1280 cm⁻¹ region. Likewise, oxidized

Table 1 Process and Deuteron NMR Chemical Shifts for Conner and Silver Pershvers and Their One-Electron Oxidation Products*

perphyria	a-phonyl	m-phenyl	p-phonyl	8-pyrrale	mass	ring -CH ₁ -	ring -CH,	ethyl -CH
(TPP)Ag ³	×	7.65 (?)	7.77 (?)	×				
(ETIO)AC					×	×	×	2.31 (61)
(OEP)As					×	×		2.32 (56)
OEP-J_JAC					-15.1 (674)	17.3 (317)		
(TPP-J.)ALICIO,				9.65 (135)	•			
(OEP-J-)ALICIO				(9.9 (84)	4.39 (35)		
TTP)Cu'	7.48 (144)	7.30 (32)	2.52 (107	×	• •			
3.4.5-(OCH,),TPP)Cud	4.9 (274)	3.86 (32)	3.98 (17)4	×				
TPP)Cu'	× (0.11)	7.48 (35)	7.62 (39)	×				
TPP-d ₄)C ₄				41 (1150)				
(TPP-4)CalCIO				13.4 (177)				
(TPP-J_)CulCIO	-4.90 (24)	15.8 (23)	-1.01 (37)					
OEPIC"		1010 (00)			×	11.5 (1275)		1.88 (49)
OEP-JWCJ					-4.2 (240)	11.5 (85)		
(OEP-Ja)CulCiO,					→.I (230)	17.1 (122)		
ETIOIC"					×	11.1 (1000)	6.4 (303)	1.86 (39)
ETIO-d ₁₄)Cu'					-6.2 (205)	11.3 (66)	6.5 (19)	
(ETIO-4,,)CulCIO,					-10 (400)	12.7 (150)	12.7 (150)	

^aAll spectra were obtained at 25°C and chemical shift values are referenced to Me₄Si. Line widths, in parentheses, are given in Hz, "X" entries indicate signals not detected due to large line width and/or overlap with other signals. ^bCDCl₃ solvent. ^cCH₂Cl₂ solvent. ^dCD₂Cl₂ solvent. ^ep-CH₃ signal. ^fm-OCH₃ signal. 8p-OCH₃ signal. (From Ref. 39.)

Table 4. Proton NMR Spectra of Monomeric Iron Porphyrins

pyrrole	ortho	meta	para	CIL
79.4	-6	13.3,	6.35	
66.1	37.6, 34.4	-12.4	29.5	
79.6	→	12.8,		5.21
		-9.8 (125)*		-5.7 (57)*
58.5	47.3	-9.2		-4.8
CI	н,	CH,	me	20
		6.64 3.16	-5	
	79.4 66.1 79.6 59.9 (170) ⁶ 58.5 C1	66.1 37.6, 34.4	79.4 ~6 13.3, 12.2 66.1 37.6, -12.4 34.4 79.6 ~6 12.8, 11.9 59.9 48.1 -9.8 (170) ⁶ (277) ⁶ (125) ⁶ 58.5 47.3 -9.2 CH ₁ CH ₁ 43.1, 39.5 6.64	79.4 -6 13.3, 6.35 12.2 66.1 37.6, -12.4 29.5 34.4 79.6 -6 12.8, 11.9 59.9 48.1 -9.8 (170) ⁶ (277) ⁶ (125) ⁶ 58.5 47.3 -9.2 CH ₁ CH ₂ me 43.1, 39.5 6.64 -5

^aExcept as noted oxidized species in CD₂Cl₂ solvent, others in CDCl₃ solvent, iron porphyrin ~ 10 mM, 26°C, Me₄Si reference. ^bLine widths at half height. ^cCD,CN solvent. ^d30°C. ^e20°C. (From Ref. 49.)

Table 5. Proton NMR Resonances for Bis(imidazole)iron(III) Porphyrin Radicals®

proton	TPP- (p-OCH,)b	TPP	ET104	
pyrrole o-phenyl	-32.7 -36.3	-40.1 -31.7	-40.4	
m-phenyl p-phenyl	24.8	30.4 -22.1	26.7	
ρ -OCH, σ -OCH,	12.9		9.5 1 2.8	
ring CH, ring CH,			\$1.7	50.4 133.1

^aCD₂Cl₂ solvent, 0.01 M iron porphyrin, 0.5 equivalent of imidazole, referenced to (CH₃)₄Si; downfield shifts are given positive sign. ^b-38°C. ^c-30°C, 1.0 equivalent imidazole present. ^d-51°C; ethyl-CH₃ groups were obscured by the solvent signal; the meso proton signal was not detected. (From Ref. 50.)

OEP radicals display a diagnostic band in the 1550 cm⁻¹ region. Other workers⁵³ have criticized the use of this band as a diagnostic criterion, and produce evidence suggesting that it could arise from the trapped chlorocarbon solvent molecules in the crystalline cation radicals. Hinman and coworkers have recently studied the cation radicals of several metallotetraphenylporphyrins and concluded that the formation of the π -cation radical results in two characteristic absorbance decreases near 1485 and 1600 cm⁻¹, and five characteristic absorbance increases near 1005, 1225, 1285, 1350, and 1415 cm⁻¹.54 Investigation of the cation radicals of OEP complexes was also recently carried out by Itoh and coworkers.⁵⁵ The tentative assignments of infrared bands of these radicals indicate frequency shift patterns relative to the unoxidized molecules that can be used for determining the ground electronic states of the π -cation radicals.

7. Resonance Raman. The application of RR spectroscopy to biological systems is an area of intense activity. RR spectroscopy is potentially able to furnish information about a molecule and its environment under experimental conditions which are not favorable to classical vibrational spectroscopy (low concentration, complex media, aqueous solution). Due to the phenomenon of resonance enhancement, specific parts of complicated molecules (e.g., hemoproteins) may be probed without interference from other parts of the molecule or from the solvent. The utility of this technique as a structural probe of the chromophore in hemoproteins has stimulated studies on protein-free metalloporphyrins,

yielding a great deal of information about structural, spectroscopic and physical properties. Sea Laser excitation into porphyrin Soret or visible bands enhances the scattered intensity by 10^3 - 10^4 and provide selective excitation of porphyrin vibrational modes. Empirical correlations between the positions of Raman lines and metal oxidation, ligation and spin state and the core size (center-to-nitrogen) distances exemplify some of the information accessible by RR spectroscopy. Seb Identification of peripheral substituents and the dependence of the depolarization ratio $\rho = \frac{LL}{I \mid I}$ of certain lines as a function of the wavelength of incident radiation is interpreted as evidence for electronic symmetry reduction, i.e., $CuOEP(D_{4h}) \rightarrow CuOEC(C_{2v})$.

The dominant RR bands in the 1000 - 1700 cm⁻¹ region correspond to the in-plane stretching of C-C, C-N partial double bonds and the bending of C-H bonds. At low frequencies, < 1000 cm⁻¹, the RR spectra are dominated by out-of-plane modes of planar MP, which correspond to the bending of the in-plane bonds, as well as by modes that involve the central metal. Experimentally, it has been found that an intense band at ~ 1360 cm⁻¹, for pyrrole-substituted MPs, is sensitive to the metal oxidation state. This band, which is commonly referred to as the "oxidation-state marker, v4" corresponds to the breathing mode of C-N bonds. Shifts to higher frequency in this line result from lower π -electron density back-donation to the porphyrin $e_g(\pi^*)$ antibonding orbitals (e.g., Fe^{III} \rightarrow Fe^{IV}).58 Essentially, all the porphyrin skeletal modes in the high-frequency region (1450 - 1700 cm⁻¹) show a negative

linear correlation with core size for planar porphyrins. Roughly, a decrease in frequency of 1 cm⁻¹ in a core size line represent an increase in core size of $\sim 0.002 \text{\AA}.56a$ Certain porphyrin modes in this region show sensitivity to the metal spin-state. This is especially true of the band at $\sim 1580 \text{ cm}^{-1} \text{ (v}_{19}, \text{C}_{a}\text{C}_{m})$ which is relatively insensitive to the metal oxidation state. Other spin-state marker bands appear at $\sim 1490 \text{ (v}_{3}, \text{C}_{a}\text{C}_{m})$ and $\sim 1630 \text{ cm}^{-1} \text{ (v}_{10}, \text{C}_{a}\text{C}_{m})$. For example, in high-spin iron(III) porphyrin complex, electrons populate the antibonding orbitals (e.g., d_x2-y2) and the lengthened bonds are accompanied by the expansion of the porphyrin core, followed by the decrease in the force constants of roughly 75% of the Raman active vibrational modes. Doming and ruffling of the porphyrin ring also alters these frequencies, but their influence is less important than the dominant core size effect.

Upon removal of an electron from the highest filled porphyrin π -bonding orbitals, a_{1u} or a_{2u} , we find that the frequencies of the stretching modes with predominantly C_bC_b character increase, whereas those with C_aC_m and C_aN character decrease in the RR spectra of the cation radicals relative to the neutral metalloporphyrins, Figure 8. These structural trends seem to be essentially insensitive to ${}^2A_{2u}$ vs. ${}^2A_{1u}$ radical designation, at least for the cation radicals studied here, Figure 10.59

An Overview of this Thesis

For a complete and systematic investigation of redox, vibrational, electronic and structural properties of metalloporphyrin π -cation radicals, we begin by addressing the oxidation products of cobalt porphyrins in Chapter 2. The versatility of cobalt(II) porphyrin system

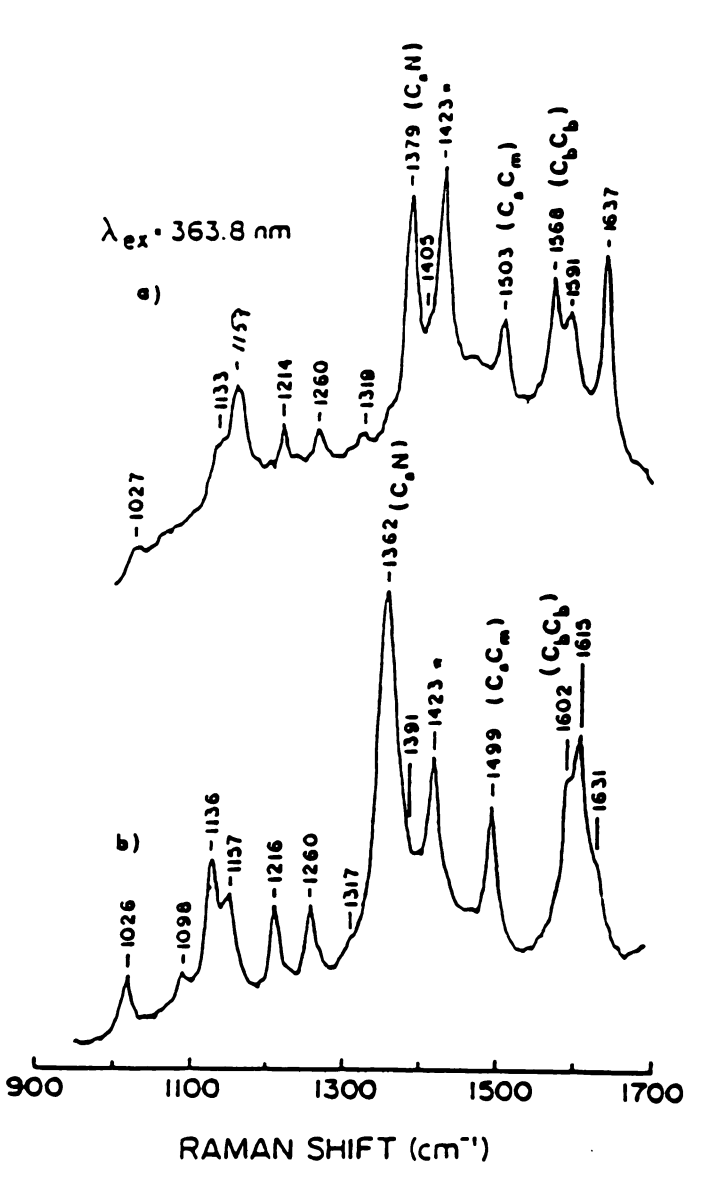


Figure 10. RR spectra of (a) CuOEP; (b) CuOEP+-ClO₄-. CH₂Cl₂ bands are marked with an *. CW laser power 20-35 mW.

allows us to compare the RR spectral characteristics of metal- vs. porphyrin- centered oxidized species all with the same metalloporphyrin complex. Additionally, cobalt spin-state remains constant upon variation in the ring oxidation and metal ligation states. Thus, the effects of ring-centered oxidation may be highlighted in the absence of any complication from changes in the spin-state, the contribution of which is significant in the RR spectra of metalloporphyrins in the high-frequency region (1450 - 1700 cm⁻¹). The oxidation products of biologically-relevant iron porphyrins will be covered in Chapter 3. Characterization of oxidized iron porphyrins include a wider range of variables owing to several oxidation, ligation and spin states that are available to iron atom.

As an appropriate extension of our metalloporphyrin π -cation radical interest, we present, in Chapter 4, some preliminary results of the RR vibrational analysis of metallochlorin π -cation radicals. This study aims to develop a better understanding of the photosynthetic primary charge-separating event involving oxidized chlorophylls. Relative to the Raman spectra of metalloporphyrins, those of metallochlorins are considerably more complex owing to the symmetry reduction, to increased macrocycle conformational flexibility and to the likelihood of changes in normal mode composition of the chlorin macrocycle vibrations compared to those of the analogous porphyrin.

Preliminary results and future perspectives on two topics that are still being pursued in our laboratories will be discussed in Chapters 5 and 6. Respectively, they are:

- 1. Novel β -pyrrolic substitution reactions of tetraperfluorophenyl porphyrin and
- 2. Metal-axial ligand vibrations in metalloporphyrins, their π -cation radicals and other related systems a preliminary vibrational study in the low-frequency region (< 1,000 cm⁻¹).

these topics will be presented in this chapter.

REFERENCES

- 1. Reid, L. S.; Mauk, M. R.; Mauk, A. G., J. Am. Chem. Soc. 1984, <u>182</u>.
- 2. Suslick, K. S.; Reinert, T. J., J. Chem. Ed. 1985, <u>62</u>, 974.
- 3. (a) Dawson, J. H.; Sono, M. Chem. Rev. 1987, 1255. (b) Hewson, W. D.; Hager, L. P. In "The Porphyrins," Vol. 7, Delphin, D. Ed., Academic Press, New York, 1979, Chapter 6.
- 4. Renger, G., Angew. Chem. Int. Ed. Engl. 1987, 26, 643.
- 5. Chang, C. K.; Fajer, J., J. Am. Chem. Soc. 1980, <u>102</u>, 848.
- 6. Johnson, E. C.; Neim, T.; Dolphin, D., Can. J. Chem. 1978, <u>56</u>, 1381.
- 7. Frew, J. E.; Jones, P., Adv. Inorg. Bioinorg. Mech. 1984, 3, 175.
- 8. Hanson, L. K.; Chang, C. K.; Davis, M. S.; Fajer, J., J. Am. Chem. Soc. 1981, 103, 663.
- 9. (a) O'Malley, P. J.; Babcock, G. T., Proc. Nat. Acad. Sci. USA 1984, 81, 1098.
 (b) Chang, C. K.; Kuo, M. -S., J. Am. Chem. Soc. 1979, 101, 3413.
- 10. Fuhrhop, J.-H.; Mauzerall, D., J. Am. Chem. Soc. 1969, 91, 4174.
- 11. Wolberg, A.; Manassen, J., J. Am. Chem. Soc. **1970**, <u>92</u>, 2982.
- 12. Hambright, P.; Bearden, A. In "Porphyrins and Metalloporphyrins," Smith, K. M., Ed., Elsevier: New York, 1975, Chapter 12.
- 13. Phillippi, M. A.; Goff, H. M., J. Am. Chem. Soc. 1982, <u>104</u>, 6026.
- 14. Commoner, B.; Townsend, J.; Pake, G. Nature 1954, 174, 689.
- 15. Gibson, J. F.; Ingram, D. J. E., Nature **1956**, <u>178</u>, 871.

- 16. (a) Dolphin, D.; Muljiani, Z.; Rousseau, K.; Borg, D. C.; Fajer, J.; Felton, R. H., Ann. N.Y. Acad. Sci. 1973, 206, 177.
 - (b) Spaulding, L. D.; Eller, D. G.; Bertrand, J. A.; Felton, R. H., J. Am. Chem. Soc. 1974, 96, 982.
- 17. Gouterman, M., J. Mol. Spectrosc. 1961, 6, 138.
- 18. Edwards, W. D.; Zerner, M. C., Can. J. Chem. 1985, <u>63</u>, 1763.
- 19. Fajer, J.; Davis, M. S. In "The Porphyrins," Vol. 4, Dolphin, D., Ed., Academic Press: New York, 1979, Chapter 4.
- 20. Fajer, J.; Borg, D. C.; Ferman, A.; Felton, R. H.; Vegh, L.; Dolphin, D., Ann. N.Y. Acad. Sci. 1973, 206, 349.
- 21. (a) Carnieri, N.; Harriman, A., Inorg. Chim. Acta 1982, 62, 103.
 - (b) Fajer, J.; Borg, D. C.; Forman, A.; Dolphin, D.; Felton, R. H., J. Am. Chem. Soc. 1970, 92, 3451.
- 22. Gouterman, M., J. Chem. Phys. 1959, 30, 1139.
- 23. Castro, C. E. In "The Porphyrins," Vol. 5, Dolphin, D., Ed., Academic Press: New York, 1978, Chapter 1.
- 24. Balch, A. L.; Latos-Grazynski, L.; Renner, M. W., J. Am. Chem. Soc. 1985, 107, 2983.
- 25. Reid, L. S.; Lim, A. R.; Mauk, A. G., J. Am. Chem. Soc. 1986, 108, 8197.
- 26. Fuhrhop, J. -H., Struc. Bonding (Berlin) **1974**, <u>18</u>, 1.
- 27. (a) Brown, G. M.; Hopf, F. R.; Meyer, T. J.; Whitten, D. G., J. Am. Chem. Soc., 1975, 97, 5385.
 - (b) Balch, A. L.; Renner, M. W., J. Am. Chem. Soc. 1986, <u>108</u>, 2603.
- 28. Spiro, T. G.; Stong, J. D.; Stein, P., J. Am. Chem. Soc. 1979, <u>101</u>, 2648.
- 29. Teraoka, J.; Kitagawa, T., J. Phys. Chem. 1980, 84, 1928.
- 30. Dolphin, D.; Felton, R. H.; Borg, D. C.; Fajer, J., J. Am. Chem. Soc. 1979, 92, 743.
- 31. Kadish, K. M.; Lin, X. Q.; Han, B. C., Inorg. Chem. 1987, 26, 4161.
- 32. Salehi, A.; Oertling, W. A.; Babcock, G. T.; Chang, C. K., J. Am. Chem. Soc. 1986, 108, 5630.

- 33. Dolphin, D.; Niem, t.; Felton, R. H.; Fujita, I., J. Am. Chem. Soc. **1975**, <u>97</u>, 5290.
- 34. Mashiko, T.; Kastner, M. E.; Spartalian, K.; Scheidt, W. R.; Reed, C. A., J. Am. Chem. Soc. **1978**, <u>100</u>, 6354.
- 35. (a) Huang, Y.-P.; Kassner, R. J., J. Am. Chem. Soc. 1979, <u>101</u>, 5807.
 - (b) Scheidt, W. R.; Geiger, D. K.; Haller, K. J., J. Am. Chem. Soc. 1982, <u>104</u>, 495.
- 36. Hill, A. O.; Skyte, P. D.; Buchler, J. W.; Leuken, H.; Tonn, M.; Gregson, A. K.; Pellizer, G., J. C. S. Chem. Comm. 1979, 151.
- 37. Spellane, P. J.; Gouterman, M.; Antipas, A.; Kim, S.; Liu, Y. C., Inorg. Chem. 1980, 19, 386.
- 38. Perrin, M. H.; Gouterman, M.; Perrin, C. L., J. Chem. Phys. 1969, 50, 4137.
- 39. Godziela, G. M.; Goff, H. M., J. Am. Chem. Soc. 1986, 108, 2237.
- 40. Kadish, K.; Davis, D. G.; Fuhrhop, J. H., Angew. Chem. Int. Ed. Engl. 1972, 11, 1014.
- 41. Ichimori, K.; Ohya-Nishiguchi, H.; Hirota, N.; Yamamoto, K., Bull. Chem. Soc. JPn. 1985, 58, 623.
- 42. Konishi, S.; Hoshino, M.; Imamura, M., J. Am. Chem. Soc. 1982, <u>104</u>, 2057.
- 43. Hambright, W. P.; Thorpe, A. N.; Alexander, C. C., J. Inorg. Nucl. Chem. **1968**, <u>30</u>, 3139.
- 44. Evans, D. F., J. Chem. Soc. 1959, 2003.
- 45. Erler, B. S.; Scholz, W. F.; Lee, Y. J.; Scheidt, W. R.; Reed, C. A., J. Am. Chem. Soc. **1987**, <u>109</u>, 2644.
- 46. Scholz, W. F.; Reed, C. A.; Lee, Y. J.; Scheidt, W. R.; Lang, G., J. Am. Chem. Soc. **1982**, <u>104</u>, 6791.
- 47. Kadish, K. M., Prog. Inorg. Chem. 1986, 34, 435.
- 48. McConnell, H. M., Chestnut, D. B., J. Chem. Phys. 1958, 28, 107.
- 49. Phillippi, M. A.; Goff, H. M., J. Am. Chem. Soc. 1982, 104, 6026.
- 50. Goff, H. M.; Phillippi, M. A., J. Am. Chem. Soc. 1983, 105, 7567.

- 51. Morishima, I.; Takamuki, Y.; Shiro, Y., J. Am. Chem. Soc. 1984, 106, 7666.
- 52. Shimomura, E. T.; Phillippi, M. A.; Goff, H. M., J. Am. Chem. Soc. **1981**, 103, 6778.
- 53. Spreer, L. O.; Maliyackel, A. C.; Holbrook, S.; Otvos, J. W.; Calvin, M., J. Am. Chem. Soc. 1986, 108, 1949.
- 54. Hinman, A. S.; Pavelich, B. J.; McGarty, K., Can. J. Chem., submitted.
- 55. Itoh, K.; Nakahasi, K.; Toeda, H., J. Phys. Chem. 1988, 92, 1464.
- 56. (a) Parthasarathi, N.; Hansen, C.; Yamaguchi, s.; Spiro, T. g., J. Am. Chem. Soc. 1987, 109, 3865.
 - (b) Kitagawa, T.; Ozaki, Y., Struct. Bonding (Berlin) 1987, <u>64</u>, 71.
- 57. Andersson, L. A.; Loehr, T. M.; Chang, C. K.; Mauk, A. G., J. Am. Chem. Soc. 1985, 107, 182.
- 58. Spiro, T. G., Israel J. Chem. 1981, <u>21</u>, 81.
- 59. Oertling, W. A.; Salehi, A.; Chung, Y. C.; Leroi, G. E.; Chang, C. K.; Babcock, G. T., J. Phys. Chem. **1987**, <u>91</u>, 5887.

CHAPTER II

PREPARATION METHODS AND SPECTROSCOPIC PROPERTIES OF OXIDIZED COBALT PORPHYRINS

In contrast to iron and copper, which dominate the scene of transition metal biochemistry and are components of a variety of metalloproteins, cobalt occupies a relatively modest position in biology. Although Co(II) porphyrins do not occur naturally, the related vitamin B₁₂ corrin system catalyzes molecular rearrangements via the Co(II) oxidation state in at least some of its enzymatic reactions. 1 Most of the literature on cobalt(II) in biochemistry concerns its effects in various metal-activated enzyme systems.² Many of the typical Mg^{2+} , Mn^{2+} , Fe^{2+} and Zn^{2+} activated metalloenzymes can work with Co²⁺ at a reasonable rate. A general observation seems to be that cobalt generates catalytic activity, often approaching, and sometimes exceeding that of the native enzyme.³ Thus, owing to its spectroscopic and magnetic properties, substitution of Co²⁺ for the native metal is considered to be a useful probe of the metalloenzyme active site. The utility of the Co^{2+} ion is also well-documented in hemoproteins and their synthetic analogs in which cobalt substitution has provided additional information for a better understanding of spectroscopic, structural and reactivity properties of these metalloproteins. For example, Co(II)-reconstituted hemoglobins and myoglobin have been extensively investigated in an attempt to obtain further

information on heme-heme interations.⁴ Hoffman and coworkers have shown that cobalt hemoglobin displays a reversible and cooperative uptake of oxygen that is qualitatively similar to that of hemoglobin.⁵ Cobalt porphyrins have also been applied in disproportionation reactions of hydrogen peroxide⁶, which in vivo is prompted by catalase, as "shift reagents" to determine the stereochemistry of molecules with which they associate^{7a}, and as the catalyst for various redox reactions of the axial ligands.^{7b}

The study of the oxidation products of cobalt porphyrins is also of great interest. The versatility of the cobalt porphyrin system allows us to compare metal vs. porphyrin centered oxidation products for the one-electron case, and $^2A_{2u}$ vs. $^2A_{1u}$ radicals for the two-electron case, all with the same metalloporphyrin species. The latter species are of principal interest owing to their relevance to the Compound I type enzyme intermediates. Additionally, cobalt exhibits only one spin-state (S = 1/2) and this can avoid complications from changes in spin-state upon oxidation, a phenomenon observed in iron porphyrins.

It is the aim of this chapter to present first the preparation of oxidized cobalt porphyrins, followed by their spectroscopic characterization by means of UV-vis, ESR and magnetic susceptibility, IR and particularly RR technique to highlight the vibrational properties of porphyrin π -cation radicals. As noted previously, the pyrrole-substituted porphyrins; i.e., OEP, will be utilized in this study.

Preparative Methods. OEP was synthesized according to the published method.¹⁰ The meso-tetradeuteration of OEP was carried out in D₂SO₄-D₂O as described by Bonnett and coworkers.¹¹ CH₂Cl₂, freshly distilled from CaH₂, was used as a solvent for all spectroscopic studies unless otherwise specified.

added a three-fold molar excess of cobaltous chloride-sodium acetate (1:1) dissolved in minimum amount of methanol. The progress of the reaction was followed spectrophotometrically until quantitative metallation was achieved. The crude reaction mixture was first evaporated to dryness. The residue was redissolved in minimum amount of dichloromethane and was washed successively with dilute acid (once) and with water (several times), to remove excess inorganic salts, and dried over anhydrous sodium sulfate. The dichloromethane solution was evaporated to dryness and the resulting fluffy CoOEP(1) solids were collected. Alternatively, the Co(II) derivative may readily be obtained from the reaction of free base porphyrin with cobaltous acetate (10X molar excess) in refluxing acetic acid¹² with a similar workup procedure as described above.

COIIIOEPX⁻ 2: Method 1. For X⁻ = Br, Co^{II}OEP (30 mg) was suspended in methanol (30 ml) containing ~ 3 ml of 48% hydrobromic acid. ¹³ When the suspension was stirred at room temperature for several hours, the solution gradually changed to a deep red color, until the red crystals were precipitated. The resulting crystalline precipitates where collected, washed subsequently with water, methanol, petroleum ether and dried at room temperature. Yield: > 90%.

Method 2. Co^{II}OEP (50 mg) was dissolved in 10 ml of chloroform, and to this solution was added 10 ml of methanol and \sim 0.2 ml of 48% hydrobromic acid. 14 The mixture was stirred at room temperature for 2 h. and then an additional 10 ml of chloroform was added. The

reaction mixture was washed with water, dried over anhydrous sodium sulfate and evaporated to dryness. Yield: > 90%.

The iodo- and chloro- derivatives may also be prepared as above by using an appropriate concentration of 57% hydriodic and 37% hydrochloric acid, respectively.

Co^{II}OEP+·X⁻ 3: This species was obtained by stirring a dry dichloromethane solution of 1 with a three-fold molar excess of solid anhydrous silver perchlorate at room temperature for about 1 h.¹⁵ The bright red solution of the neutral Co^{II}OEP turns brownish-red upon completion. The solution is then filtered and the product can be isolated by precipitation with hexane. The cobaltous porphyrin cation radical is stable only in the presence weakly coordinating ligands such as ClO₄⁻, BF₄⁻ and PF₆⁻ but not Br⁻ where the formation of bromocobaltic derivative is favored.

Co^{III}OEP+·2X⁻ 4: When X⁻ = Br⁻, a dichloromethane solution of 1 may be oxidized by means of molecular bromine. The first step, which requires ~ 0.5 moles of bromine, brings about the oxidation of 1 to 2. Further oxidation of this trivalent complex, using an additional ~ 0.5 moles of bromine gives the green cationic radical species 4. When $X^- = ClO_4^-$, this dibromide species dissolved in dichloromethane is treated with silver perchlorate 16a or, alternatively, a direct two-electron oxidation of Co^{II}OEP may be achieved in dichloromethane by using a large excess of ferric perchlorate salt. 16b

 $Co^{III}(ROH)_2OEPX^-$ 5: When R = CH₃, this complex was obtained by oxidation of 1 with $HX(X^- = ClO_4^-, Br^-)$ in dichloromethanemethanol

- (3:1). The diaquo adduct may be prepared in the same manner. Weakly coordinated methanol and water molecules are readily placed with stronger ligands such as pyridine.¹⁷
- 4 may also be prepared indirectly by titrative addition of methanol or water to a dichloromethane solution of Co^{II}OEP+·X⁻, Co^{III}OEPX⁻, and Co^{III}OEP+·2X⁻ in the order of increasing the required volume of ROH for complete conversion.¹⁸

Instrumentation: UV-vis spectra were recorded by using Shimadzu UV-160 and Cary 219 spectrophotometers. The ESR spectra were measured on a Varian E-4 spectrometer. The g-value calibration and spin quantitation were obtained by using Fremy's Salt. 15a,b Magnetic susceptibility was obtained on an SHE SQUID susceptometer at a field of 5kG. Infrared spectra of Co OEP compounds were examined as KBr disks by using a Perkin-Elmer 599-IR spectrophotometer. Raman Spectra were measured with a Spex 1877 Triplemate and OMA II electronics (Oertling et al., J. Phys. Chem. 1987, 91, 5887-5898). Laser emission at 363.8 nm was provided by a Coherent Innova 90-5. Argon Ion Laser.

2. Electronic Absorption Spectra: As described by Johnson¹⁹, the various cobalt porphyrin complexes can be differentiated by their visible spectra and changes can be followed conveniently by using a spectrophotometer.

The general pattern of a normal pyrrole-substituted metallopor-phyrin spectra is well known. ^20 A dichloromethane solution of 1 exhibits such a pattern with two moderately intense bands, the so-called α and β bands ($\epsilon \sim 10^4$ M⁻¹Cm⁻¹) at 551 and 517 nm, respectively, and the

strong Soret band at 391 nm ($\varepsilon \sim 10^5$ M⁻¹Cm⁻¹). Of the two visible bands, the α band has the higher intensity, Figure 1.

Formation of the Co(III) complex is accompanied by the red-shift of both Soret and visible peaks with respect to those in Co(II), a phenomenon pointed out by Corwin and coworkers. They suggested that this is a general trend for square planar porphyrins bonded to ligands in the octaehedral positions. The electronic spectrum is always "normal", but the ratios of the visible α and β bands, as well as the exact position of the Soret band are solvent-dependent to an exceptional degree, Figure 1. A more recent study by Wang and Hoffman²¹ support the earlier results but also demonstrates that the perturbations by the ligand not only shift the overall spectrum but also systematically change both the frequency difference between the Soret and the visible bands and the relative intensity of $\varepsilon_{\alpha}/\varepsilon_{\beta}$. Thus, the position of the α band shifts less rapidly than that of the Soret band and the individual axial ligands affect the spectra in the following order of increasing red shift and decreasing $\varepsilon_{\alpha}/\varepsilon_{\beta}$ ratios: "e-"(phantom ligand) $< H_2O < F^- < O_2^-, Im, NMeIm , OH^- < N_3^- <$ CN⁻. This is consistent with the earlier observation that the Soret and the visible bands of the Co(III) complex are displaced by ~ 20 and 9 nm, respectively, toward higher wavelength relative to the Co(II) complex and the relative intensity of the α and β bands become nearly equal.

In the optical spectrum of $Co^{II}OEP^+\cdot ClO_4$, Figure 2b, the Soret band occurs at 376 nm and is ~ 1/3 as intense as that of $Co^{II}OEP$ at 391 nm. The region between 500-700 nm is broad and featureless, similar to that of other well-characterized porphyrin π -cation radicals. The contribution of

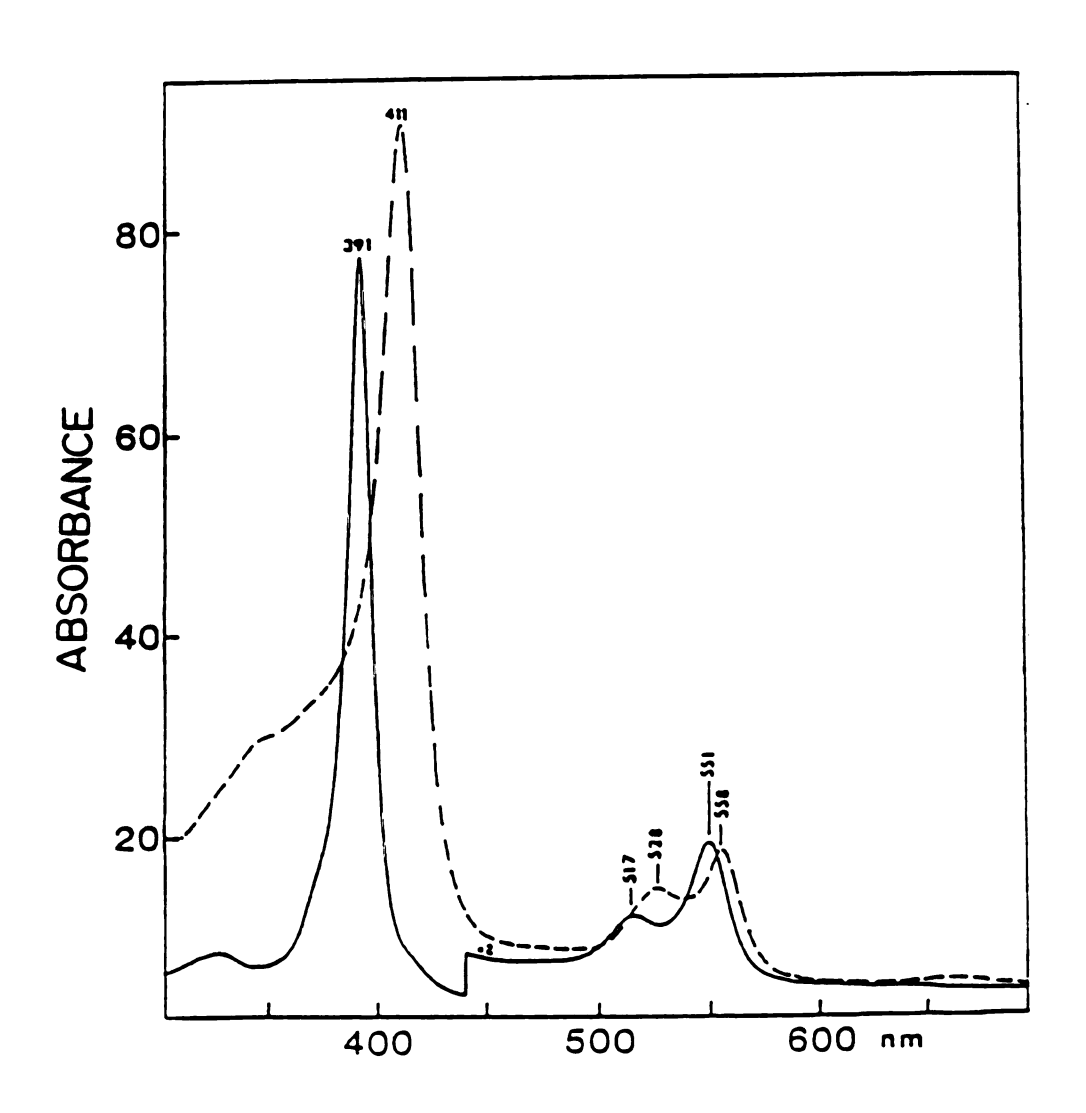


Figure 1. Visible absorption spectra of CoOEP (Soret = 391 nm) and $Co^{III}(MeOH)_2OEPBr^-$ (Soret = 411 nm) in dichloromethane.

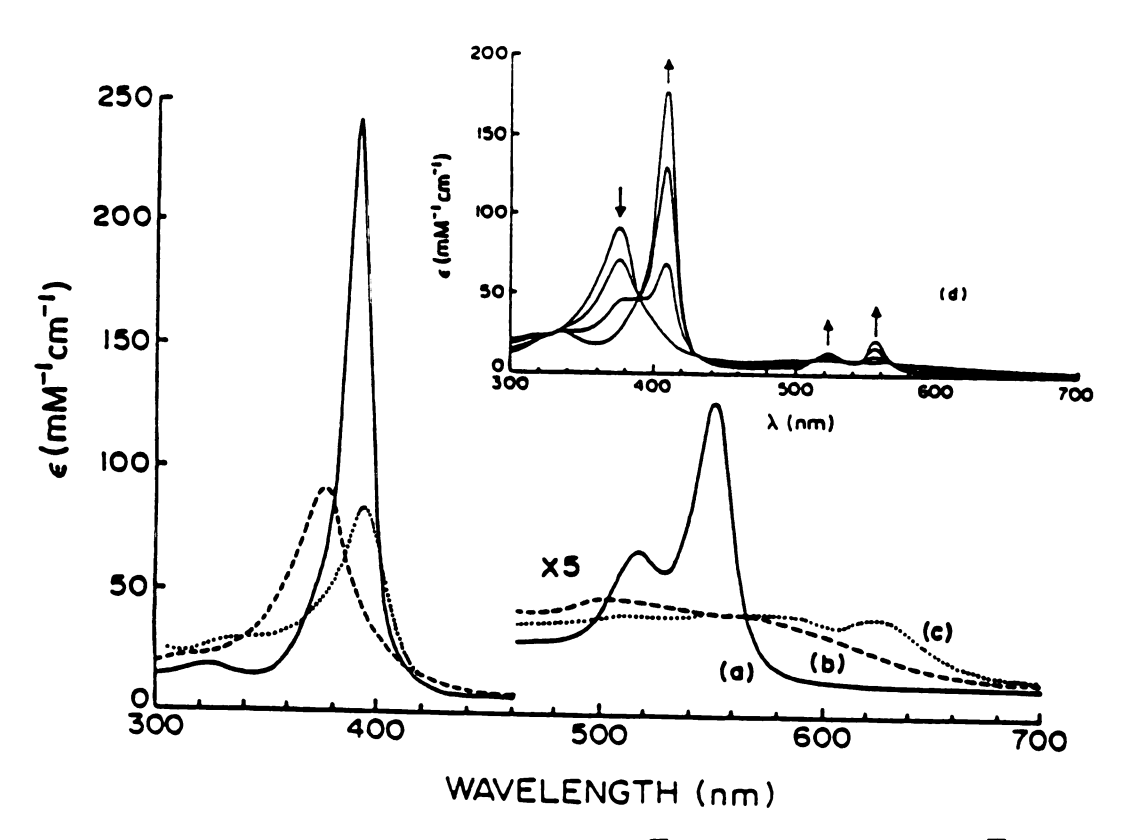


Figure 2. Electronic absorption spectra of $Co^{II}OEP$ derivatives: (a) $Co^{II}OEP(---)$; (b) $Co^{II}OEP+\cdot ClO_4^-(---)$; (c) $Co^{III}OEP+\cdot 2ClO_4^-(---)$, in CH_2Cl_2 ; (d) spectral changes on addition of methanol to a methylene chloride solution of (b) producing $Co^{III}(CH_3OH)_2OEPClO_4^-$, total methanol content < 0.01%.

3 is apparent in some previously reported optical spectra of "CoIIIOEPClO4" and CoIIIOEP+.2ClO4 as a high-energy shoulder on the Soret absorptions.²² The presence of this radical is overlooked in earlier reports, most likely because this species is only stable in anhydrous noncoordinating solvents, i.e., dichloromethane. It seems that an authentic Co^{III}OEPClO₄⁻ species, stripped of other coordinating solvents or ligands, does not exist. Titrative addition of water or methanol to a dry dichloromethane solution of Co^{II}OEP+• results in appearance of species with absorption maxima at 409, 522 and 558 nm, Figure 2d. This new species presumably is Co^{III}(MeOH)₂OEPClO₄⁻ as its optical characteristics are identical with those of typical Co(III) porphyrin spectra; i.e., the Soret peak is red-shifted by ~ 20 nm compared with that of 1 and the relative intensity of the visible bands are decreased. The effect of "wet" solvent is reversible: if the solvent of the 409 nm species is evaporated to dryness and the residue is redissolved in dry dichloromethane, the 376 nm species This is also demonstrated by a temperature study on Co^{II}OEP+· in which an increasing amount of 5 is formed as the temperature is lowered. As the 376 nm Soret band decreases in intensity, absorptions characteristic of the cobaltic complex become apparent, Figure 3. Thus, lowering the temperature of this sample has much the same effect on the absorption spectrum as the addition of methanol, presumably due to increased diaxial ligation by water with decreasing temperature. Freeze-pump-thawing to remove water vapor over the sample prior to cooling minimizes the conversion to the six-coordinate diaquo cobaltic complex, consistent with diaxial ligation by water.

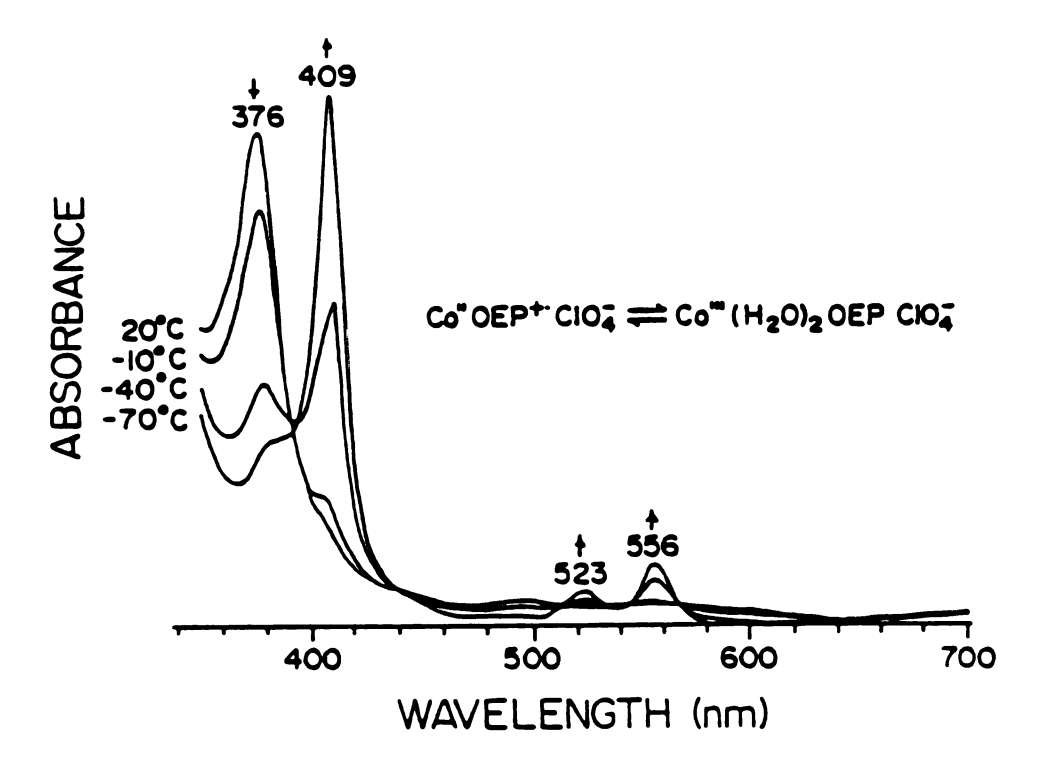


Figure 3. Electronic absorption spectra showing the conversion of $Co^{II}OEP^+\cdot ClO_4^-$ to $Co^{III}(H_2O)_2OEPClO_4^-$ as the temperature is lowered. Solvent, "dry" CH_2Cl_2 ; path length ~ 2mm (EPR tube).

The absorption spectra of $Co^{III}OEPX^{-}(X^{-} = Br^{-},Cl^{-},I^{-})$ appear to be quite unlike other Co(III) diamagnetic porphyrin spectra due to the extremely low intensity and rather large blue shift to 373 nm of the Soret band, Figure 4b. Additionally, the α band shifts to \sim 546 nm with a slight increase in intensity, while the β band envelope almost disappears. Because of the anomalous nature of these spectra, a dimeric form has been suggested for these Co(III) complexes.²² The formation of the cobaltic porphyrin as a diamagnetic low-spin Co(III) system is supported by ¹H-NMR spectrum which shows sharp lines with no paramagnetic broadening or contact shifts, Figure 5. The doubling of the α -CH₂ protons in the spectrum of Co^{III}OEPBr⁻, however, is indicative of the displacement of Co from the plane of the macrocycle. This characteristic has precedence in the ¹H-NMR spectrum of OEPFe^{III}Cl, but not in OEPFe^{III}(Im)₂⁺ in which a single α -CH₂ proton is observed.²³ The diastereotopic nature of -CH2 protons are indicative of the removal of a plane of symmetry through the methylene protons. counterion X⁻ remains bound to the metal in non-coordinating solvents, it is replaced in coordinating solvents, L, to form the species Co^{III}(L)₂OEPX⁻, Figure 4a, particularly at high concentrations.

There are also distinct changes in the absorption spectra when $Co^{II}OEP$ is oxidized by two electrons to $Co^{III}OEP+\cdot 2X^-$ (where $X^-=ClO_4^-,Br^-$), Figures 2c and 4c. The optical characteristics of these species as a function of the counterion have exemplified the two possible radical ground states and they were described in detail in Chapter 1.

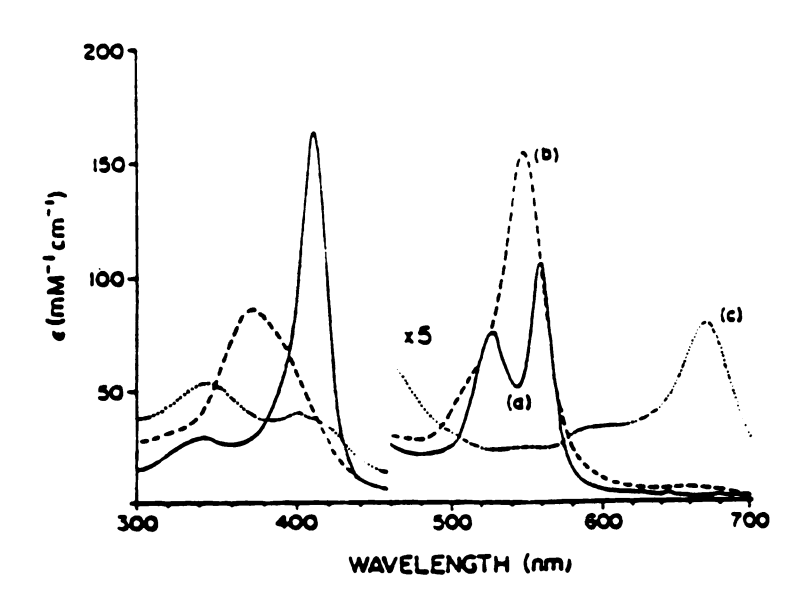


Figure 4. Electronic absorption spectra of oxidation products of CoOEP.

- (a) Co^{III}(MeOH)₂OEPBr⁻(-);
- (b) Co^{III}OEPBr⁻(---);
- (c: Co^{III}OEP+·2Br⁻(···), the small feature at 401 nm is due to 1% H₄OEP²+2Br⁻ contamination as discussed in the text. Solvent, drv CH₂Cl₂, except for (a) which contains ~ 5% methanol (MeOH).

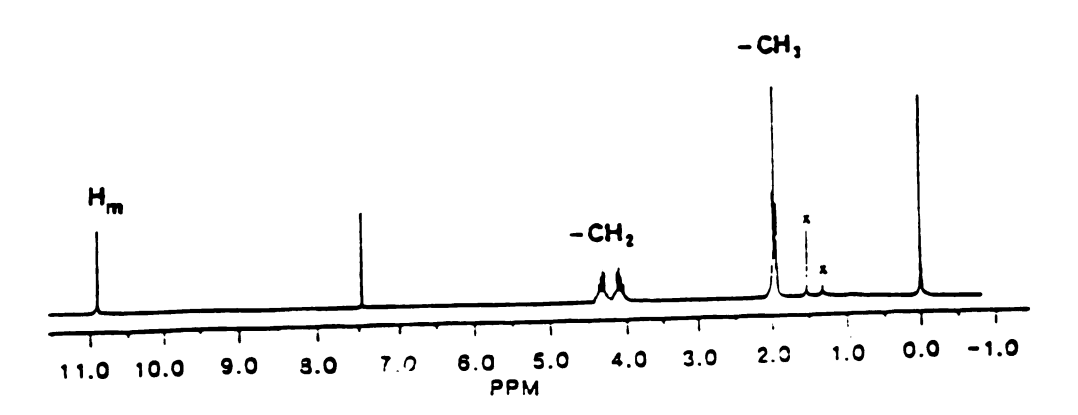


Figure 5. 250-MHZ proton NMR spectrum of Co^{III}OEPBr⁻ in CDCl₃ at 25°C. Impurity peaks labeled X.

Figure 6 shows that titrative addition of a dichloromethane solution of the diperchlorate species with methanol also results in the formation of 5.

3. **ESR and Magnetic Susceptibility.** The unpaired electron in the low-spin Co(II) porphyrins is in the d_Z^2 orbital, and since the major lobes are not directed at the porphyrin nitrogen atoms, electron delocalization into the π orbitals of the porphyrin ring is not allowed. Indeed, the observed electronic interaction is shown to arise primarily from changes in the metal-porphyrin σ bond.²⁴ The unpaired electron, however, is directly involved in axial interaction and can alter the energy separation between the d_Z^2 orbital and the d_{XZ} , d_{YZ} orbitals which, in turn, affects the ESR g-values, i.e., $g_{\perp} \equiv 1$ /energy gap. Hence the ESR parameters can be used to identify adducts of Co(II) porphyrins with π -or σ -donors or acceptors.²⁵ Hambright has reported an observed magnetic moment of 2.89 μ B for Cobalt(II) mesoporphyrin-IX dimethyl ester compared with the spin-only value of 1.73 μ B.²⁶

Co(III) porphyrin, on the other hand, shows no ESR signal, consistent with a square-planar 3d⁶ configuration. An interesting observation was recently made with cobaltic complexes which are involved in a disproportionation reaction leading to two paramagnetic species in equal proportions. Studies by ESR and NMR methods have indicated that Co^{III}TPPX⁻ is converted partially and reversibly into Co^{III}TPP+·2X⁻ and Co^{II}TPP in chlorinated hydrocarbons by thermal or light activation in aerated solution.^{27b} The mechanism of the formation of the radical is initiated by a homolytic cleavage of the Co-X

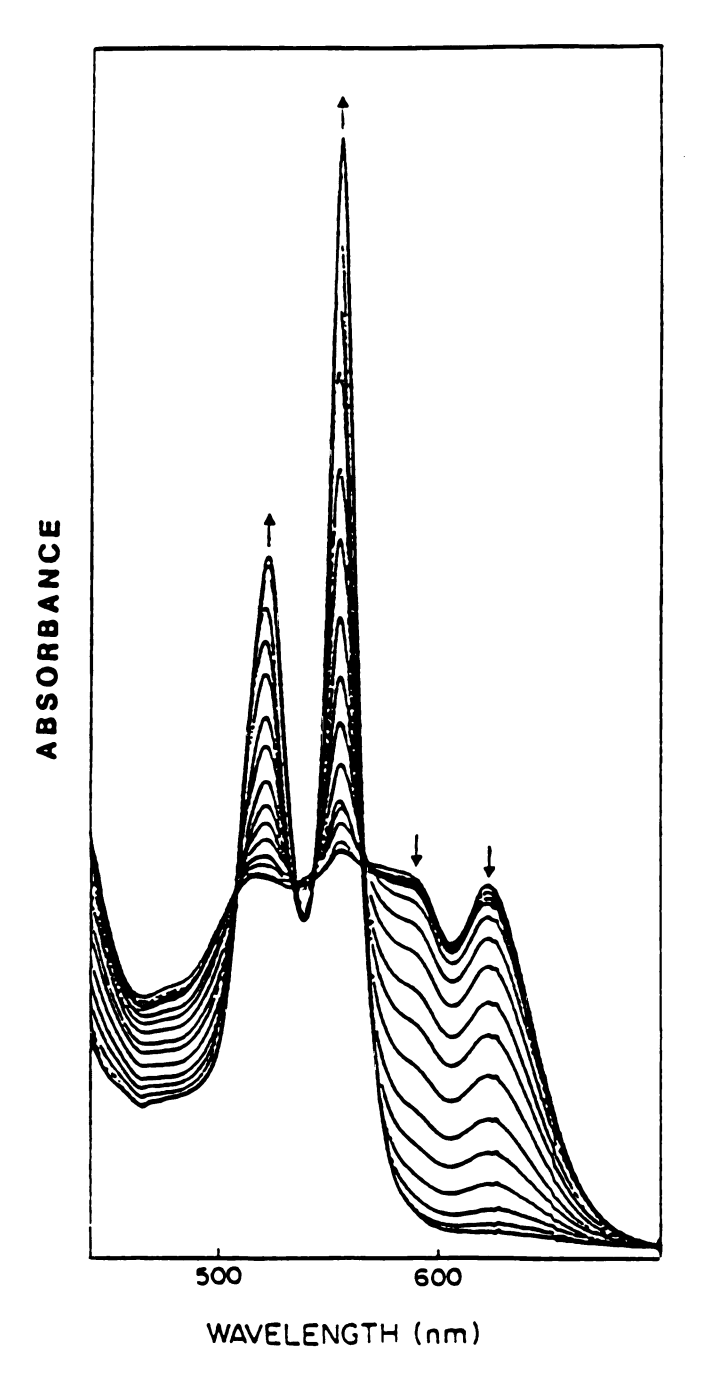


Figure 6. Spectral changes on addition of methanol to a dichloromethane solution of Co^{III}OEP+·2ClO₄⁻ in the visible region producing Co^{III}(CH₃OH)₂OEPClO₄⁻, total methanol content ~ 2%.

bond to yield Co^{II} porphyrin and chlorin atoms. The subsequent hydrogen abstraction from the chlorohydrocarbon solvent (i.e., CH₂Cl₂) produces solvent radicals which then react with oxygen molecules to form oxidant radicals; oxidant radicals may, however, be formed by photolysis of aerated dichloromethane. These radicals oxidize Co^{III}TPPX⁻ to produce the porphyrin π -cation radical, Co^{III}TPP2X⁻. The amount of π -cation radical (~ .5%) that has an $^2A_{2u}$ structure increases in the order $X = I < Br < Cl < PF_6 < ClO_4$.

 CoIIOEP+-ClO_4^- is ESR silent.¹⁵ This indicates that the unpaired electron of low-spin coII in the d_{Z^2} orbital of this radical is spin-coupled with the porphyrin unpaired electron. The magnetic susceptibility of 3 at 50°K indicates a magnetic moment of $0.215\mu_B$, most of which is likely to arise from contaminants for the following reasons:

- (a) Upon conversion by additional of methanol of 3 to 5, which is a diamagnetic d⁶ Co^{III} species, the signal persisted with the same intensity.
- (b) Increasing the initial ratio of silver perchlorate resulted in a higher signal intensity.
- (c) The intensity of residual contaminant diminished upon repeated evaporating-redissolving 3 in dichloromethane. All these observations suggest the presence of a trace amount (1-2%) of 4 in the preparation of 3.

The two-electron oxidation product, on the other hand, exhibits a room-temperature, free-electron-like ESR signal for $X^- = ClO_4^-$. As in the Co^{III}TPP+•2X⁻, spin density is transferred from the oxidized ring onto the

metal, and the ESR spectrum can be simulated by using a hyperfine-splitting constant of ~ 1.2 G for cobalt (I = 7/2); this represents a small spin density on the cobalt ion.²⁸ The dibromide complex has no ESR signal at room temperature, but as the solution is cooled, a broad signal appears that narrows with further cooling. Thus, the bromide ligand cause a significant change in the ESR spectrum. In fact, Dolphin and coworkers have shown that the bromide ions are so strongly complexed to the dication that the parent peak in the mass spectrum (m/e 749) is 1/10 as intense as the base peak (CoOEP), whereas the parent peaks of either FeOEPCl or MnOEPCl are only 1/200 as intense as the base peaks (FeOEP and MnOEP, respectively).²⁸ Thus, the absence of an ESR signal at room temperature and the broadened nature of the spectrum at low temperatures suggest a strong coupling interaction between the cobalt and the cation radical centers caused by conformational and/or electronic effects of bromide ion coordination.

Infrared Diagnostic Band of the Cation Radicals: Figure 7 shows the IR spectra of CoOEP and of its one- and two-electron radical species obtained as the KBr disk. A feature around 1550 cm-1 increases in intensity in the spectra of the cation radicals compared with that of the neutral ring compounds. This band was originally assigned by Shimomura and Goff as the diagnostic band of the radicals.²⁹ However, dispute as to the authenticity of this band has recently prompted further studies on a more quantitative basis to expand the diagnosis of the radicals to other IR bands and to establish vibrational frequency shifts upon cation radical formation.³⁰ As to the mode composi-

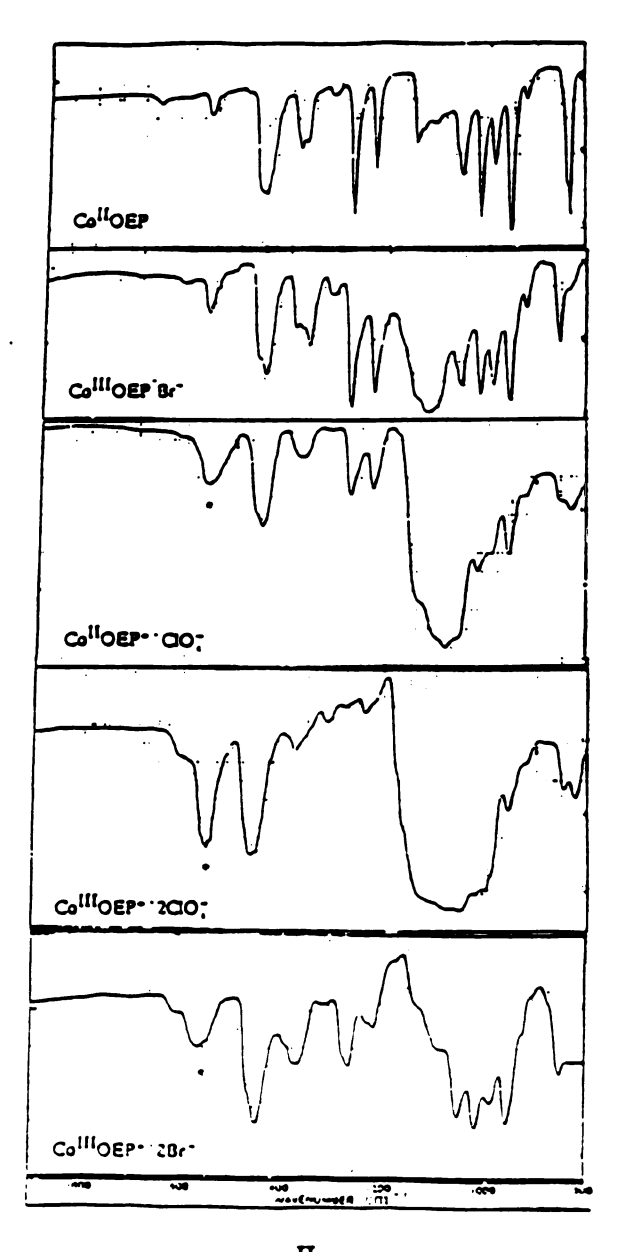


Figure 7. Infrared spectra (in KBr) of Co^{II}OEP and its oxidized products. The porphyrin cation radical diagnostic band is labeled with an asterisk.

tion of the original diagnostic band, Shimomura et al. observed at 10 cm⁻¹ decrease in the frequency of this mode upon meso-tetradeuteration of the porphyrin macrocycle. If the corresponding modes are correctly correlated in the -h₄ and -d₄ species, the isotopic shift is then consistent with the pattern observed for the vibrations that are predominantly of C_aC_m stretching character (v₃ and v₁₀) in the RR spectra of metalloporphyrin derivatives (Section).

RR Vibrational Analysis of Co^{II} OEP and its Oxidized Products-Spectral Characteristics of the Cation Radicals in the High-Frequency Region (1450-1700 cm⁻¹: Figures 8-12 show the RR spectra (1000 - 1700 cm⁻¹) obtained with near -UV excitation of various products of CoOEP oxidation. Comparison of the vibrational spectra of h₄ vs. d₄ derivatives of CoOEP, Figure 8a,b, reflects the involvement of the C_m atoms in the individual normal modes. Vibrations of C_aC_m stretching character are expected to exhibit a wavenumber decrease upon substitution of d₄ for h₄. The bands above 1450 cm⁻¹ are known to reflect porphyrin core geometry and are of principal interest to this study.

From the mode designations established by Abe et al., 31 the v₃, v₁₁, v₂ and v₁₀ modes of CoOEP are identified at 1512, 1575, 1599, and 1647 cm⁻¹, respectively, in Figure 8a. The deuterium shifts of -11 and -8 cm⁻¹ for the v₁₀(C_aC_m) and v₃ (C_aC_m) vibrations, respectively, confirm their compositional assignments. The absence of significant change in the wavenumbers of the features occurring at 1599 and 1575 cm⁻¹ in 1 is consistent with the assignment of v₂ (C_bC_b) and v₁₁ (C_bC_b) for these

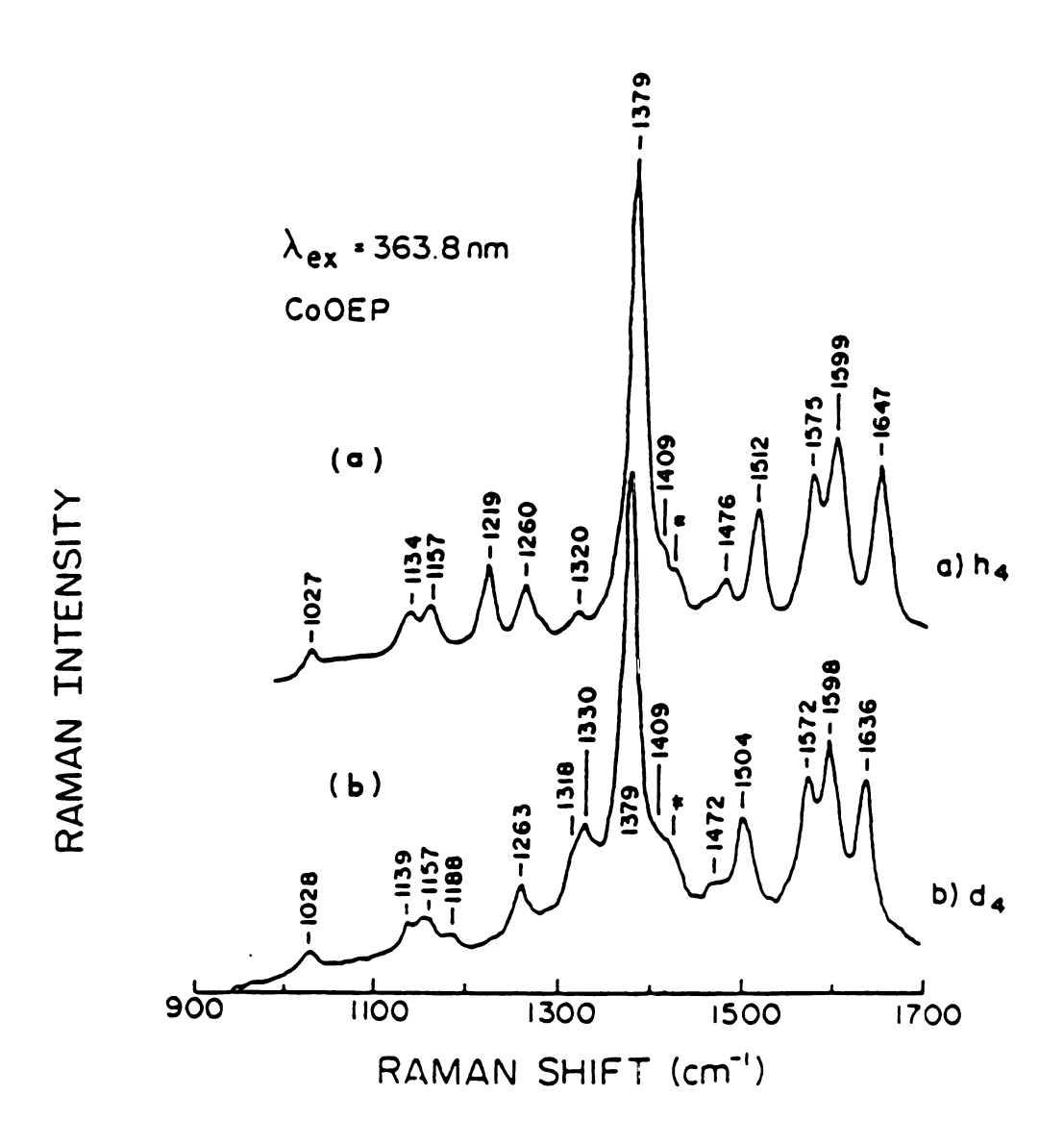


Figure 8. RR spectra of cobaltous octaethylporphyrin in CH₂Cl₂.

vibrations. The weak mode at 1476 cm⁻¹ may correspond to v_{28} (C_aC_m), also reported for NiPP (PP = protoporphyrin-IX) at 1482 cm⁻¹.³² The intense polarized oxidation-state marker band (v_4) appears at 1379 cm⁻¹ in Figure 8a and is predominantly of C_aN stretching character. The depolarization ratio, the absence of a deuterium shift, Figure 8b, and the clear spectral analogy to the other well-characterized metalloporphyrins³¹, ³² forms the basis of this assignment.

The effects of metal-centered, one-electron oxidation accompanied by axial metal ligation are demonstrated by comparing the spectra of $Co^{II}OEP$ and $Co^{III}(MeOH)_2OEPClO_4^-$ depicted in Figure 9a,b. The oxidation-state marker, v_4 , increases from 1379 to 1383 cm⁻¹, reflecting depopulation of the porphyrin π^* orbitals caused by metal oxidation.³³ There is little systematic change in frequency of modes above 1450 cm⁻¹, indicating that the core size of the porphyrin ring does not change significantly upon metal oxidation and addition of axial methanol ligands.^{32,34}

Figure 9c, d, shows the spectra of the cobaltous and cobaltic OEP+· complexes. Neglecting differences in relative intensity produced by the differences in Soret absorption, the RR spectra of 3 and 4 are essentially identical and (above 1300 cm⁻¹) radically different from those of the neutral ring compounds in Figure 9a, b. We assign the v_3 , v_{11} , v_2 and v_{10} frequencies of $Co^{II}OEP+·ClO_4-$, for example, at 1505, 1604, 1620, and 1642 cm⁻¹, respectively, the assignments of which are based upon similarity in depolarization ratio measurements and isotope data with the authentic π -cation radical $Co^{III}OEP+·2ClO_4-$, Figures 9c, d and 10.

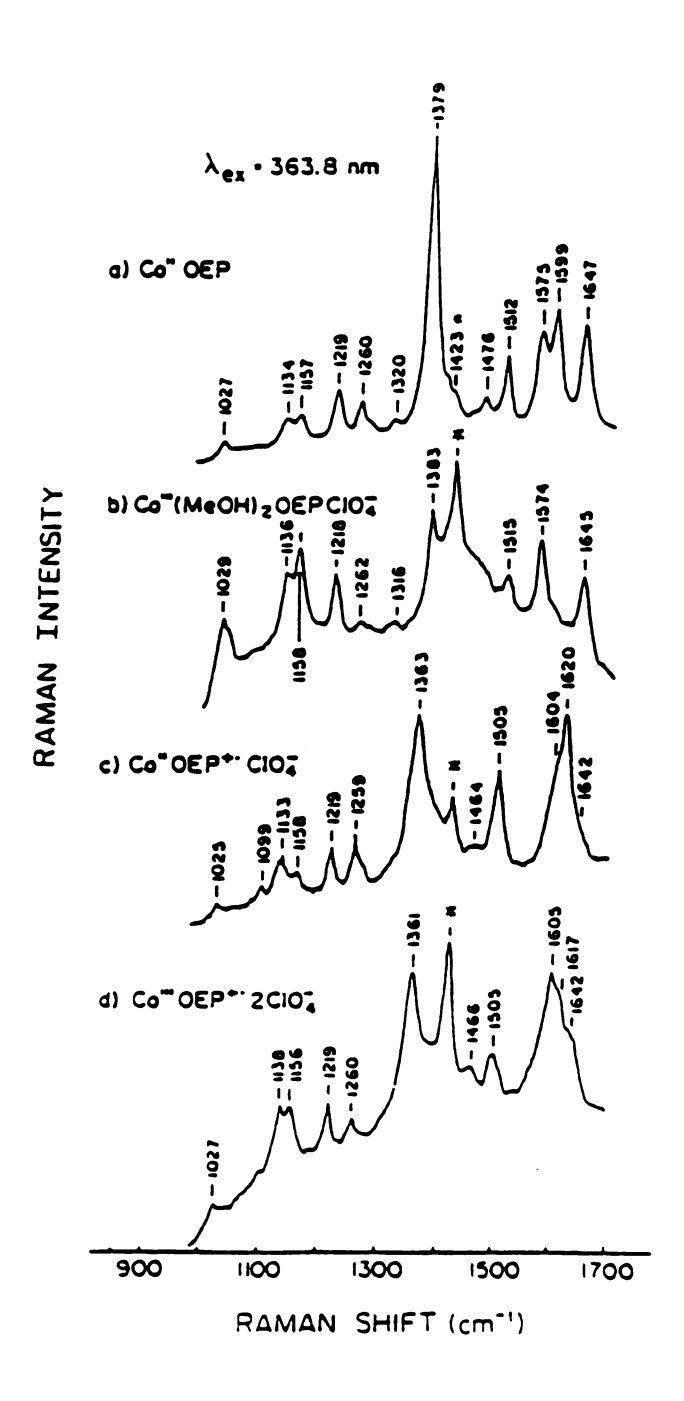


Figure 9. RR spectra excited at 363.8 nm (~ 35 mW) of CoOEP and its oxidation products. (a) CoOEP; (b) Co^{III}(MeOH)₂OEPClO₄⁻; (c) Co^{III}OEP+-ClO₄⁻; (d) Co^{III}OEP+-2ClO₄⁻; (e) Co^{III}(MeOH)₂OEPBr⁻; (f) Co^{III}OEPBr⁻; (g) Co^{III}OEP+-2Br⁻. Solvent, dry CH₂Cl₂ except (b) and (e) which contain ~ 5% methanol. Solvent bands are marked with an *

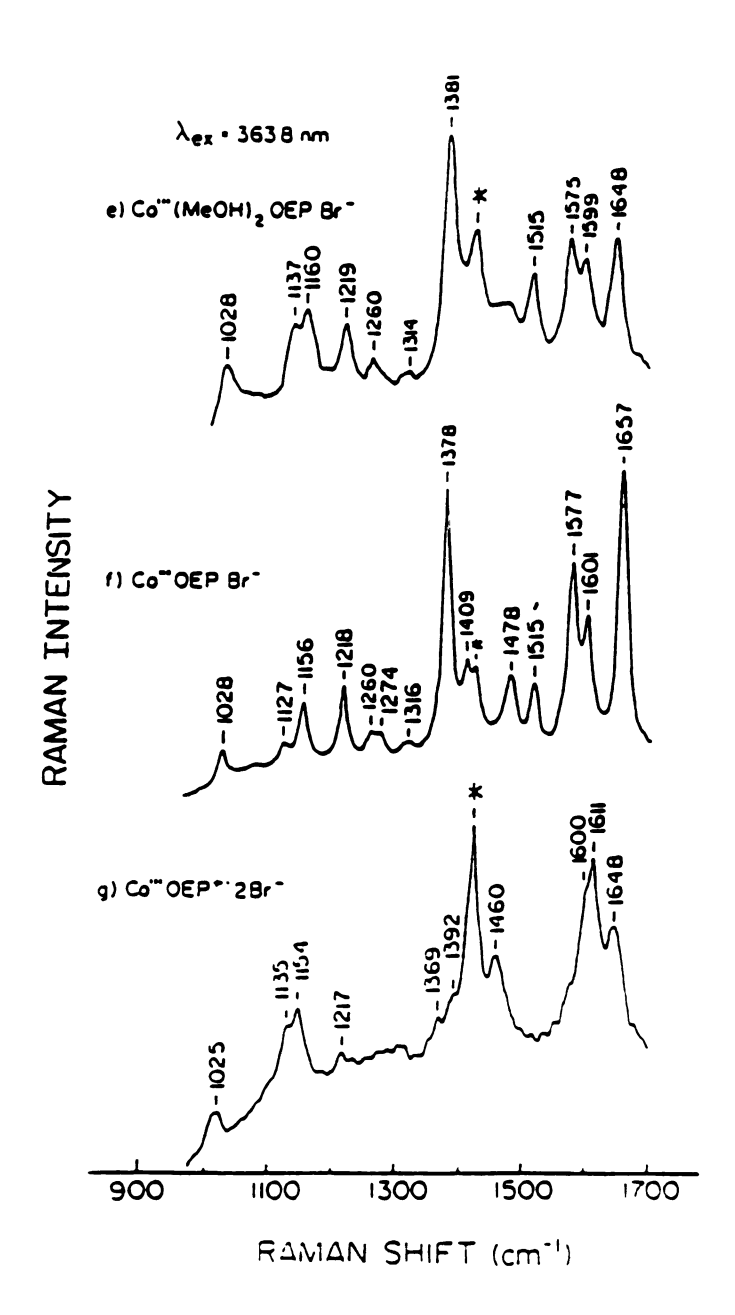


Figure 10. Electronic absorption spectra of oxidation products of CoOEP. (a) Co^{III}(MeOH)₂OEPBr⁻(-); (b) Co^{III}OEPBr⁻ (---); (c) Co^{III}OEP+·2Br⁻ (···), the small feature at 401 nm is due to 1% H₄OEP²+2Br⁻ contamination as discussed in the text. Solvent, dry CH₂Cl₂, except for (a) which contains ~5% methanol (MeOH).

The RR spectra excited at 363.8 nm of the bromide adducts of oxidized CoOEP are shown in Figure 11. The RR spectrum of $Co^{III}(MeOH)_2OEPBr^-$, Figure 11a, is similar to that of CoOEP and $Co^{III}(MeOH)_2OEPClO_4^-$, Figure 9a, b. The RR spectrum of $Co^{III}OEPBr^-$ is shown in Figure 11b. While v4 (1378 cm⁻¹) is slightly lower than in the other Co(III) compounds, the core-sensitive bands above 1450 cm⁻¹, particularly v₁₀ (1657 cm⁻¹), have increased in frequency, supporting a slight core contraction in this species.^{32,34}

The spectrum of the π -cationic radical species, Co^{III}OEP+·2Br⁻(Figure 11c) is dominated by v₂ (1611 cm⁻¹) and v₁₁ (1600 cm⁻¹) modes, similar to the other π -cations discussed earlier. There is, however, no band easily assignable to v₄. The features at 1460 and 1648 cm⁻¹ are assigned to v₂₈ and v₁₀, respectively. The v₃ vibration, which is enhanced in Soret RR spectra of neutral metalloporphyrins, does not appear in these spectra, but a polarized feature at 1497 cm⁻¹ present in the spectra obtained in resonance with the 670-nm transition of the dibromide cation radical is assigned to v₃. (Spectrum not shown).¹⁸

Table 1 summarizes the vibrational frequencies of CoOEP derivatives. Thus, in the high-frequency region, the modes involving primarily C_aC_m stretching character (v3 and v10) decrease in frequency upon oxidation of the porphyrin ring, while modes involving primarily C_bC_b stretching character (v11 and v2) increase in frequency. The frequency of v4, primarily a C_aN stretch, decreases upon formation of porphyrin π -cation radical. These trends are common to other metalloporphyrin system (i.e., CuOEP, ZnOEP) not presented here. ¹⁸

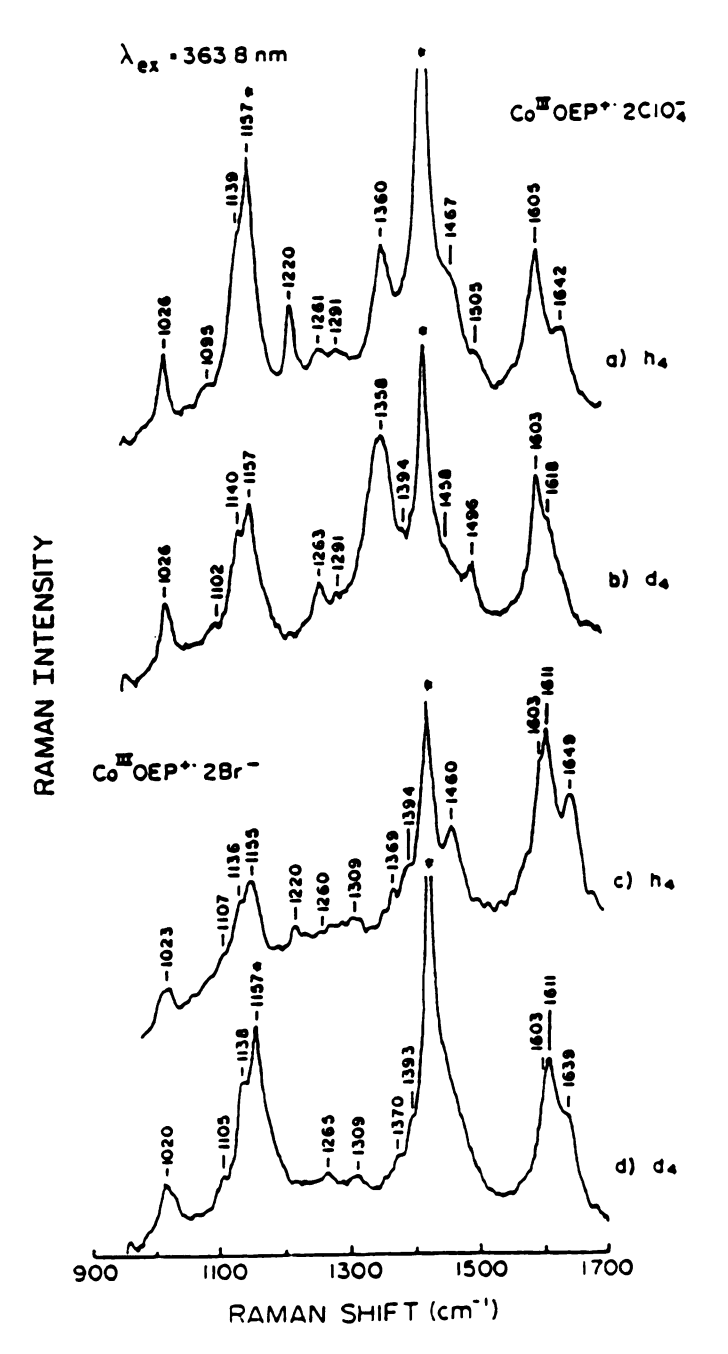


Figure 11. RR spectra of cobaltic octaethylporphyrin π cation radicals in CH₂Cl₂.

Table 1: Resonance Raman Frequencies (cm⁻¹) for the Parent CoOEP and its Oxidation Products

	v ₄ C _a N	v ₃ C _a C _m	v ₁₁ C _b C _b	v ₂ C _b C _b	v ₁₀ C _a C _m	Soret, nm
Co ^{II} OEP-h ₄ d ₄	1379(.2) 1379(.3)	1512(.2) 1504(.2)	1575(.6) 1572(.9)	1599(.3) 1598(.4)	1647(0.7) 1636(1.0)	391
Co ^{III} (MeOH) ₂ OEPx ⁻						
$x^- = ClO_4^-$	1383	1515	1574	?	1645	409
Br ⁻	1381	1515	1575	1599	1648	411
Co ^{III} OEPBr	1378	1515	1577	1601	1657	373
Co ^{II} OEP+•ClO ₄ -	1363	1505	1604	1620	1642	376
Co ^{III} OEP+·2x-						
$x^- = ClO_4^-, h_4$	1360(.3)	1505w	1605(.8)	1617w	1642	sh392
d ₄	1360(.4)	1496(.6)	1603(.8)	1618sh	?	
$x^- = Br^-, h_4$?	1497(.3)	1603(.5)	1611(.4)	1649(.7)	410,
d ₄	?	?	1603	1611	1639	344

Depolarization ratios, given in parentheses, were also measured with 363.8-nm excitation.

Perhaps the most interesting aspect of the RR spectra of $Co^{III}OEP^{+}\cdot 2X^{-}$ is the apparent insensitivity of the RR frequencies to radical electronic state. Aside from differences in relative intensities, the RR spectra of the two radicals are similar; however, the vibrational frequencies of the dibromide complex $(^{2}A_{1u})$ are 6-7 cm⁻¹ lower than those of the diperchlorate $(^{2}A_{2u})$, with the exception of v_{10} with no explanation offered as yet. Because the

frequency differences are small, we speculate that they can be attributed to differences in porphyrin core geometry caused by the different axial ligation of these two species. Although these vibrations of the porphyrin macrocycle may well be insensitive to the radical electronic state, the abnormally high values of the $v(C_bC_b)$ modes provide a clear basis to identify ring-centered oxidations.¹⁵

Co^{III}OEP+·2ClO₄- is the only species that remains identified in the literature as a ²A_{2IJ} radical among the MOEP+ complexes, thus, our suggestion regarding the insensitivity of porphyrin RR vibrations to the radical electronic state is not strongly supported. Since the ESR data is inconclusive as to the ²A_{2II} assignment of the diperchlorate adduct (e.g., lack of Co hfs), it may be that this species belongs to a ²A_{1U} ground state as well. Reed and coworkers have recently stressed the importance of the evaluation of porphyrin stereochemistry as well as π -orbital occupancy for the analysis of the magnetic properties of metalloporphyrin π -cation radicals. Thus, the structural factors, in our opinion, may also play a significant role in the analysis of the electronic and vibrational spectra of these complexes. It is likely that the absorption spectra of Co^{III}OEP+·2ClO₄- and Co^{III}OEP+·2Br-, which were originally thought to be characteristics of the ²A_{2U} and ²A_{1U} states, respectively, actually reflect the stereochemistry of the porphyrin core and that a planar conformation exists in the solution for the diperchlorate complex, and presumably a nonplanar one is present for the dibromide adduct. The RR spectra may in turn, reflect the structural properties of these radicals and, that they are either to some extent independent of ²A₁₁₁ vs. ²A₂₁₁

designation or that all of the MOEP+ \cdot compounds we have examined belong to the $^2A_{1U}$ ground state. In order to resolve questions regarding structure we are currently studying the low-frequency RR active vibrations of the metal axial ligand and porphyrin skeleton of these complexes. In addition, ENDOR measurements are being used to determine radical ground state assignment. We will report on these efforts in the future.

REFERENCES

- 1. Dolphin, D., Ed., B₁₂ (Wiley, New York, **1982**), Vols. 1 and 2.
- 2. LindsKog, S., Struct. Bonding (Berlin) **1970**, 8, <u>153-196</u>.
- 3. Smith, E. L.: In: Mineral Metabolism 2, Part B, 349. Ed. by C. L. Comar and F. Bronner. New York--London: Academic Press, Inc. 1962.
- 4. Yonetani, T.; Yamamoto, H.; Woodrow, G. V., J. Biol. Chem. 1974, 249, 682.
- 5. HSU, G. C.; Spilburg, c. A.; Bull, C.; Hoffman, B. M., Proc. Natl. Acad. Sci., USA 1972, 69, 2122.
- 6. Lee, W. A.; Bruice, T. C., Inorg. Chem. 1986, 25, 131.
- 7 (a) Hill, H. A. O.; Sadler, P. J.; Williams, R. J. P.; Berry, C. D., Ann. N.Y. Acad. Sci., **1973**, <u>206</u>, 247.
 - (b) Setsune, J. I., Dolphin, D., Organometallics, 1984, 3, 440.
- 8. Hanson, L. K.; Chang, C. K.; Davis, M. S.; Fajer, J., J. Am. Chem. Soc., **1981**, <u>103</u>, 663.
- 9. Scholz, W. F.; Reed, C. A.; Lee, Y. J.; Scheidt, W. R.; Lang, G., J. Am. Chem. Soc., 1982, 104, 6791.
- 10. Wang, C. B.; Chang, C. K., Synthesis, 1979, 548.
- 11. Bonnett, R.; Gale, I. A. D.; Stephenson, G. F., J. Chem. Soc. (c), 1967, 1168.
- 12. Adler, A. D.; Longo, F. R.; Kampas, F.; Kim, J., J. Inorg. Nucl. Chem., 1970, 32, 2443.
- 13. Sakurai, T.; Yamamoto, K.; Naito, H.; Nakamoto, N., Bull. Chem. Soc. Jpn. 1976, 49, 3042.

- 14. Datta-Gupta, N.; Bardos, T. J., J. Pharm. Sci. 1968, <u>57</u>, 300.
- 15 (a) Salehi, A.; Oertling, W. A.; Babcock, G. T.; Chang, C. K., J. Am. Chem. Soc., **1986** <u>108</u>, 5630.
 - (b) Wertz, J. E.; Reitz, D. C.; Dravneiks, F. In "Free Radicals in Biological System," Blois, Jr., M. S., Ed., Academic: New York, 1961, 183.
- 16. (a) Dolphin, D.; Muljiani, Z.; Rousseau, K.; Borg, D. C.; Fajer, J.; Felton, R. H. Ann. N. Y. Acad. Sci., 1973, 206, 177.
 - (b) Groves, J. T.; Quinn, R.; McMurry, T. J.; Lang, G.; Boso, B., J. Chem. Soc., Chem. Commun., 1984, 1455
- 17. Sugimoto, H.; Ueda, N.; Mori, M., Bull. Chem. Soc. Jpn. 1981, <u>54</u>, 3425.
- 18. Oertling, W. A.; Salehi, A.; Chung, Y. C.; Leroi, G. E.; Chang, C. K.; Babcock, G. T., J. Phys. Chem., 1987, 91, 5887.
- 19. Johnson, A. W.; Kay, I. T., J. Chem. Soc., 1960, 2979.
- 20. Edwards, L.; Dolphin, D. H.; Gouterman, M. J., Mol. Spectrosc., 1970, 35, 90.
- 21. Wang, M. -Y. R.; Hoffman, B. M., J. Am. Chem. Soc., 1984, 106, 4235.
- 22. Browett, W. R.; Stillman, M. J., Inorg. Chim. Acta, 1981, 49, 69.
- 23. (a) Walker, F. A.; La Mar, G. N. Ann. N. Y. Acad. Sci., 1973, 206, 328.
 - (b) LaMar, G. N.; Walker, F. A., J. Am. Chem. Soc., 1973, 95, 1782.
- 24. Walker, F. A., J. Mag. Res., 1974, 15, 201.
- 25. Fulton, G. P.; LaMar, G. N., J. Am. Chem. Soc., **1976**, <u>98</u>, 2119.
- 26. Hambright, P.; Thorpe, A.; Alexander, C. J. Inorg. Nucl. Chem., **1968**, <u>30</u>, 3139.
- 27. (a) Huet, J.; Gaudemer, A.; Boucly-Goester, C.; Boucly, P., Inorg. Chem., 1982, 21, 3413.
 - (b) Yamamoto, K.; Hoshino, M.; Kohno, M.; Ohya-Nishiguchi, H., Bull. Chem. Soc. Jpn., 1986, 59, 351.
- 28. Dolphin, D.; Forman, A.; Borg, D. C.; Fajer, J.; Felton, R. H., Proc. Natl. Acad. Sci. USA, 1971, 68, 614.
- 29. Shimomura, E. T.; Phillippi, M. A.; Goff, H. M., J. Am. Chem. Soc., 1981, 103, 6778.

- 30. (a) Itoh, L.; Nakahasi, K.; Toeda, H., J. Phys. Chem., 1988, 92, 1464.
 - (b) Hinman, A. S.; Pavelich, B. J.; McGarty, K., Can. J. Chem., submitted.
- 31. Abe, M.; Kitagawa, T.; Kyogoku, Y., J. Chem. Phys., 1978, 69,m 4526.
- 32. Choi, S.; Spiro, T. G.; Langry, K. C.; Smith, K. M.; Budd, D. L.; La Mar, G. N., J. Am. Chem. Soc., 1982, 104, 4345.
- 33. Spiro, T. G.; Strekas, t. C., J. Am. Chem. Soc., 1974, 96, 338.
- 34. Spiro, T. G., In "Iron Porphyrins," Lever, A. B. P.; Gray, H. B., Eds.; Addison-Wesley: Reading, MA, 1983; Part 2, 89.

CHAPTER III

IRON PORPHYRIN Π-CATION RADICALS: SOLUTION RESONANCE RAMAN SPECTRA OF OEP+•Fe^{III}(X)(X')

Heme catalysis in peroxidases, catalases and cytochromes P-450 proceeds through high valent intermediates, some of which are likely to be oxidized at the porphyrin macrocycle as well as the central iron. An understanding of the role of these species in the enzymatic cycle requires insight into the interplay between the oxidation state, geometry and electron density distribution of the porphyrin ring and the valence, spin and ligation states of the iron. Raman spectroscopy is potentially able to provide this kind of information and its utility was demonstrated in the previous chapter in the detection of cobalt porphyrin oxidation products. This work, however, was confined only to the cobalt complexes in which the spin state remains unchanged upon variation in the ring oxidation and metal ligation states. Characterization of oxidized iron porphyrins, on the other hand, covers a wider range of variables owing to several oxidation, ligation and spin states that are available to the iron atom, and has not yet been achieved by Raman spectroscopy. 4

For example, for ferric porphyrins, which serves as the neutral precursor in this study, the spin-state and stereochemistry of the iron(III)

center are controlled by the nature of axial ligands.⁵ The coordination of two strong field ligands leads to low-spin (S = 1/2) six-coordinate hemes, e.g., bis(imidazole) iron(III) derivatives. Weaker field ligands, typically anionic ones such as chloride and azide, lead to five-coordinate high-spin (S = 5/2)derivatives. The high-spin five-coordinate species have the iron(III) atom displaced out of the porphyrin plane by ~ 0.5Å with concomitant longer Fe-N The low-spin, six-coordinate complexes have the iron(III) atom bonds. essentially centered in the porphyrin plane and relatively short Fe-N bonds. The stereochemical differences are associated with the population of the 3d_x2_{-v}2 orbital in the high-spin complexes and its depopulation in the lowspin derivatives. The coordination of two weak field ligands to the ferric porphyrins leads to still another structural type for iron(III) porphyrins; namely, high-spin six-coordination. Ligands which lead to this type are commonly neutral oxygen donor ligands: sulfoxide, dimethylformamide, pyridine N-oxide, triphenylphosphine oxide and water.

When the axial ligands are extremely weak anionic ligands, such as perchlorate or tricyano methanide $[C(CN)_3^-]$, the resulting ferric porphyrin derivatives are not high-spin. Rather these complexes have magnetic properties and stereochemical features consistent with a ground-state assignment of intermediate (S = 3/2) or a quantum mechanical admixture of S = 3/2 and S = 5/2 spin state.⁶ This formulation is to be distinguished from a thermal mixture of magnetically distinct S = 3/2 and S = 5/2 states. Quantum mechanical admixing is presumably the result of small energy separation between pure spin states.⁷ For the iron (III) porphyrin perchlorate derivative, the molecular structure reveals a shortened Fe-N distance, a small Fe-out-of

plane displacement (0.3Å), and a lengthened Fe-perchlorate oxygen distance with respect to high-spin derivatives.⁸

To address these properties at the oxidized level, we report here the solution RR characterization of iron(III) octaethylporphyrin cation radicals of general formula OEP+·Fe^{III}(X)(X'), where X⁻ = Cl⁻, ClO₄⁻, and X' = ClO₄⁻ and SbCl₆⁻. We focus on the determination of the solution coordination number and spin state of the iron atom in the porphyrin radicals, as monitored by high-frequency (1450 - 1700 cm⁻¹) vibrational modes that are sensitive to porphyrin core conformation. Our data demonstrate the utility of Raman spectroscopy in characterizing iron porphyrin radicals and indicate a preference for the five-coordinate state in solution, at least for the ligand combinations used here. We discuss our results in light of recent NMR, crystal structure, magnetic, and IR data available on the related TPP derivatives.

EXPERIMENTAL SECTION

Instrumentation. UV-vis spectra were recorded by using a Cary 219 spectrophotometer. The 363.8 and 351.1 nm lines used to record the RR spectra were obtained from a Coherent Innova 100-20 argon ion laser; the Raman equipment is described in detail elsewhere. Magnetic susceptibility measurements were performed on an SHE SQUID susceptometer at a field of 5KG.

Materials and Methods. The free base porphyrin H_2OEP and H_2EPI (etioporphyrin-I) were synthesized according to the published methods.^{9,10}

Iron insertion was achieved by using ferric chloride Salt.¹¹ Exchange of hydrogen (h₄) for deuterium (d₄) at the meso position of the porphyrin was accomplished by using the D₂SO₄/D₂O method and confirmed by NMR measurements.¹²

Chemical Oxidations. Typically, samples were prepared at room temperature in dry CH₂Cl₂ by using a slight stoichiometric excess of the oxidant, according to the published reports.^{2a},¹³ The progress of the reaction was followed spectrophotometrically until complete oxidation was achieved. OEP+·Fe^{III}(ClO₄-)₂ (1) was prepared from (OEPFe)₂O by using Fe(ClO₄)₃·xH₂O (yellow) in the presence of trace HClO₄ to assist in the breaking of the μ -oxo bridge of the dimer. UV-vis (CH₂Cl₂) λ_{max} (ϵ x10⁻³) for 1 are as follows: 357 (86), 517 (14.5), 578 nm (broad), Figure 1; μ_{eff} = 6.7 μ_{B} (solid state, 300K). OEP+·Fe^{III}(Cl-)(SbCl₆-) (2) was prepared from OEPFeCl by using phenoxathiin hexachloroantimonate as the oxidant.^{2c} UV-vis (CH₂Cl₂) λ_{max} (ϵ x10⁻³) for 2 were similar: 357 (84), 519 (14.7); μ_{eff} = 2 μ_{B} (solid state, 300K).

Integrity of the samples was verified by monitoring the absorption spectra before and after the RR spectra. The choice of the excitation line, however, is of importance to minimize contributions from ferric porphyrin and diacid salt contaminations, 3b which may be difficult to observe in the optical spectra, and to select predominantly for the porphyrin radical.

Results and Discussion. Our magnetic susceptibility data for 1 ($\mu_{eff} = 6.7\mu_{B}$) and 2 ($\mu_{eff} = 5.2\mu_{B}$) show that the effective magnetic moment for ferric OEP π -cation radicals in the solid state is a function of the axial ligation. A similar dependence occurs for solid state ferric TPP radicals as TPP +·Fe^{III}(ClO₄-)2 (3)

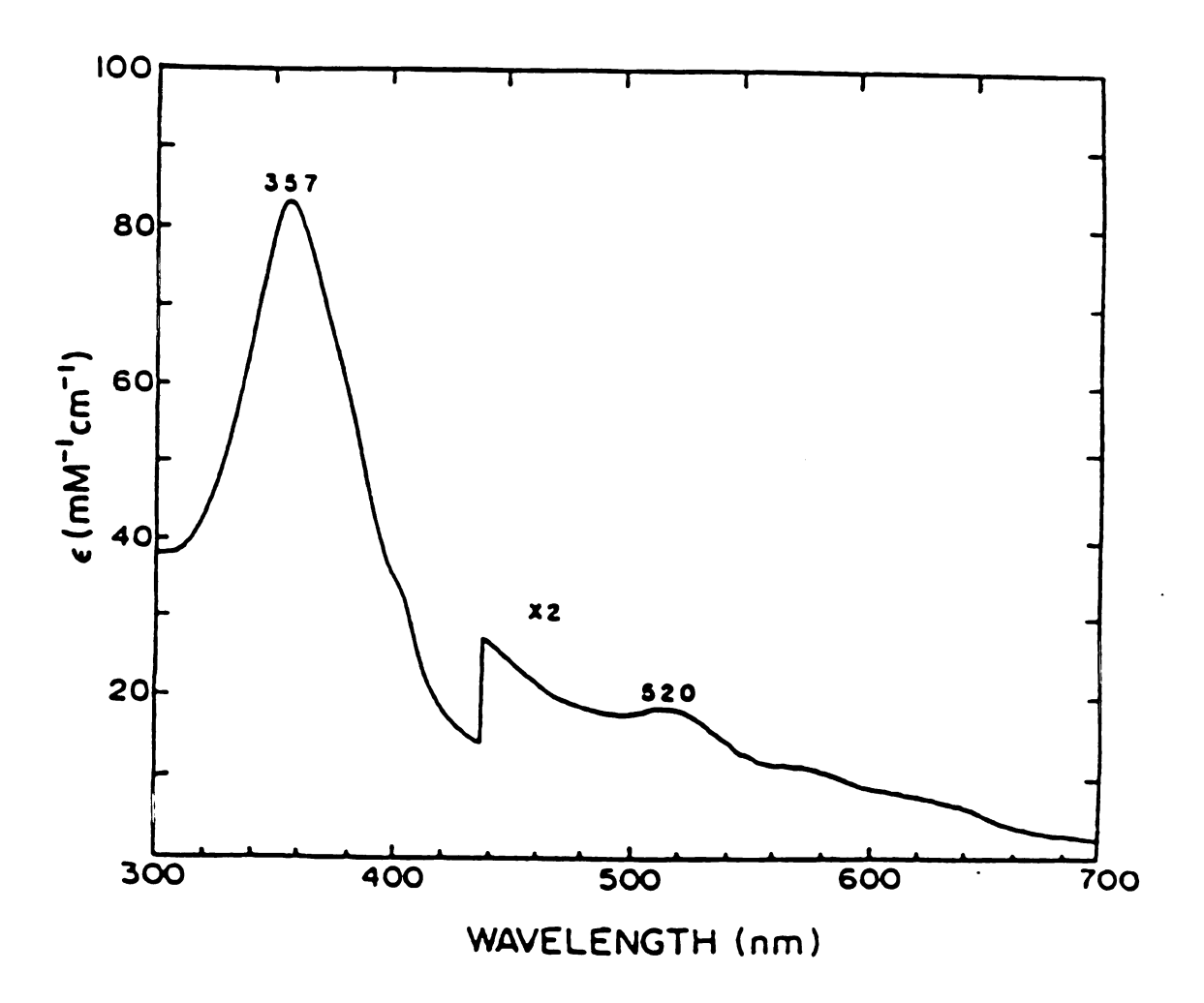


Figure 1. Absorption spectrum of Fe^{III}OEP+·(Cl⁻)(SbCl₆⁻) in CH₂Cl₂.

has $\mu_{eff} = 6.5$ while TPP+·Fe^{III}(Cl⁻)(SbCl₆⁻) (<u>4</u>) has $\mu_{eff} = 4.8\mu_{B}$.¹⁴ The latter data have been rationalized by X-ray crystallographic work.^{14,15} 3 has a planar core with both perchlorate ions ligated to the iron; this geometry apparently leads to strong ferromagnetic coupling between the high-spin ferric ion and the ring-centered radical to produce an overall spin of S = 3. Solid state IR data on 3 and its TMP analog are consistent with bisaxial ligation.^{15,16} 4, however, is five-coordinated and exhibits a ruffled core, which presumably leads to antiferromagnetic exchange and a room temperature S = 2 state.

In solution 4 maintains its five-coordinate ligation geometry. Boersma and Goff, however, have interpreted NMR and magnetic data to suggest that 3 undergoes axial ligand dissociation and also adopts a five-coordinate geometry in solution. Raman spectroscopy of these ferric cation radicals provides an independent means by which to test this suggestion; moreover such a study will assess the applicability of Raman techniques to characterizing ring-oxidized iron porphyrin species. As in our earlier work, we have focused on iron OEP derivatives owing to their biologically relevant peripheral substitution pattern. The similarity in magnetic moments between Fe^{III}OEP cation radicals and Fe^{III}TPP cation radicals noted above indicates that the altered pattern of peripheral substitution is unlikely to perturb axial ligation behavior significantly.

Figure 2 shows Raman spectra of 1 and 2 along with that of the five-coordinate ring neutral OEPFe^{III}(Cl⁻) species (5) in methylene chloride. An assignment of the principal high frequency modes for these species as well as of OEPFe^{III}(DMSO)₂+ (6)¹⁸ is given in Table I. Compositional assignment

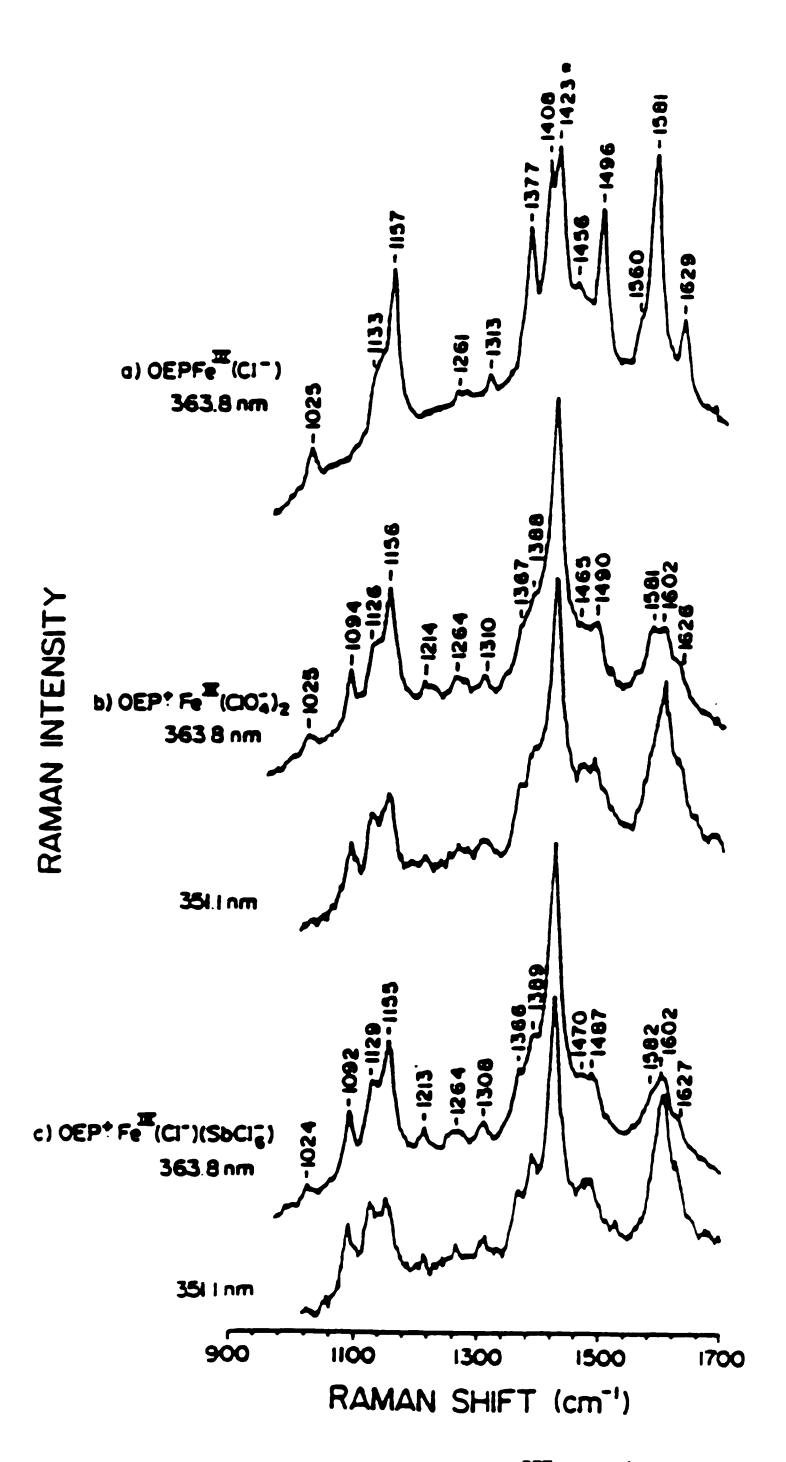


Figure 2. Near-UV RR spectra of OEP+·Fe^{III}(X)(X') complexes. The laser power was 35-40 mW. The solvent (CH₂Cl₂) band at 1423 cm⁻¹ is labeled with an asterisk (*).

for the individual normal modes has been confirmed by a combination of meso-deuterium isotope effect and spectral comparison between the analogous OEP and EPI complexes, Figures 3 and 4.19 The vibrational modes with significant C_aC_m stretching character are expected to exhibit a decrease in wavenumber upon meso-tetradeuteration. On the other hand, the frequencies of vibrations that are predominantly of CbCb character should remain unchanged. The contributions from CbCb stretching motions may, however, be more directly confirmed by comparing the spectra of OEP vs. EPI complexes, which also serves as an alternative to isotopic labelling at the β -The frequency differences apparent in comparing pyrrole positions. corresponding modes for the two ring neutral species, 5 and 6, are understood and correlate inversely with porphyrin core size. The similarities for 1 and 2 in the frequencies of these modes, which retain core-size sensitivity in the metalloporphyrin cation radicals,^{3c} indicate that the solution geometry for these two radicals is similar, in agreement with the Boersma and Goff suggestion.

We can gain further insight into the coordination state of these radicals by referring to earlier work with valence +2 metalloporphyrin derivatives. 3 C For this class of compounds we showed that vibrational modes with predominantly C_bC_b character are ~ 20 cm $^{-1}$ higher in a given radical relative to the corresponding modes in its neutral precursor, whereas those with significant C_aC_m character are ~ 5 cm $^{-1}$ lower (Table I, column 6). The physical basis for this behavior lies in the fact that there is a little change in porphyrin core geometry upon ring-centered oxidation. This correlation indicates, then, that the axial coordination for the OEP radicals in Figure 1

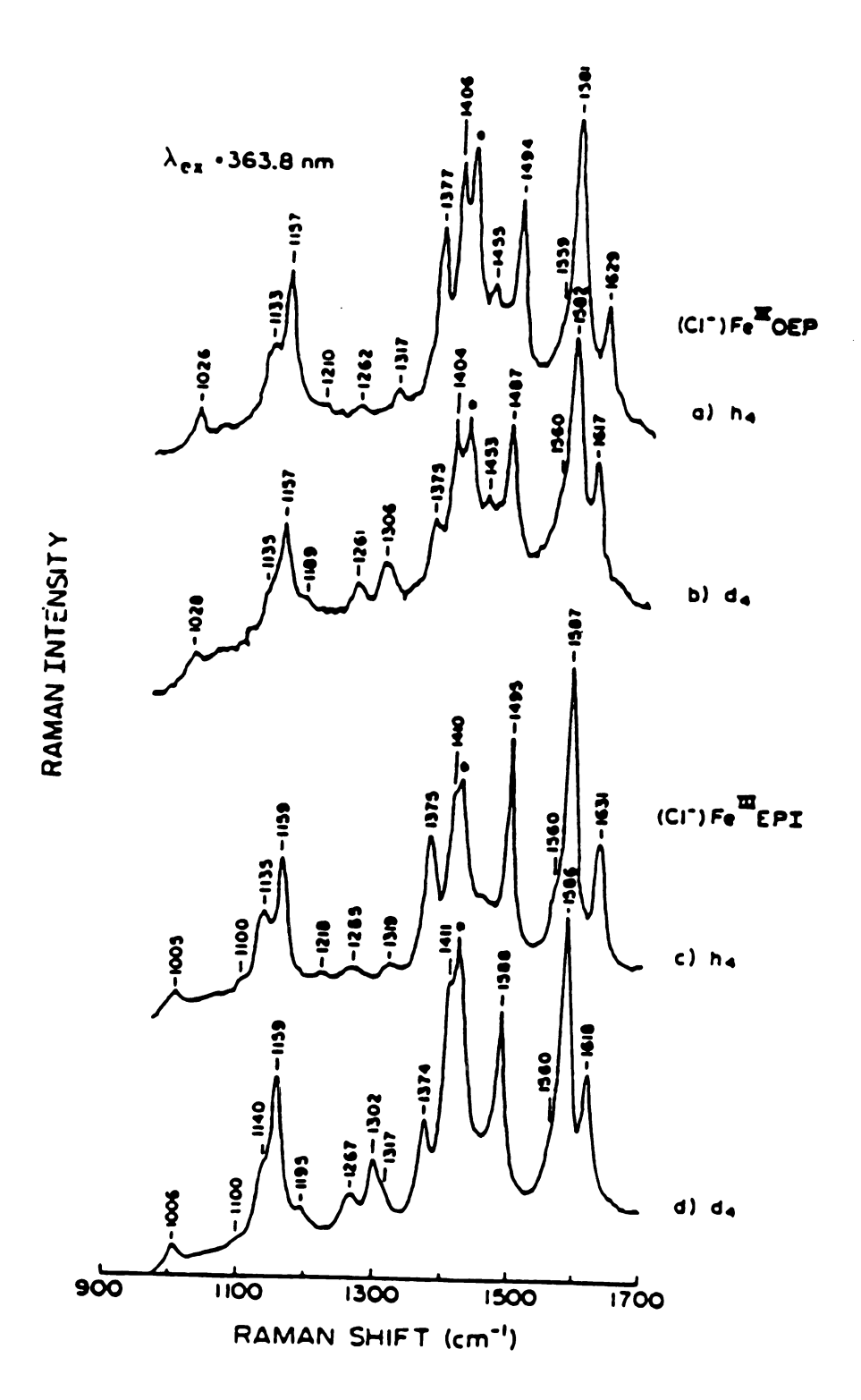


Figure 3. RR spectra of ferric chloride porphyrins in CH₂Cl₂.

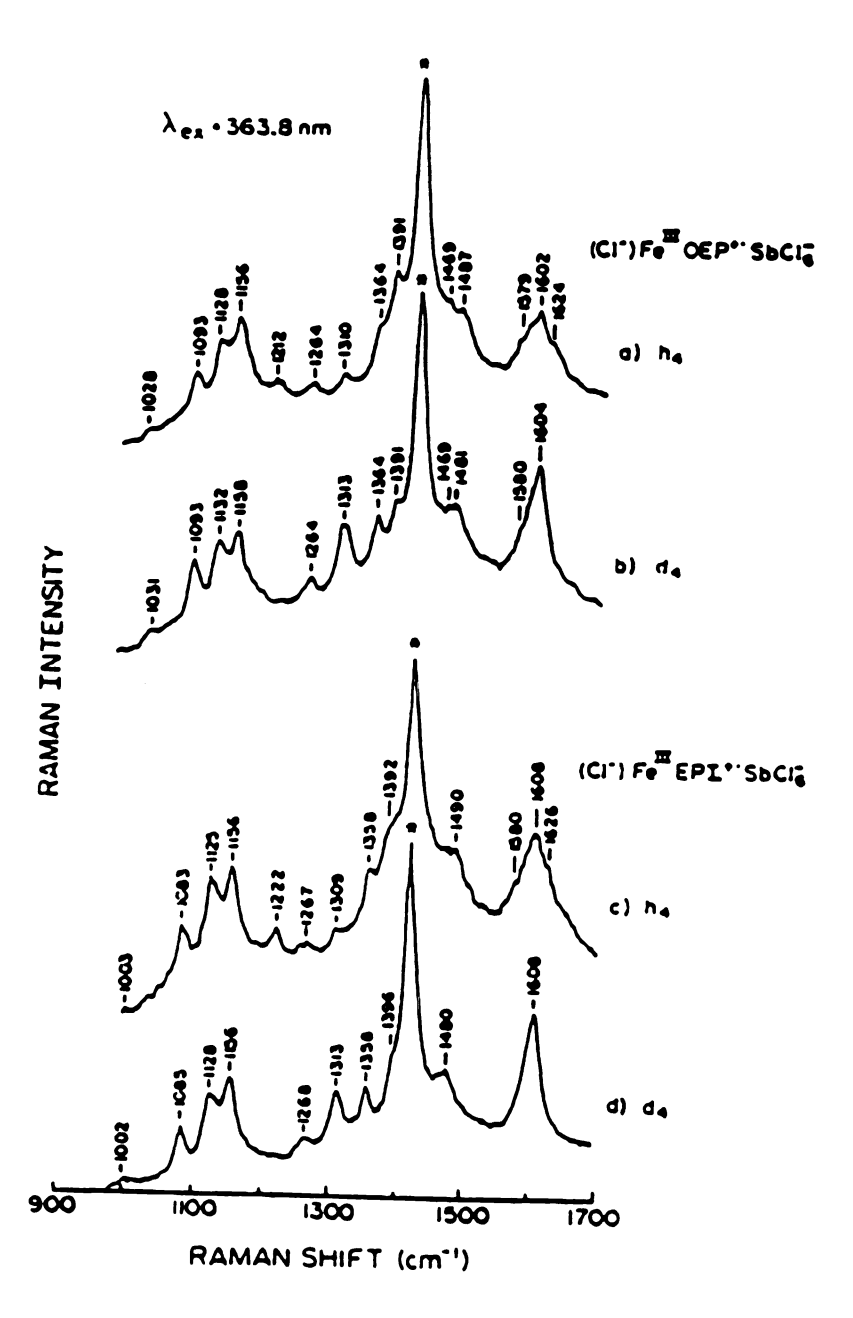


Figure 4. RR spectra of ferric chloride porphyrin π cation radicals in CH₂Cl₂.

may be assigned by considering their frequency shifts relative to the neutral five- and six-coordinate ferric OEP species. Inspection of Table I shows that the pattern of frequency shifts observed for the valence +2 metalloporphyrin derivatives is reproduced when the ferric π -cation radicals are considered to be five-coordinate in solution (column 4); assuming a six-coordinate solution state for the radicals (column 5) produces poor agreement with our earlier data.

Two conclusions follow from these data. First, the porphyrin core geometries of both 1 and 2 in solution are characteristic of a five-coordinate state, consistent with the suggestion that axial ligand dissociation occurs when 2 goes into solution.¹⁷ Second, the pattern of vibrational frequency changes that occurs upon ring oxidation of +2 metalloporphyrin derivatives^{3c} appears to hold as well for the more complex, but biologically more relevant, iron porphyrins.

High frequency RR scattering from Iron protoporphyrin-IX π -cation radical:

Figure 5 depicts the RR spectra of OEPFeCl and its one-electron oxidation product, OEP+·FeIII(Cl⁻)(SbCl₆⁻). Also shown are the spectra of the analogous protoheme species (Figure 5c and d). As demonstrated earlier, the OEP compounds exhibit a five-coordinate, high-spin (S = 5/2) configuration for the heme iron in solution; the protoheme spectra are consistent with the same spin and coordination state assignment for these species.²⁰ Table 2 compares the vibrational assignments of iron PP-IX with those of OEP complexes. The decrease in frequency for modes with significant C_bC_b character for the protoheme species relative to OEP species is expected on the basis of different pattern of peripheral substitution, also demonstrated in the

spectra of the EPI complexes. The protoheme RR spectra are more complex owing to the E_{11} modes, v_{38} and v_{37} , which occur at 1530 and ~ 1553 cm⁻¹, respectively, in the neutral form, Figure 5C.21 The position of v₃₈ in the cation radical is difficult to determine from our RR spectra excited at 351.1 nm, Figure 5d, but presumably can be measured by IR spectroscopy.3c We interpret the broad feature extending from 1570 - 1600 cm⁻¹ in the Fe^{III}PP-IX+. spectrum to be composed of three overlapping bands: v₁₁ (C_bC_b) occurring at ~ 1570 cm⁻¹, v_2 (C_bC_b) at 1593 cm⁻¹ and v_{37} (C_aC_m) at ~ 1585 cm⁻¹. The ~ 20 cm^{-1} increase in the modes (v_{11}, v_2) that are predominantly composed of C_bC_b stretches is expected upon oxidation of ferric porphyrin π -cation radical, Table 1. These frequency increases are partially obscured in the spectrum in Figure 5d by the frequency decreases of v_{37} (C_aC_m) in the cation (~ 1585 cm⁻¹) relative to the neutral (1590 cm⁻¹). These spectra demonstrate that the changes in the vibrational frequencies that accompany ring oxidation of these ferric compounds are consistent with those observed for other cation radical species. Thus, in general, we find that stretching modes with predominantly C_aN character (v₄) or C_aC_m character (v₃ and v₁₀) decrease in frequency, while those with CbCb character (v₁₁ and v₂) increase in frequency when the porphyrin ring is oxidized, Tables 1 and 2. We see these frequency shifts regardless of whether the electron is extracted from the $a_{1u}(\pi)$ or $a_{2u}(\pi)$ molecular orbital.

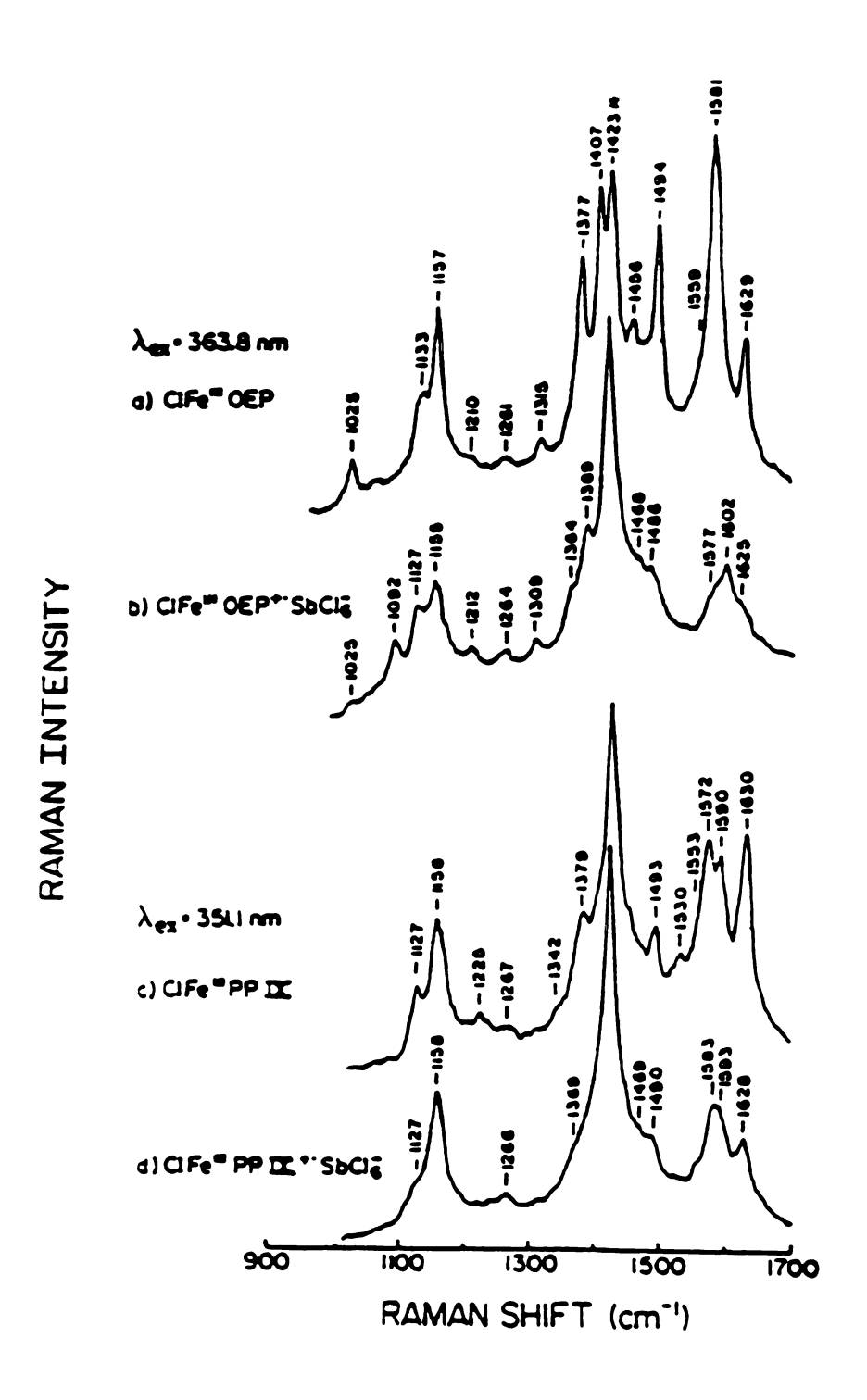


Figure 5. RR spectra of model compounds in CH₂Cl₂. Conditions: 25-30 mW incident on the sample in a spinning cell at 25°C.

Table I.

RR Frequencies (cm-1) of Selected Iron OEP Species

Mode	OEP+·Fe ^{III} (ClO ₄ ⁻)2 1	OEP+·Fe ^{III} (Cl ⁻)(SbCl ₆ ⁻) 2	OEPFe ^{III} (Cl ⁻) 5 (Δν) ^a)	OEPFe ^{III} (DMSO) ₂ +6 (Δν) ^a)	Predicted Δν _{ave} b)
$v_{10}(C_aC_m)$	1626	1627	1629 (-3)	1615 (+11)	-4
$v_2(C_bC_b)$	1602	1602	1581 (+21)	1576 (+26)	+20
$v_{11}(C_bC_b)$	1576	1577	1560 (+21)	-	+26
$v_3(C_aC_m)$	1490	1487	1496 (-7)	1483 (+6)	-7

- a) Obtained as the average frequency difference for the indicated mode in the cation radicals and either the neutral five-coordinate species (column 4) or the neutral six-coordinate species (column 5).
- b) From ref. 3c.

Table II. $\mbox{Vibrational Assignments (1450-1700 cm$^{-1}$)} \label{eq:Vibrational Assignments} \mbox{for Ferric Porphyrins and their π Cation Radicals}$

	C1FeOEP	C1FeOEP+•	C1FePPIX	C1FePPIX+•
v ₃ (C _a C _m)	1494	1486	1493	1490
$v_{11}(C_bC_b)$	1559	-1577	1553	-1570
$v_2(C_bC_b)$	1581	1602	1572	-1593
$v_{37}(C_aC_m)$		-	1590	-1585
$v_{10}(C_aC_m)$	1629	1625	1630	1628

REFERENCES

- 1. (a) Edwards, S. L.; Xuong, N. H.; Hamlin, R. C.; Kraut, J., Biochemistry, 1987, 26, 1503.
 - (b) Hanson, L. K.; Chang, C. K.; Davis, M. S.; Fajer, J., J. Am. Chem. Soc., 1981, 103, 663.
 - (c) Guengerich, F. P.; MacDonald, T. L., Acc. Chem. Res., 1984, 17.
- 2. (a) Phillippi, M. A.; Goff, H. M., J. Am. Chem. soc., 1982, 104, 6026.
 - (b) Phillippi, M. A.; Shimomura, E. T.; Goff, H. M., Inorg. Chem., 1981, 20, 1322.
 - (c) Gans, P.; Marchon, J.-C.; Reed, C. A.; Regnard, J. -R., Nouv. J. Chim., 1981, 5, 203.
 - (d) Furhop, J. H., Struc. Bonding (Berlin), 1974, 18, 1.
 - (e) Groves, J. T.; Quinn, R.; McMurry, T. J.; Lang, G.; Boso, B., J. Chem. Soc. Chem. Comm., 1984, 1455.
 - (f) Erler, B. S.; Scholz, W. F.; Lee, Y. J.; Scheidt, R.; Reed, C. A., J. Am. Chem. Soc., 1987, 109, 2644.
- 3. (a) Salehi, A.; Oertling, W. A.; Babcock, G. T.; Chang, C. K., J. Am. Chem. Soc., **1986**, <u>108</u>, 5630.
 - (b) Oertling, W. A.; Salehi, A.; Chang, C. K.; Babcock, G. T., J. Phys. Chem., 1987, 91, 3114.
 - (c) Oertling, W. A.; Salehi, A.; Chung, Y. C.; Leroi, G. E.; Chang, C. K.; Babcock, G. T., J. Phys. Chem., 1987, 91, 5887.
- 4. (a) Goff, H. M.; Phillippi, M. A., J. Am. Chem. Soc., 1983, 105, 7567.
 - (b) Lee, W. A.; Calderwood, T. S.; Bruice, T. C., Proc. Natl. Acad. Sci. U.S., 1982, 82, 4301.
 - (c) Balch, A. L.; Latos-Grazynski, L.; Renner, M. W., J. Am. Chem. Soc., 1985, 107, 2983.
- 5. Sheidt, W. R. In The Porphyrins, Dolphin, D. H. Ed., Academic press: New York, 1978, Vol. 3, 463.

- 6. Dolphin, D. H.; Sams, J. R.; Tsin, T. B., Inorg. Chem., 1977, 16, 711.
- 7. Goff, H. M.; Shimomura, E. T., J. Am. Chem. Soc., 1980, 102, 31.
- 8. Reed, C. A.; Mashiko, T.; Bentley, S. P.; Kastner, M. E.; Scheidt, W. R.; Spartalian, K.; Lang, G., J. Am. Chem. Soc., 1979, 101, 2948.
- 9. Wang, C. B.; Chang, C. K., Synthesis, 1979, 548.
- 10. Fuhrhop, J. -H.; Smith, D. M. in Porphyrins and Metalloporphyrins, Smith, K. M., Ed., Elsevier: Amsterdam, 1975, 765.
- 11. Chang, C. K.; Dinello, R. K.; Dolphin, D., Inorg. Synth., 1980, 20, 147.
- 12. Fuhrhop, J. -H.; Smith, K. M. in Porphyrins and Metalloporphyrins, Smith, K. M., Ed., Elsevier: Amsterdam, 1975, 816.
- 13. Carnieri, N., Harriman, A., Inorg. Chim. Acta, 1982, 62, 103.
- 14. Gans, P., Buisson; G., Duee, E.; Marchon, J. -C.; Erler, B. S.; Scholz, W. F.; Reed, C. A., J. Am. Chem. Soc., 1986, 108, 1223.
- 15. (a) Scholz, W. F.; Reed, C. A.; Lee, Y. J.; Scheidt, W. R.; Lang, G., J. Am. Chem. Soc., **1982**, <u>104</u>, 6791.
 - (b) Buisson, G.; Deronzier, A.; Duee, E.; Gans, P.; Marchon, J. -C.; Regnard, J. -R., J. Am. Chem. Soc., 1982, 104, 6793.
 - (c) Groves, J. T.; Quinn, R.; McMurry, T. J.; Nakamura, M.; Lang, G.; Boso, B., J. Am. Chem. Soc., 1985, 107, 354.
- 16. WARNING: Laser irradiation of solid perchlorate salts may cause explosion.
- 17. Boersma, A. D.; Goff, H. M., Inorg. Chem., 1984, 23, 1671.
- 18. Callahan, P. M.; Babcock, G. T., Biochemistry, 1981, 20, 952.
- 19. Oertling, W. A.; Salehi, A.; Chang, C. K.; Babcock, G. T., J. Phys. Chem., submitted.
- 20. Oertling, W. A.; Babcock, G. T., Biochemistry, in press.
- 21. Choi, S.; Spiro, T. G.; Langry, K. C.; Smith, K. M.; Budd, D. L.; LaMar, G. N., J. Am. Chem. Soc., 1982, 104, 4345.

CHAPTER IV

RESONANCE RAMAN SPECTRA OF THE II-CATION RADICALS OF COPPER, COBALT, AND NICKEL METHYLOCTAETHYLCHLORINS:

VIBRATIONAL CHARACTERISTICS OF CHLOROPHYLL MODELS

The primary charge-separating event in photosynthetic higher organisms proceeds via the light-induced generation of chlorophyll a radical ions in the reaction centers of Photosystems I and II.^{1,2} The nature of the resulting oxidized chlorophyll species has been controversial and both monomer and dimer formulations have been suggested for P-700⁺ in Photosystem I and P-680⁺ in Photosystem II.^{3,4,5} Lutz and coworkers have provided Raman data that suggest that the radical may be localized in the related bacterial system, at least on the vibrational time scale.⁶

Although there is uncertainty in the extent of the delocalization of the unpaired electron, it is clear that the chlorophyll species is well-suited to its role in photosynthetic systems. A major factor in this function is the relative ease of chlorophyll cation radical formation. This is primarily due to the fact that chlorophyll contains a chlorin ring as its basic structural feature and metallochlorins are oxidized at potentials that are as much as 0.3V lower than those of their metalloporphyrin counterparts.^{7,8,9}

A variety of spectroscopic methods have been used to characterize metallochlorin π -cation radicals, including UV-vis, ESR, ENDOR, and cyclic voltammetry.7,3,10,11,12 These methods have provided information regarding the optical properties, electron-density distribution, ground-state assignments, and redox properties of the radical species; however, their vibrational characteristics have not been explored in any detail. This may partially result from the limited stability of the one-electron oxidized metallochlorin system and its tendency to convert to the corresponding metalloporphyrin derivative. 10,12 Stability of these radicals may, however, be enhanced if one of the substituents on the reduced ring is an alkyl group. This substitution inhibits oxidative dehydrogenation of the chlorin ring to porphyrin, a reaction common to chlorins in which the reduced ring contains vicinal protons. 13 In this regard, methyloctaethylchlorin (MeOEC), Figure 1, represents a simple form of the alkyl chlorins that is ideally suited for oxidation study; moreover, its structure closely resembles the more commonly-studied cis/trans octaethylchlorin (OEC). Additionally, an alkyl chlorin has been suggested as the prosthetic group in the catalytic cycle of Neurospora crassa catalase. 14 Earlier, we demonstrated the application of RR spectroscopy for the vibrational characterization of metalloporphyrin π -cation radicals, MP+.15,16 We present here the RR spectra obtained with excitation at 363.8 nm of Cu(II), Co(II) and Ni(II) complexes of MeOEC and their π -cation radicals. Additionally, the Raman spectra of the Cu(II) derivatives of t-OEC are presented for comparison. This study aims to compare the vibrational characteristics in the high-frequency region (1450-1700 cm⁻¹) of the oxidized metallochlorins (MC+ \cdot) to those of the corresponding metalloporphyrin π cation radical (MP+·) derivatives.

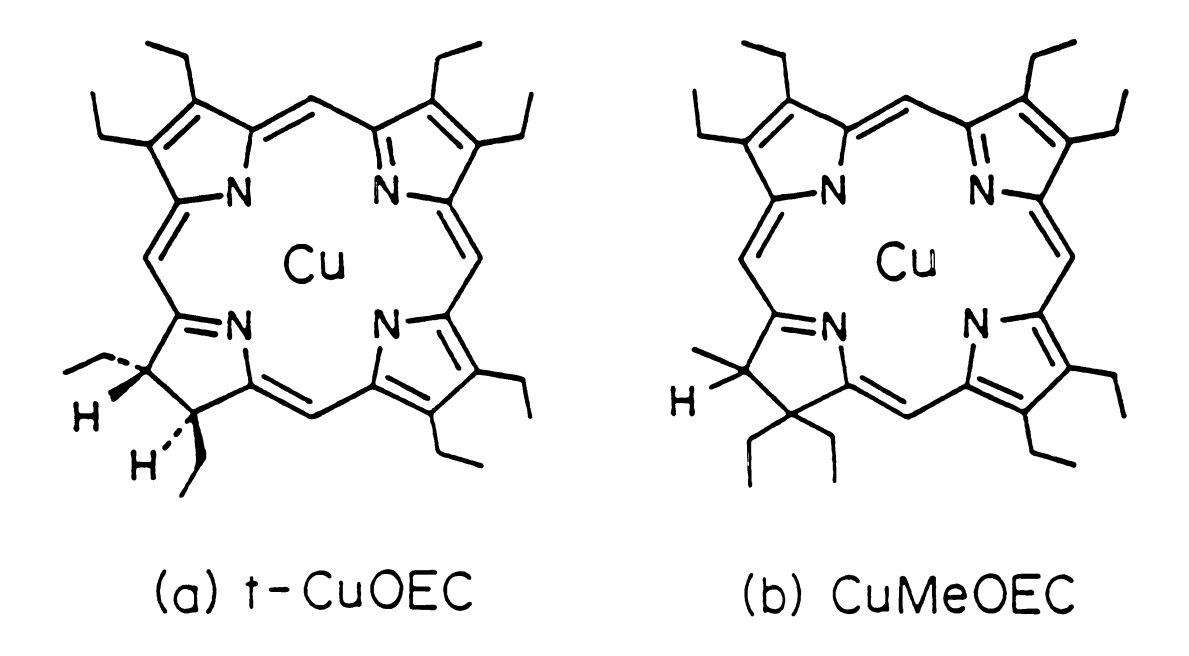


Figure 1. Chemical structures of copper(II) derivatives: (a) trans-octaethylchlroin (t-OEC); (b) methylcotaethylchlorin (MeOEC).

Materials and Methods. t-H₂OEC and H₂MeOEC were prepared according to the published methods.^{17,18} Metal insertion was carried out by adding a saturated CH₃OH solution of M(OAC)₂·XH₂O-NaOAC to a CH₂Cl₂ solution of the free base chlorins. Metallochlorins were oxidized chemically at room temperature according to the AgClO₄/CH₂Cl₂ method.¹⁹ The progress of the reaction was followed spectrophotometrically until complete oxidation was achieved. The color change is diagnostic: the initial purple-blue (Cu) or green (Co,Ni) color of the neutral chlorin complex changes to yellow.

Absorption spectra were measured on Shimadzu UV-160 and Cary 219 spectrophotometers. The 363.8 nm line used to record the RR spectra was obtained from a Coherent Innova 100-20 argon ion laser, the Raman equipment is described in detail elsewhere.¹⁵

The integrity of the samples was verified by monitoring the absorption spectra before and after recording the Raman spectra. Cu(II), Co(II), and Ni(II) complexes of MeOE, as well as that of t-CuOEC, were sufficiently stable under aerobic conditions, and for this reason samples were not routinely degassed. The corresponding cation radicals were also tractable over the course of RR study with minimal decomposition. On prolonged irradiation, t-CuOEC+• decomposed to CuOEP (Soret = 397 nm) for the most part, whereas MeOEC+• complexes returned to the neutral state.

Results and Discussion. Optical spectra of CuMeOEC and its one-electron oxidation product are shown in Figure 2. The cation radical exhibits a split Soret band compared with that of the neutral species, which shows a single maximum. The characteristic band in the 600 nm region disappears in the spectrum of the cation radical and is replaced by several weak, broad bands

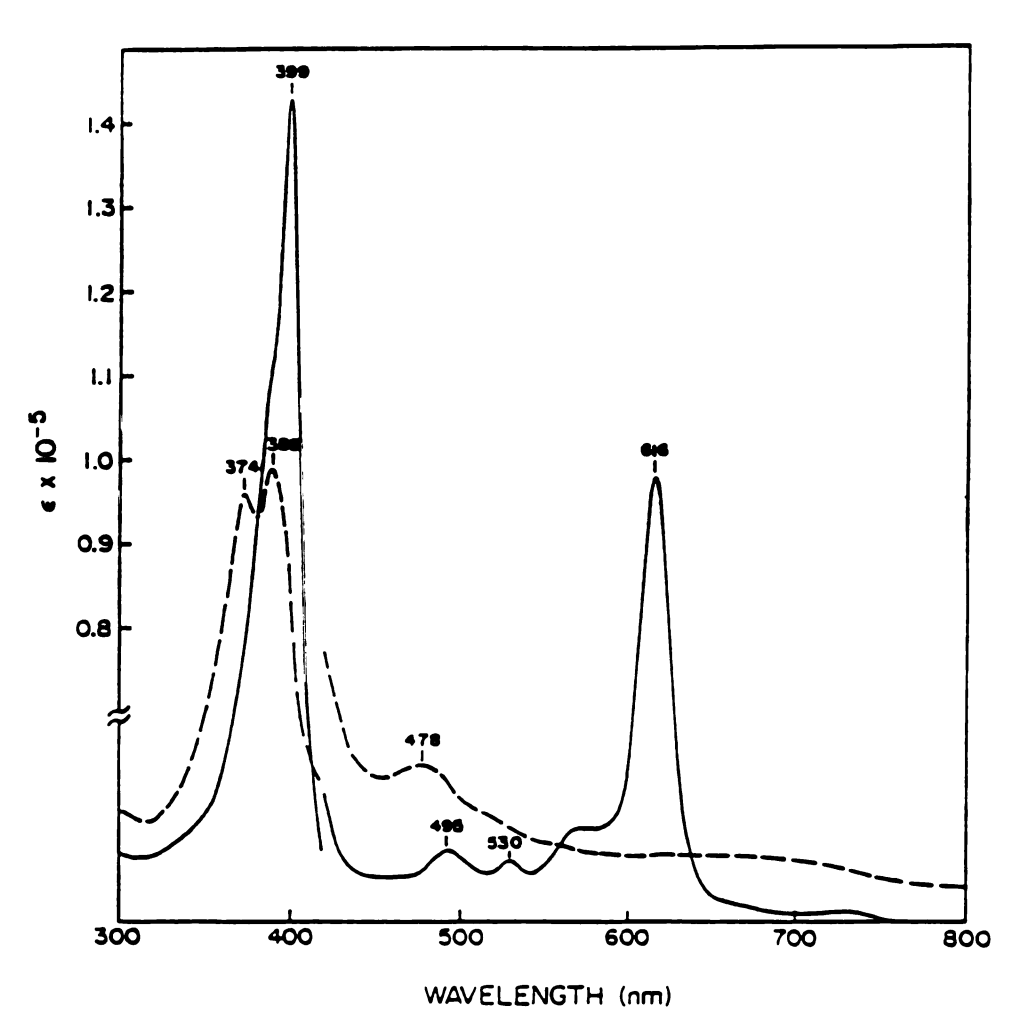


Figure 2. Optical absorption spectra of CuMeOEC(-) and its one-electron oxidation product, CuMeOEC+-ClO₄- (---) in CH₂Cl₂.

that extend into the near infrared region. Figures 3 and 4 show the RR spectra of t-CuOEC 1, and the Cu(II) 2, Co(II) 3, and Ni(II) 4 complexes of MeOEC and their one-electron oxidation products, respectively. The methyl substituted Cu chlorin complex, 2, exhibits a Raman spectrum that is nearly identical to that of the corresponding Cu trans-OEC complex, 1, in both its neutral and its oxidized state. The only clear exceptions to this generalization are slight frequency shifts in lines that occur at 1508 and 1602 cm⁻¹ in 1 and the splitting of the line that occurs at 1204 cm⁻¹ in 2 into two features at 1198 and 1212 cm⁻¹ in 1. We conclude that the added stability imparted by alkyl substitution of the chlorin radicals may be gained without serious alterations to the vibrational properties of the dihydro trans-octaethylchlorin macrocycle.

Relative to the Raman spectra of MP, those of MC are considerably more complex owing to the symmetry reduction in proceeding from D4h in the MP case to at least C_{2V} for the MC complexes, to increased macrocycle conformational flexibility, and to the likelihood of changes in normal mode composition of the chlorin macrocycle vibrations compared to those of the analogous porphyrin. 20,21,22 As a result, additional modes become Raman allowed in the metallochlorins. This effect is evident in the spectra in Figures 3 and 4. For example, in the 1360-1390 cm⁻¹ region of the neutral MC species at least three modes are apparent; in the case of the corresponding metalloporphyrins only a single mode (v4) is generally observed. Likewise, in the higher frequency region $\Delta \nabla > 1500$ cm⁻¹), where macrocycle stretching modes with $C_a C_m$ and $C_b C_b$ character occur, the MC spectra are more complex. For example, Boldt et al. have identified ten vibrations in the 1450-1700 cm⁻¹ region of the RR spectra of t-NiOEC (solid state) by using excitation at various wavelengths. In the present study, we focus on two

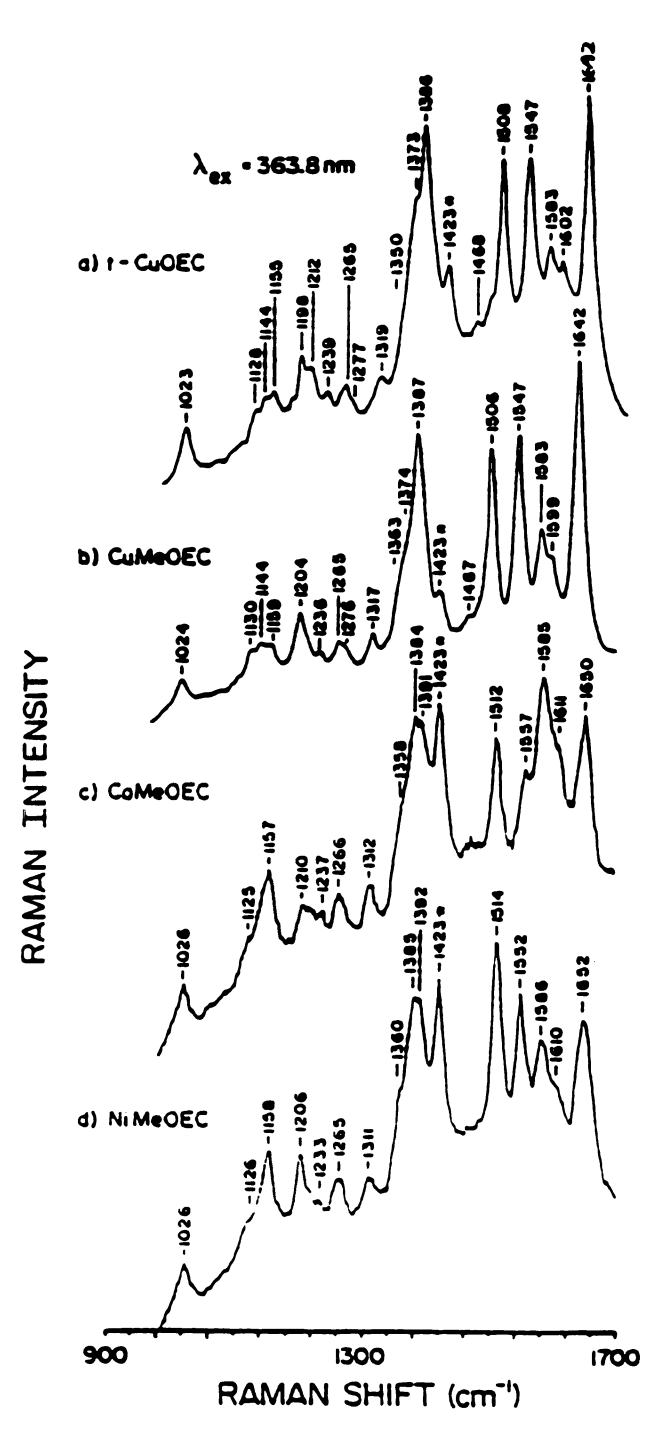


Figure 3. Near-uv RR spectra of t-CuOEC (a), Cu (b), Co (c), Ni (d) complexes of MeOEC. The laser power was 20-30 mw. The solvent (CH₂Cl₂) band at 1423 cm⁻¹ is labeled with an asterisk (*).

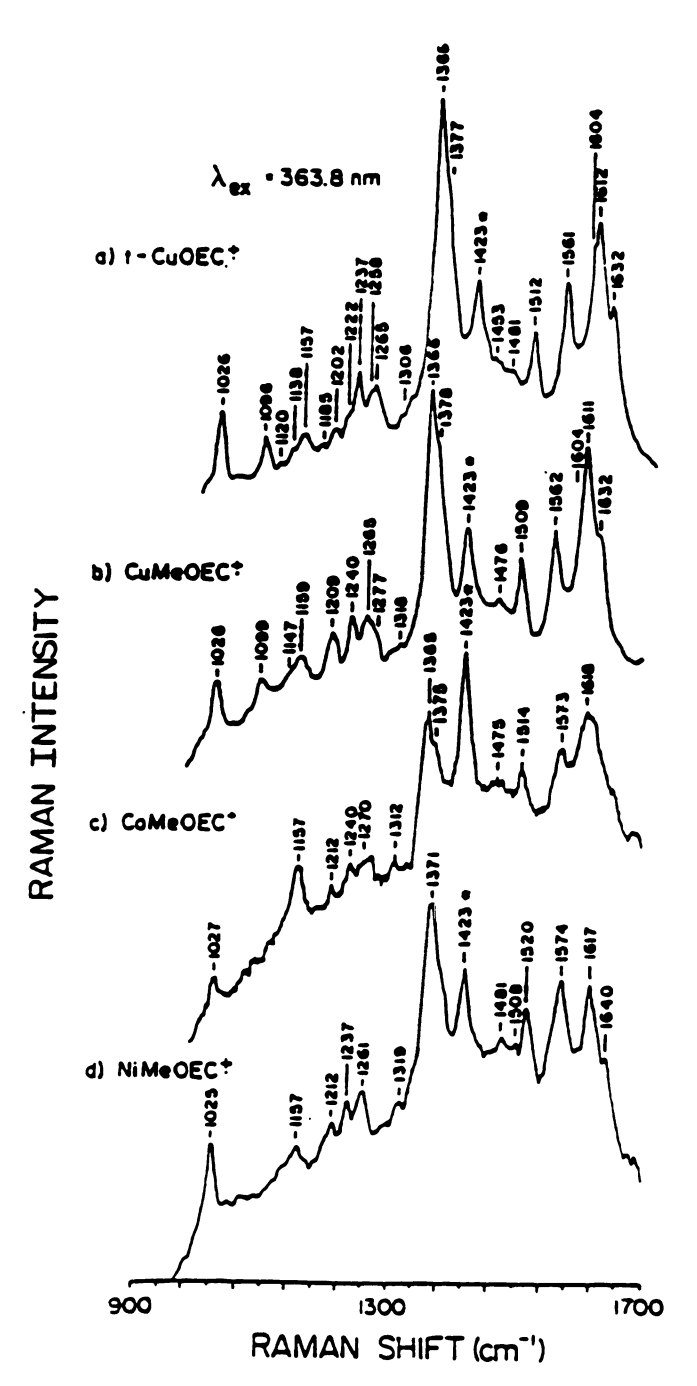


Figure 4. RR spectra of (a) t-CuOEC++, (b) CuMeOEC++, (c) CoMeOEC++, (d) NiMeOEC++. The laser power was 20-30 mw. The solvent (CH₂Cl₂) band at 1423 cm⁻¹ is labeled with an asterisk (*).

modes in the 1500-1520 cm⁻¹ and 1620-1650 cm⁻¹ region that have analogy to those that are referred to as v_3 and v_{10} vibrations, respectively, in the porphyrin analogs. These modes are clearly defined in all species and exhibit a strong core-size dependency in the porphyrin complexes.

We have applied the empirical correlation first reported by Spaulding et al. between the Raman frequency and the macrocycle core-size to the v_{10} -and v_{3} - like vibrations of the chlorins.²⁴ The parameters $K(cm^{-1}/Å)$ and A(Å) in the relationship, $\Delta \nabla = K(A-d)$, have been estimated by making the following assumptions. First, the core size (d,Å) remains constant upon oxidation of the macrocycle in the chlorin complexes, as we have found for the metalloporphyrin systems¹⁵ and second, we may use the core-size distances already established for the porphyrin counterparts.²⁴ Based on limited x-ray crystal data on the chlorin system, however, the latter assumption may not be fully accurate.²⁵

Table 1 summarizes the pattern of frequency shifts observed for the v_{10} - and v_3 -like vibrations, as well as the optical absorption shifts of the Soret band maxima, associated with both porphyrin and chlorin metal complexes when they are oxidized at the ring. Table 2 lists the K and A values for these vibrations. A number of observations concerning the v_{10} and v_3 vibrations of the MC/MC+· and MP/MP+· complexes require comment. Because the relatively high K values for the v_{10} modes of both systems are similar (- 400 cm⁻¹/Å), we conclude that these vibrations are predominantly C_aC_m character in both cases. On the other hand, for the v_3 mode, we see that the K values for the MP/MP+· system (~ 380 cm⁻¹/Å) are significantly higher than those of Mc/MC+· system (~ 300 cm⁻¹/Å). This implies that the percentage

 C_aC_m character in chlorin vibration is correspondingly lower than in the porphyrin v₃ vibration. In MOEP, the v₃(C_aC_m) vibration has no C_bC_b character. However, the v₃-like chlorin vibration around ~ 1500 cm⁻¹ may have substantial C_bC_b character. The contribution of C_bC_b character to this mode in the chlorins is implied by the lower K value and may also be realized by comparing its frequency in copper cis-dihydroxyoctaethyl chlorin²¹ at 1500 cm⁻¹ with those of 1 and 2 at 1508 and 1506 cm⁻¹ in the neutral species and at 1512 and 1509 cm⁻¹ in the cation radicals, respectively. The frequency variation with the change in peripheral substituents on the chlorin ring implies a contribution from the C_bC_b stretching coordinate to this normal mode.²⁶ Thus, attaching the v₃ label to this chlorin macrocycle vibration does not imply that the normal mode composition is the same as in the porphyrin case. For this mode, at least, our analysis supports that of Boldt et al.²² who argued that the normal coordinates in the metallochlorins may be significantly different than those in metalloporphyrins.

In previous work, we found that a general pattern of frequency shifts occurred in the MP+ \cdot relative to their neutral MP precursors. Modes that have significant C_bC_b character were found to increase; whereas, those that are principally C_aC_m and C_aN in character decrease relative to the neutral metalloporphyrin.¹⁵ We also concluded that there was little expansion or contraction of the macrocycle core upon oxidation and that the normal mode composition in the neutral precursor was largely preserved in the π -cation radicals, at least for those high-frequency modes. Specific deuteration experiments on the MP and MP+ \cdot species provide support for these conclusions.²⁷

The data in Table 2 indicate that the K values for the v_3 and v_{10} vibrations in both the MP and MC systems do not change significantly upon oxidation to the corresponding MP+ and MC+ system. This implies that the PED of these chlorin vibrations also remains relatively constant upon oxidation. Table 1 reveals, however, that the empirical observations made concerning frequency change due to oxidation for the v₃ and v₁₀ modes in the MP/MP+· system do not apply directly to the corresponding MC/MC+· vibrations. In the chlorin case, the v3 frequency increases upon oxidation. We consider this as further evidence for C_bC_b stretching contribution to this mode, as the small increase (~ 3 cm⁻¹) in the frequency of this mode upon oxidation in 1-4 may be the result of offsetting effects. metalloporphyrin case, CbCb character causes a strong frequency increase, whereas C_aC_m stretching coordinate contributions cause a weak frequency decrease. Thus, the result of mostly C_aC_m and small C_bC_b character is a slight frequency increase upon oxidation. We also note that the change in v_{10} frequency that occurs upon oxidation, though qualitatively similar, is perhaps larger in the chlorin than in the porphyrin case.

In the 1540-1620 cm⁻¹ region of the CuMeOEC+· spectrum, we recognize two modes at 1604 and 1612 cm⁻¹ that appear to have substantial C_bC_b stretching character. These modes have similarities to the v₁₁ and v₂ vibrations that occur in CuOEP+· at 1600 and 1610 cm⁻¹, respectively. Further confirmation and resolution of the modes in this region will be provided by selective isotopic labelling, core-size plots, IR, and both visible and Soret excitation RR measurements, which are in progress.

Two points follow from the data presented in this study.

- The alkyl-substituted MMeOEC complex serves as a suitable system for the resonance Raman characterization of its ring-centered oxidized species; serious alteration of the vibrational properties of the chlorin macrocycle in this species, as compared to those of t-OEC system, does not occur.
- 2. The preliminary core-size plots as well as the pattern of frequency shifts observed for the v3 and v10 vibrations upon oxidation reveal similarity of the chlorin and porphyrin complexes; however, differences in the normal mode composition and the number of Raman allowed vibrational modes between the two systems will provide an additional source of complexity in the spectral analysis of the metallochlorin species.

Table I Resonance Raman Frequencies (cm $^{-1}$) and Optical Absorption Maxima (nm) for Parent MOEP and MMeOEC and Their Corresponding π -Cation Radicals

Compound	v 3	v3 ⁺ ·	Δv ₃ OX	v 10	v ₁₀ +•	Δν ^{OX} ₁₀	Sore Neutral	et, nm Oxidized
Mi OEP	1519	1511	-8	1655	1651	-4	391	377
MeOEC	1514	1520	•6	1652	1640	-12	399	368, 391
Co OEP	1512	1505	-7	1647	1642	-5	391	376
MeOEC	1512	1514	•2	1650	-1639	-11	392	368, 382
Cu OEP	1502	1497	-5	1636	1631	-5	397	383
MeOEC	1506	1509	•3	1642	1632	-10	399	374, 389
Zn OEP	1485	1477	-8	1618	1617	-1	400	387
MeOEC ^b	1490	1490	0	1619	1608	-11	400	381, 392

Abbreviations: v_3^+ , the v_3 frequency (cm-1) of the cation radical: Δv_3^{OX} frequency shift (cm⁻¹) for the v_3 vibration due to one-electron oxidation ($\Delta v_3^{OX} \cdot v_3^+ \cdot v_3^-$): the preceding descriptions also apply to v_{10}^+ and Δv_{10}^{OX} , respectively.

^a porphyrin data taken from: Oertling et al. (J. Phys. Chem. 1987, 91, 5887 - 5898): chlorin data from this work.

^b ZnMeOEC was oxidized by a dilute methanolic solution of iodine in CH₂Cl₂ (RR spectra not shown).

Table II

Estimated K(cm⁻¹/Å/) and A(Å) Values for the ν and ν Vibrations of the Parent MOEP, MMeOEC and Their π -cation Radicals

Parameters	Parameters		v ₃ +•	v ₁₀ v ₃ +·		
MOEP,	K	383	384	415	377	
	A	5.93	5.90	5.94	6.33	
MMeOEC,	K	278	334	385	375	
	A	7.41	6.51	6.26	6.34	

Abbreviations: v_3^+ and v_3^+ , the v_3 and v_{10} frequencies (cm⁻¹) of the cation radical, respectively.

REFERENCES

- 1. Mathies, P.; Rutherford, A. W. In "Photosynthesis," Amesz, J. Ed., Elsevier: Amsterdam, 1987, 63.
- 2. Ranger, G., Angew. Chem. Int. Ed. Engl., 1987, 26, 643.
- 3. Davis, M. S.; Forman, A.; Fajer, J., Proc. Nat. Acad. Sci. (USA), 1979, 76, 4170.
- 4. O'Malley, P. J.; Babcock, T. G., Proc. Nat. Acad. Sci. (USA) 1984, 81, 1098.
- 5. Hoff, A. J., In "Antennas and Reaction Centers of Photosynthetic Bacteria", Michal-Beyerle, M. E., Ed., Springer: Berlin, 1985, 150.
- 6. Lutz, M., In "Advances in Infrared and Raman Spectroscopy", Clark, R. J. and Hester, R. e., Ed., Wiley Heyden: New York, 1984, Vol. 11, 211.
- 7. Fuhrhop, J.-H., Z. Naturforsch, 1970, 256, 255.
- 8. Chang, C. K.; Hanson, L. K.; Richardson, P. F.; Young, R.; Fajer, J., Pre. Nat. Acad. Sci. (USA), **1981**, <u>78</u>, 2653.
- 9. Chang, C. K., In "The Biological Chemistry of Iron", Dunford, H. B., Ed., Reidel, D.: Philadelphia, 1982, 313.
- 10. Hanson, L. K.; Chang, C. K.; Davis, M. S.; Fajer, J., J. Am. Chem. Soc., 1981, 103, 663.
- 11. Fujita, E.; Chang, C. K.; Fajer, J. Am. Chem. Soc., 1985, 107, 7665.
- 12. Stolzenberg, A. M.; Stershic, M. T., Inorg. Chem., 1987, 26, 1790.

- 13. Scheer, H.; Inhoffen, H. H., In "The Porphyrins", Dolphin, D., Ed., Academic Press: New York, 1978, Vol. II, 45.
- 14. Jacob, G. S.; Orme-Johnson, W. H., Biochemistry, 1979, <u>18</u>, 2967.
- 15. Oertling, W. A.; Salehi, A.; Chung, Y. C.; Leroi, G. E.; Chang, C. K.; Babcock, G. T., J. Phys. Chem., 1987, 91, 5887.
- Salehi, A.; Oertling, W. A.; Babcock, G. T.; Chang, C. K., Inorg. Chem., 1987, 26, 4296.
- 17. Whitlock, Jr., H. W.; Hanauer, R.; Oester, M. Y.; Bower, G. K., J. Am. Chem. Soc., 1969, 91, 7485.
- 18. Chang, C. K., Biochemistry 1980, 19, 1971.
- 19. Salehi, A.; Oertling, W. A.; Babcock, G. T.; Chang, C. K., J. Am. Chem. Soc., 1986, 108, 5630.
- 20. (a) Ozaki, Y.; Iriyama, K.; Ogoshi, H.; Ochia, T.; Kitagawa, T., J. Phys. Chem. 1986, 90, 6105.
 - (b) Ozaki, Y., Iriyama, K.; Ogoshi, H., Kitagawa, T., J. Phys. Chem., **1986**, 90, 6113.
- 21. Andersson, L. A.; Sotiriou, C.; Chang, C. K.; Loehr, T. M., J. Am. Chem. Soc., 1987, 109, 258.
- Boldt, N. J.; Donohoe, R. J.; Birge, R. R.; Bocian, D., J. Am. Chem. Soc., 1987, 109, 2284.
- 23. Abe, M.; Kitagawa, t.; Kyogoku, Y., J. Chem. Phys., 1978, <u>69</u>, 4526.
- 24. Spaulding, L. C.; Chang, C. C.; Yu, N. -T.; Felton, R. H., J. Am. Chem. Soc., 1975, 97, 2517.
- 25. Strauss, S. H.; Silver, M. E.; Ibers, J. A., J. Am. Chem. Soc., 1983, 105, 4108.
- 26. Callahan, P. M.; Babcock, G. T., Biochemistry, 1981, 20, 952.
- 27. Oertling, W. A.; Salehi, A.; Chang, C. K.; Babcock, G. T., J. Phys. Chem., submitted.

Supplementary Material: In order to facilitate a detailed investigation of vibrational mode assignments of the chlorin ring macrocycle at both the neutral and π -cation radical levels, selectively deuterated transoctaethylchlorin derivatives have been prepared which will be addressed in the following section; the normal mode assignments, however, will be the subject of a future work and will be presented elsewhere by other coworkers (Harold N. Fonda and Anthony W. Oertling).

Preparation of trans-octaethylchlorin- $d_2(\alpha,\beta)$, $-d_2(\gamma,\delta)$, and $-d_4$ as well as octaethylporphyrin- d_2 using acid-catalyzed exchange reaction

Deuteration of the methine (meso) bridges of tetrapyrrolic macrocycles has contributed to a better understanding of the hemoproteins' electronic and vibrational characteristics by utilizing methods such as ESR(1,2), ENDOR (3,4), NMR (5,6), IR(7,8) and resonance Raman (9,10) spectroscopy. The relative reactivities of the four methine carbons for hydrogen-deuterium (H/D) exchange result primarily from the ease of electrophilic substitution at these sites which, in turn, depends upon the nature of the substituents on the adjacent pyrrole rings (11,12,13). For example, it has been shown that transoctaethylchlorin (t-OEC) undergoes facile H/D exchange at γ ,8-meso carbons in refluxing acetic acid-d1; whereas, α , β -bridges are not affected (14). The exchange reactions, carried out on metal free systems, are generally acid-catalyzed and a number of acidic media have been reported, including D2SO4-D2O (11), toluenesulfonic acid-d1 (15), TFA-d1 (12), and acetic acid-d1 (16). The D2SO4-D2O method represents a strong acidic condition which is routinely used to induce H/D exchange reaction at all four methine carbons

in symmetrically substituted ring systems (12). In one instance, however, it has been applied to the oxoporphyrin complexes in which deuteration occurs predominantly at two bridging carbons and the other two sites undergo minimal exchange (17). The D2SO4-D2O method is usually carried out at ambient temperature in contrast with the refluxing and/or anaerobic condition required by other methods.

We report here a modification of the original D₂SO₄-D₂O reaction condition (11) which may be used for the preparation of three forms of selectively deuterated trans-octaethylchlorin(t-OEC-d₂(α , β),-d₂(γ , δ), and -d₄), Figure 5a. The dideuterated chlorin species may then be oxidized to the corresponding octaethylporphyrin-d₂, Figure 5b, which would otherwise be difficult to prepare and may reveal interesting spectroscopic properties.

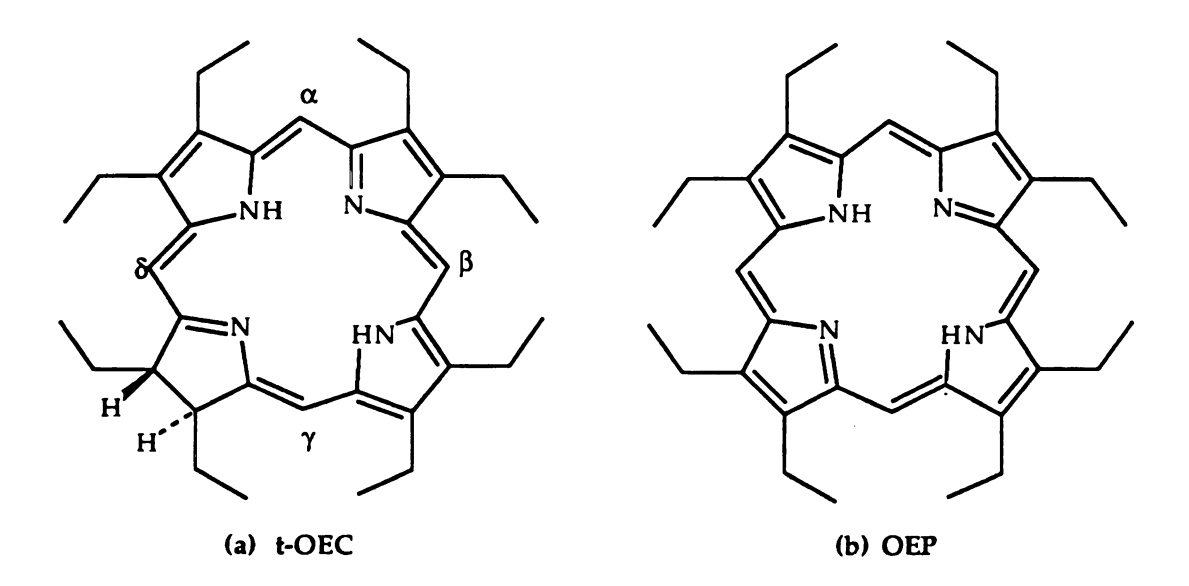


Figure 5. Chemical Structures

EXPERIMENTAL

OEP and t-OEC were synthesized according to the published methods (18, 19). Proton NMR spectra were obtained at 250 MHz on a Bruker spectrometer in deuterated chloroform with the solvent signal as an internal standard. Chloroform-d1 (99.8 atom percent D), D2O (99.8 atom percent D) and 98 percent sulfuric acid-d2 in D2O (99.5 atom percent D) were obtained from Aldrich Chemical Co. Dichloromethane was freshly distilled from CaH2. All other solvents were reagent grade and were used without further purification. The extent of deuteration was estimated by integration of the proton NMR spectra. Column chromatography was performed on Alcoa basic alumina (type F-20).

trans-octaethylchlorin-d2(γ , δ)

In a typical experiment, 10 mg of t-OEC was equilibrated in 2.1 ml of D₂SO₄:D₂O (6:1,v/v) and allowed to sit at room temperature in a desiccator for 20 hours. The solution was then quenched with ice water and extracted with dichloromethane. The extract was washed with sodium bicarbonate and with water and dried over anhydrous sodium sulfate. At this point, the sample may contain about 2-3 percent OEP which results from oxidation of t-OEC. This was demonstrated by t.l.c. and by proton NMR spectrum (OEP meso-proton peak at δ 10.2). Purification was carried out on alumina with benzene as eluant. Quantitative deuteration was established by the disappearance of the γ , δ - proton signal at 8.9 ppm, Figure 6c. MS: m/e 538(M+), 509(M+-29), 269(M++), Figure 7b; m.p. 231-232°C.

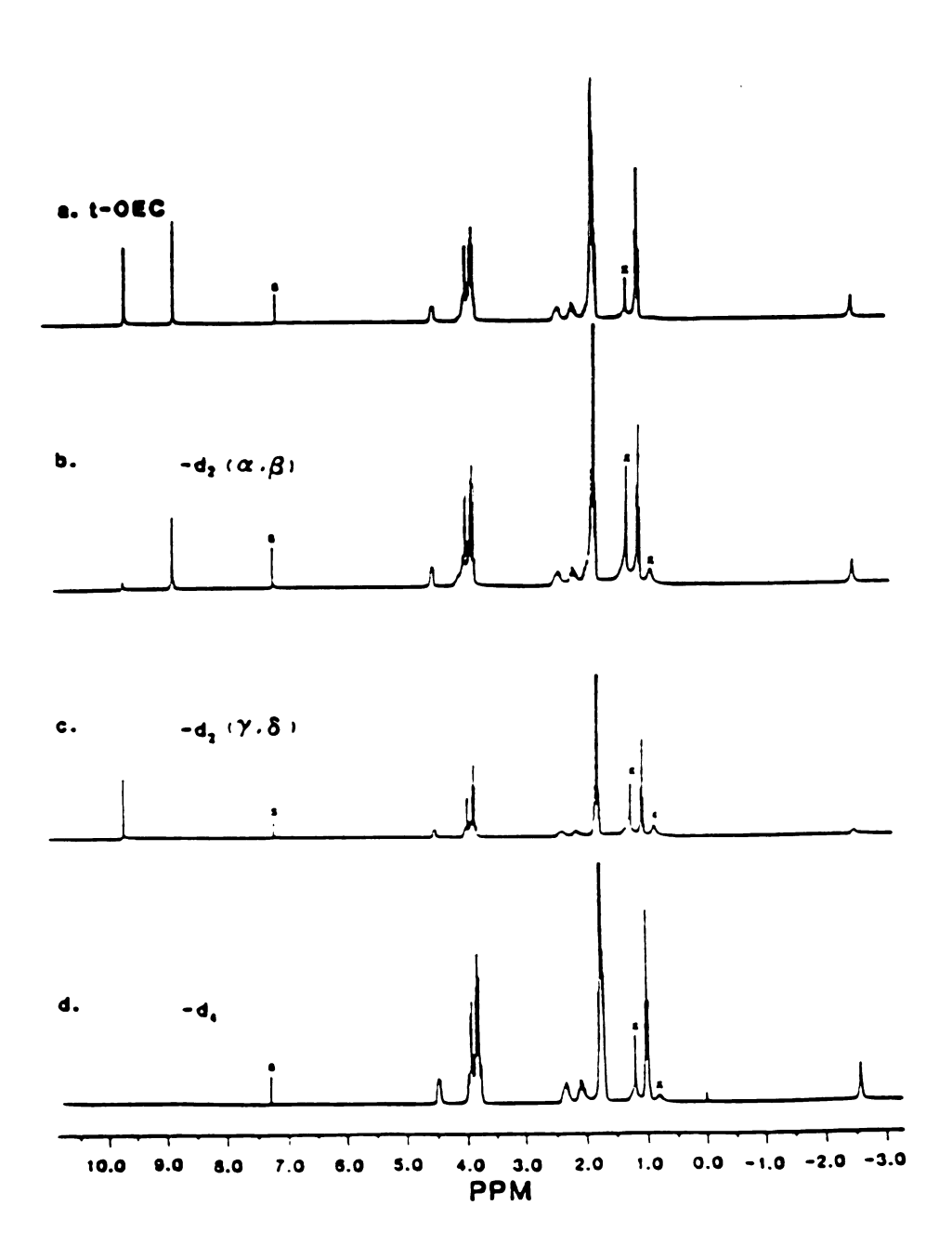
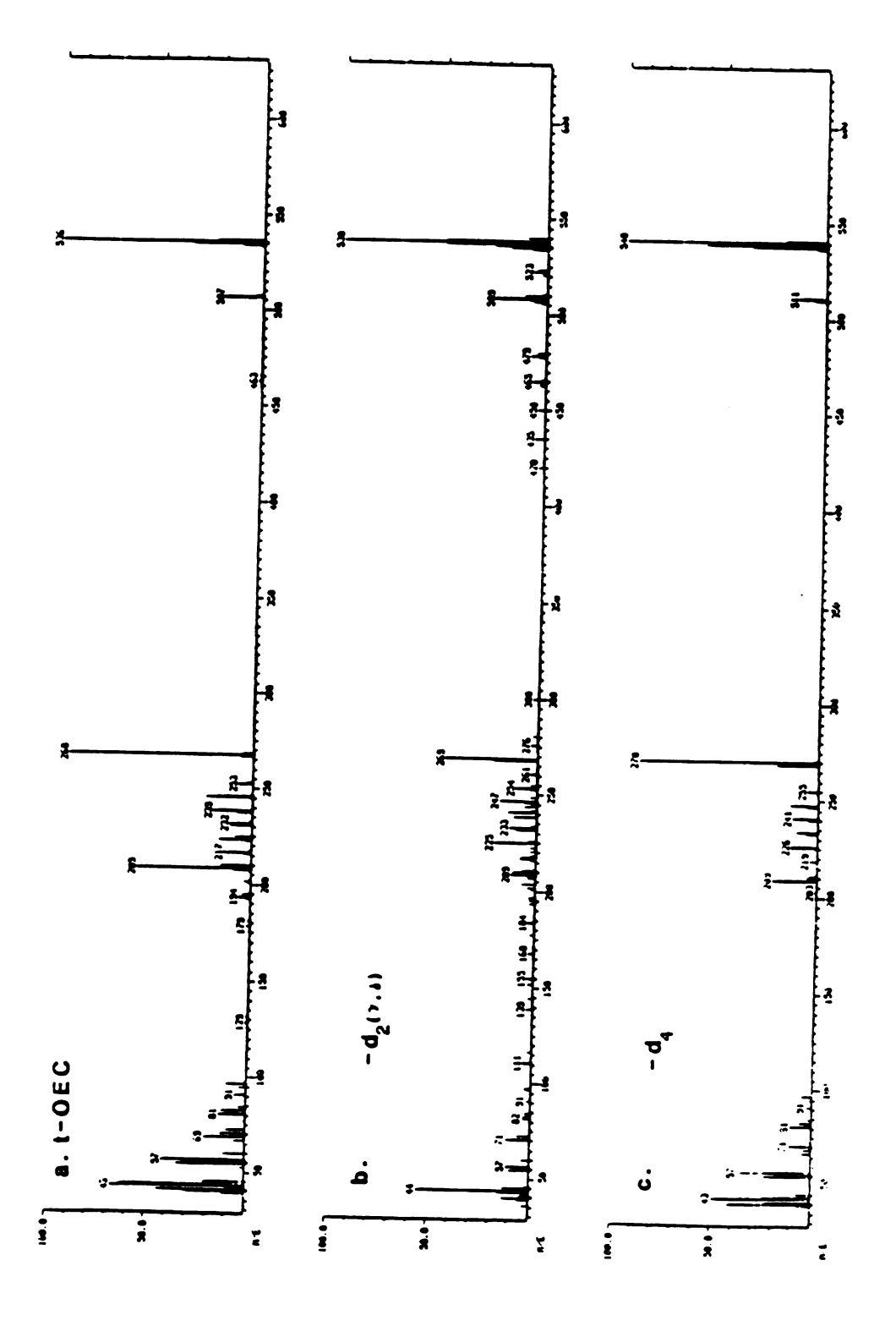
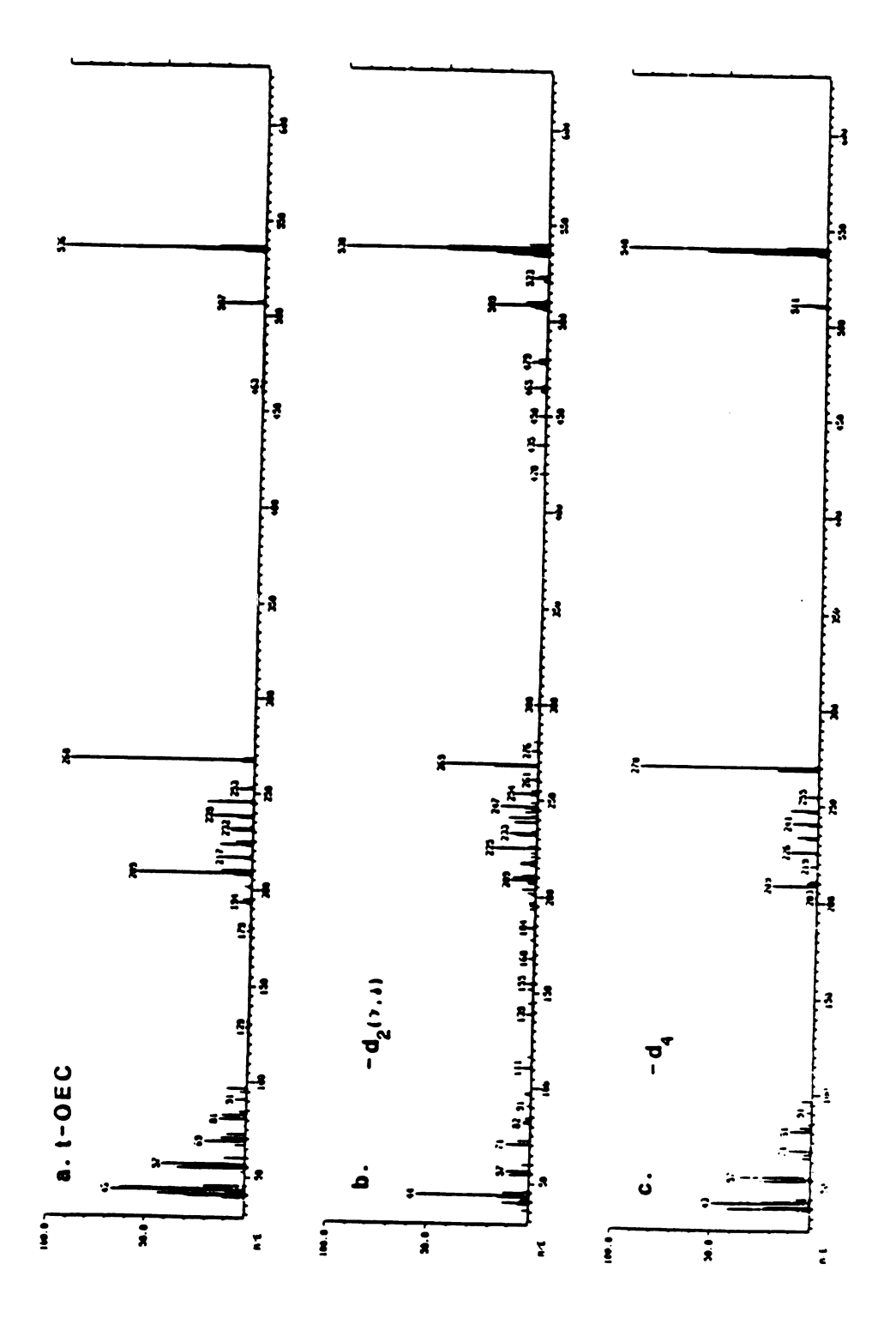


Figure 6. 250-MHZ proton NMR spectra of t-OEC and its deuterium labeled derivatives in CDCl₃. S indicates residual undeuteriated solvent and X represents other impurities.



The electron impact mass spectra (EI-MS) of trans-octaethylchlorin and its deutero derivatives at 70 ev. Figure 7.



The electron impact mass spectra (EI-MS) of trans-octaethylchlorin and its deutero derivatives at 70 ev. Figure 7.

trans-octaethylchlorin-d4

The tetradeuterated species was prepared by the same method as described above; however, the sample was permitted to sit at room temperature for ~ 72 hours. One hundred percent deuteration was established by the disappearance of proton NMR signals at 8.9 and 9.7 ppm due to γ , δ - and α , β - protons, respectively, Figure 6d. MS: m/e 540(M+), 511 (M++), Figure 7c.

trans-octaethylchlorin- $d_2(\alpha, \beta)$

t-OEC-d4 (10 mg) was subject to "back-exchange" in 2.1 ml of H2SO4(96.4 percent):H2O(6:1, v/v) followed by the same work-up as mentioned above. This method gave ~ 90 percent deuteration at α,β -position and complete proton recovery at the γ,δ - sites, Figure 6b.

octaethylporphyrin-d2

To a refluxing dichloromethane solution of dideuterochlorin was added a solution of DDQ (excess) in benzene according to the published methods (20,21). The green color of the chlorin solution turned red almost instantaneously. After refluxing for an additional 0.5 h, the solution was evaporated to dryness and chromatographed on alumina with chloroform. The visible absorption spectrum and the proton NMR signal at δ 10.2 showed the characteristic OEP spectrum. MS: m/e 536(M+), 507(M+-29), and 268(M++); m.p. 322-324°C.

CONCLUSION

The original procedure reported for the tetradeuteration of OEP (80 mg in D2SO4:D2O, 2 ml; 9:1, w/v) has been modified to prepare three forms of selectively deuterated trans-octaethylchlorin; namely, $-d_2(\alpha,\beta)$, $-d_2(\gamma,\delta)$, and $-d_4$ derivatives. This method offers an alternative approach to that of acetic acid-d1 for H/D exchange at ambient temperature in unsymmetrically substituted tetrapyrrolic macrocycles. It is also particularly attractive for deuterium labeling in systems where prolonged refluxing conditions are not desirable. The partially-deuterated porphyrin and chlorin complexes are currently being utilized to verify the proposed "quadrant-localized" vibrational modes in the chlorin macrocycles²², by means of IR and resonance Raman spectroscopy.

REFERENCES

- Fajer, J., Borg, D.C., Forman, A., Dolphin, D., J. Am. Chem. Soc., 1970, 42: 3451.
- 2. Mengersen, C., Subramanian, J., Fuhrhop, J.W., Smith, K. M., Z. Naturforsch, 1974, 29a: 1827.
- 3. Norris, J. R., Scheer, H., Druyan, M.E., Katz, J.J., Natl. Acad. Sci. USA, 1974, 71: 4897.
- 4. Feher, G., Hoff, A.J., Isaacson, R.A., Ackerson, L.C., Ann. N. Y. Acad. Sci., 1975, 244: 239.
- 5. Morishima, I., Takamuki, Y., Shiro, Y., J. Am. Chem. Soc., 1984, 106: 7666.
- 6. Godziela, G.M., Goff, H.M., J. Am. Chem. Soc., 1986, <u>108</u>: 2237.
- 7. Urban, M. W., Nakamoto, K., Kincaid, J., Inorg. Chim. Acta, 1982, 61: 77.
- 8. Kincaid, J. R., Urban, M. W., Watanabe, T., Nakamoto, K., J. Phys. Chem., 1983, 87: 3096.
- 9 Ozaki, Y., Kitagawa, T., Ogoshi, H., Inorg. Chem., 1979, <u>18</u>: 1772.
- 10. Andersson, L. A., Sotiriou, C., Chang, C. K., Loehr, T. M., J. Am. Chem. Soc., 1987, 109: 258.
- 11. Bonnett, R., Stephenson, G.F., Proc. Chem. Soc., 1964, 291.
- 12. Bonnett, R.; Gale, I. A. D., Stephenson, G. F., J. Chem. Soc. (c), 1967, 1168.
- 13. Smith, K. M., Langry, K. C., deRopp, J. S., J. Chem. Soc. Chem. Comm., 1979, 1001.

- 14. Cavaleiro, J. A. S., Smith, K. M., J. Chem. Soc., Perkin Trans. 1973, 1, 2149.
- 15. Hickman, D.L., Goff, H.M., J. Am. Chem. Soc., 1984, <u>106</u>: 5013.
- 16. Woodward, R. B., Skaric, V., J. Am. Chem. Soc., 1961, 83: 4676.
- 17. Stolzenberg, A. M., Laliberte, M. A., J. Org. Chem., 1987, <u>52</u>: 1022.
- 18. Wang, C. B., Chang, C. K., Synthesis, 1979, 548.
- 19. Whitlock, Jr., H. W., Hanauer, R., Oester, M. Y., Bower, B. K., J. Am. Chem. Soc., 1969, 91: 7485.
- 20. Eisner, V., Linstead, R. P., J., 1955, 3749.
- 21. Barnett, G. H., Hudson, M. F., Smith, K. M., Tet. Lett., 1973, 2887.
- 22. Boldt, N. J., Donohoe, R. J., Birge, R. R., Bocian, D., J. Am. Chem. Soc., 1987, 109: 2284.

CHAPTER V

NOVEL β-PYRROLIC SUBSTITUTION REACTIONS OF TETRAPERFLUOROPHENYLPORPHYRIN

Tetraperfluorophenylporphyrin (TFPP) is an electron-deficient porphyrin having highly electron-withdrawing yet chemically inert mesoperfluorophenyl substituents. This pattern of peripheral substitution is expected to raise the redox potentials of the porphyrin macrocycle dramatically. For example, half-wave potentials of TFPPFeCl are positively shifted by 0.4 and 0.32 V with respect to those of TPPFeCl for the first and second oxidation waves, respectively. On the other hand, flouring substitution, particularly on phenyl C-2 and C-6 positions, provide the porphyrin ring with added steric protection against oxidative attack which is commonly directed at the meso carbons. This reaction often results in the cleavage of the ring and formation of an open-chain tetrapyrrolic structure.2 This type of electrophilic substitution is operative in biological heme catabolism and it has also been demonstrated with the OEP and TPP model compounds.³ Thus, increased stability against self-destruction as well as higher oxidation potentials make the TFPP system a powerful oxidation catalyst for the study of cytochrome P-450 mediated reactions.⁴ For example, Chang and Ebina have shown that the TFPPFeCl-catalyzed hydroxylation of cyclohexane to cyclohexanol proceeds in 71% yield compared with the 5%

yield obtained from TPPFeCl.⁵ Apparently, the electron-deficient TFPP complex forms a more reactive and electrophilic oxene complex (TFPP+•Fe^{IV}=0).

During a chemical and spectroscopic investigation of the metallo TFPP complexes, Gouterman and coworkers observed a new series of TFPP adducts. These adducts were formed when the free base was treated with AgNO3 in acetic acid or, alternatively, the corresponding metal derivatives (e.g., Ag^{2+} , Nz^{2+} , Zn^{2+} and Cu^{2+}) were dissolved in acetic acid in the presence of catalytic amount of concentrated nitric acid, under refluxing condition.

This work aims to elucidate the structures of these TFPP, derivatives by Uv-vis, FAB-MS and ¹H-NMR studies.

General Characteristics of TFPP

- a. Reduced Affinity to Metal Ions: The insertion of Co^{2+} ion, for example, into $H_{2}TPP$ may be carried out by refluxing a chloroform-methanol solution of the free base containing cobaltous chloride (or acetate), while under identical condition, most of $H_{2}TFPP$ remains as a free base even after 24 hours. Thus, CoTFPP may be prepared by refluxing an acetic acid solution of $H_{2}TFPP$ which contains a large molar excess (10x) of cobaltous acetate.
- b. Resistance Toward Acid Demetallation: NiTFPP, for example, resists demetallation considerably. NiTPP can be completely demetallated with H₂SO₄ at RT, while a super acid (e.g., FSO₃H) is required for the TFPP derivative. Gouterman et al. reported an alternative method by refluxing a trifluoro acetic acid solution of NiTFPP for ~ 72 hours. 14
- c. Reduced Proton Affinity: H₂TFPP exists as free base in acetic acid. In a marked contrast, H₂OEP exists as a monocation in acetic acid.⁶ The great dicationic salt of H₂TFPP may readily be formed by the addition of TFA,

HNO₃ and HClO₄ to a dichloromethane solution of the free base. Table I summarizes the optical changes associated with the formation of $H_4TFPP^2+2X^-$.

Table I. Absorption Spectra (nm) of Dicationic Salt of H₂TFPP in CH₂Cl₂.

Compound	Soret	IV	Ш	П	I
H ₂ TFPP H ₄ TFPP ² +·2X	412	506		583	655
$X^- = TFA^-$	430		538	574	625
NO ₃ -	434		543	579	629
ClO ₄ -	433		?	580	631

The preceding observations as well as the increase in oxidation potentials of TFPFeCl by ~ 0.4V with respect to those of TPPFeCl demonstrate that introduction of the fluoro groups on the phenyl rings results in a significant reduction in the electron density on pyrrolic nitrogens.

d. Optical Absorption Properties: TFPP complexes feature unusual electronic spectra which separate them from other tetraphenyl porphyrins.⁷ The energies of absorption maxima in the free base and the metal derivatives fall between those of OEP at higher energy and TPP at lower energy, Table 2. The most remarkable difference is observed in the spectrum of H₂TFPP in which an absorption maximum near 550 nm (band III) is absent, in contrast with that of H₂TPP.⁷

Table 2. Comparison of H_2TFPP Absorption Maxima (nm) in CH_2Cl_2 with Those of H_2TPP and H_2OEP .

Compound	Soret	IV	Ш	П	I
H ₂ TPP	416	513	547	589	645
H_2^{-} TFPP	412	506		583	655
H ₂ OEP	397	496	531	565	615

Kim and coworkers later confirmed the phenomenological cause of this anomalous behavior.⁸ They found that electron-withdrawing substituents in the phenyl ortho position cause the diminishing of the extinction coefficients of bands I, III, and Soret; whereas, bands II and IV are not affected. Moreover, phenyl substitution in other positions have minimal effect.

The visible absorption spectra of TFPP complexes exhibit strong solvent-dependent maxima shifts, Table 3. Thus, if optical changes, which are accompanied by TFPP substitution reactions, are to be used to partially characterize the newly-formed adducts, the solvent-induced shifts must also be taken into consideration.

Table 3. Solvent-induced Absorption Maxima Shifts (nm) of TFPP Adducts.

Compound	Solvent	Soret	IV	ш	П	I
H ₂ TFPP	DMF	410	504		579	654
	CH_2C1_2	412	506		583	655
	φН	417	508		586	659
	фСН3	417	509	-	586	658
NiTFPP	CH ₂ Cl ₂	404		524, 558		620
	фСН3	407		526, 559		621
	PY	429		553		621
CuTFPP	CH ₂ Cl ₂	408		534, 570		
	фСН3	416		539, 573		
ZnTFPP	CH ₂ Cl ₂	413		543, 577		606
	фСН3	421		547, 580		607

e. 1 H-NMR: H₂TFPP and its Ni²⁺ and Zn²⁺ complexes feature a single peak at 8.50, 8.77 and 8.99 ppm, respectively, in CDCl₃ characteristic of β -pyrrole protons. The upfield shifts of the β -hydrogen peaks in the TFPP adducts as compared with those observed in the TPP system (e.g., H₂TPP, H $_{\beta}$ = 8.75 ppm) has been explained in terms of the degree of buckling of the porphyrin nucleus due to meso-fluorophenyl substituents. Apparently, the steric interaction between the fluoro groups and the β -hydrogens of the pyrrole rings results in increased coplanarity of the phenyl groups with the porphyrin ring in the TFPP system. This, in turn, reduces buckling of the macrocycle and increases the ring current effect.

f. Reversible Oxidation Reactions of MTFPP Derivatives - Electronic Absorption Characteristics: Ferric perchlorate salt, Fe(ClO₄)₃·XH₂O, serves as a chemical oxidant of general utility and provides adequate redox potential for at least single-electron oxidation of all common porphyrins ($\varepsilon_{1/2} \approx 1.2 \text{V vs.}$ SCE). The utility of this oxidant has been demonstrated in several instances in the previous chapters. However, it falls short of oxidizing Cu²⁺ and Ni²⁺ complexes of TFPP. The Zn²⁺ adduct demetallates immediately upon oxidation. This may result from 1) large ionic radius of Zn²⁺ ion, 2) electron-deficient porphyrine ring and 3) further weakening of the metal-porphyrin bonds upon removal of an additional electron from the porphyrin π -system to form a cation radical.

However, the Ag^{2+} and Co^{2+} complexes of this porphyrin are readily oxidized at the metal to form the corresponding valance +3 derivatives. The absorption-shift pattern observed for both systems upon oxidation agrees well with the Ag(III) and Co(III) complexes of other porphyrins, Table 4.¹⁰, 11

Table 4. Changes in the Optical Absorption (nm) in CH₂Cl₂ of the Ag^{II} and Co^{II} Complexes of TFPP Upon One-Electron Metal-Centered Oxidation.

Compound	Soret	Visible Bands
Ag ^{II} TFPP	419	537, 570
Ag ^{III} TFPPClO ₄ -	418	527, 559
Co ^{II} TFPP	404	527
Co ^{III} TFPP(H ₂ O) ₂ ClO ₄ ⁻	422	536

Our attempt to chemically oxidize $Co^{II}TFPP$ by more than one electron resulted in the partial formation of $Co^{III}TFPP+\cdot 2ClO_4^-$ (e.g., 666 nm) and that the Co^{III} species (e.g., 422 and 536 nm) persisted for the most part. The presence of the radical was conformed by observing a broad, residual ESR signal at room temperature. Qualitatively, it is expected that the TFPP radicals are more prone than their TPP counterparts to adopt $^2A_{1U}$ electronic ground state or that the fluorophenyl groups may completely stabilize the a_{2U} orbital relative to the a_{1U} orbital by withdrawing electron density from the meso carbons. 12 The $^2A_{1U}$ vs. $^2A_{2U}$ state of the MTFPP radicals may be crucial for selective peripheral functionalization of the porphyrin ring either at the β -pyrrolic or on the bridging meso-carbon positions, as was recently reported by Catalano and coworkers for the analogous TPP complexes. 13

EXPERIMENTAL

The reaction conditions applied in this study may be divided into three categories as follows:

- 1. The free base H₂TFPP was treated in glacial acetic acid with a large excess (e.g., 10x) of metal nitrate salt (e.g., Ag^{2+} , Cu^{2+}) under refluxing condition for ~ 6 hours.
- 2. The desired MTFPP (e.g., Ag²⁺, Ni²⁺) was initially prepared from refluxing an acetic acid solution of the free base with a large molar excess (e.g., 10x) of metal acetate. Subsequently, MTFPP was treated with acetic acid in the presence of catalytic amount of concentrated nitric acid under refluxing condition for ~ 6 hours.
- 3. The free base was refluxed in acetic acid in the presence of a large molar excess of metal acetate (e.g., Zn²⁺) and catalytic amount of concentrated nitric acid for ~ 6 hours.

In all above cases, removal of the solvent gave a green solid which was redissolved in dichloromethane and chromatographed on silica gel TLC plate (dichloromethane/hexane 9:1). The individual fractions in which their optical spectra contained two bands in the 500-600 nm region and displayed no fluorescence under the UV light were subsequently demetallated in TFA under refluxing condition for 48 - 72 hours. The TFA solution was evaporated to dryness and the solid was taken up in dichloromethane and rechromatographed on silica gel (dichloromethane/hexane 9:1) to afford the free base adducts. This step, in some instances, resulted in the separation of two or more fractions, which are not separable when they are metallated. Moreover, demetallation would facilitate the ¹H-NMR analysis of paramagnetic species (e.g., Cu²⁺, Ag²⁺).

Results

Generally, three types of products were obtained based on their optical absorption characteristics:

- a. Type 1 features two bands of comparable intensity in the 500 600 nm region, characteristic of metalloporphyrins and designated as M(2-B). Although Gouterman et al. 7 have demonstrated the solvent-dependent intensity variation of MTFPP visible bands, Figures 1 and 2, the so-called α band intensifies drastically in M(2-B) species, Figure 3. This figure also demonstrates that Cu(2-B) spectrum is red-shifted relative to CuTFPP. Type 1 species may be prepared by refluxing an acetic acid-nitric acid (catalytic, ~ 3 drops) solution of MTFPP for ~ 6 hours.
- b. Type 2 species also displays a two-banded visible region; however, in the absence of the central metal. This spectrum may arise from the mono-

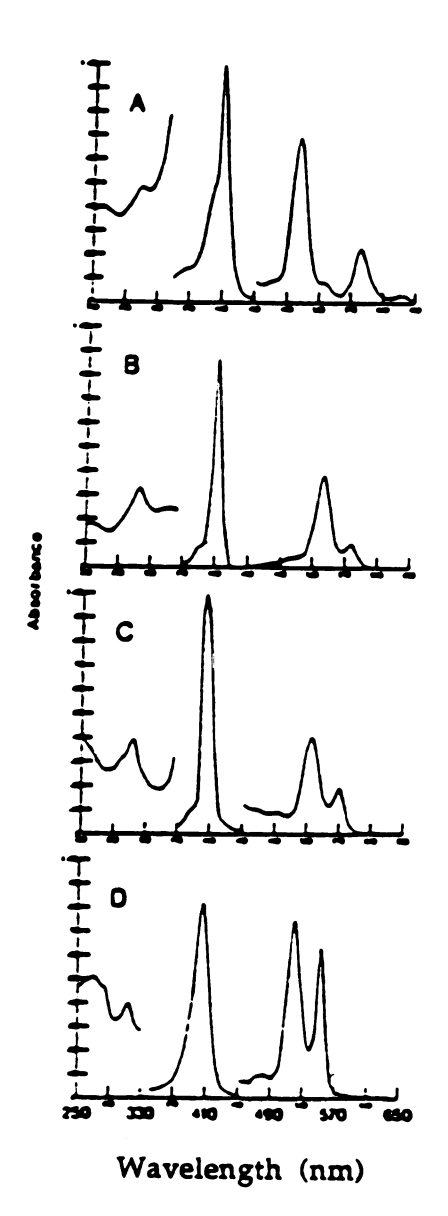


Figure 1. Absorption spectra of tetrakis(perfluorophenyl)porphyrin complexes taken in CH₂Cl₂ at room temperature: (A) free base; (B) Zn complex, (C) Cu complex; (D) Pd complex. (From Ref. 7.)

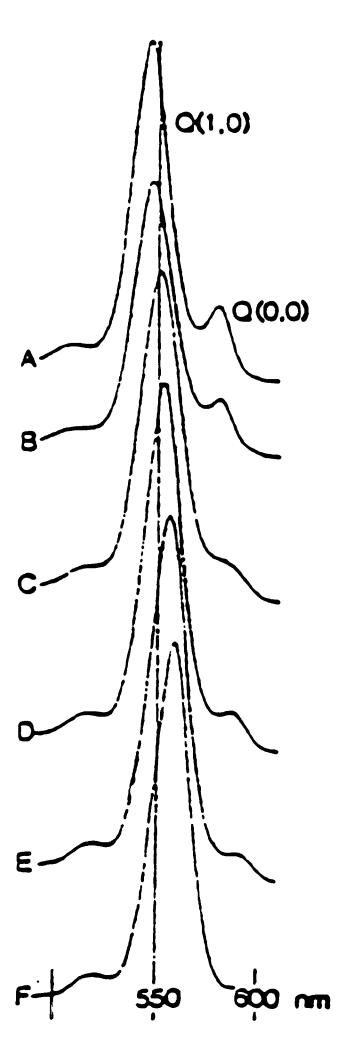


Figure 2. Solvent-dependent absorption spectra of zinc tetrakis(perfluorophenyl)porphyrin in visible region: (A) dry toluene; (B) toluene shaken with H₂O;(C) 75% toluene and 25% CH₃CN; (D) 75% toluene and 25% ethanol; (E) 75% toluene and 25% pyridine; (F) 75% toluene and 25% triethylamine. (From Ref. 7.)

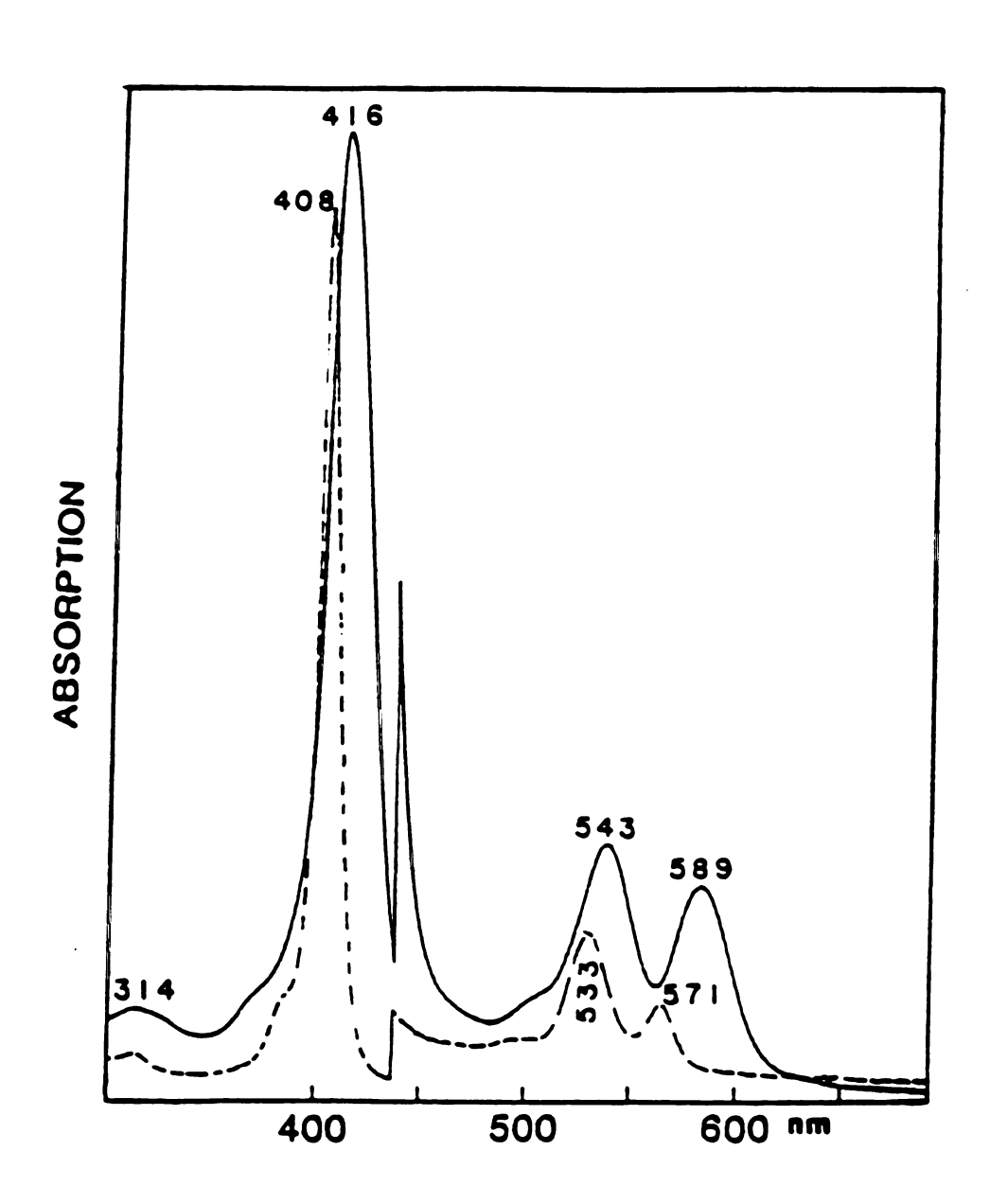


Figure 3. Electronic absorption spectra of CuTFPP(—) and Cu(2-B) in CH₂Cl₂.

and diprotonated free base of the functionalized TFPP adduct, designated as $H_M(2-B)$. In the absence of the exact identity of peripheral groups, type 2 may be distinguished from type 1 by their active emission properties. Type 2 adducts are formed as the by-products of $M(NO_3)_2/HOAC$ or $HOAC/HNO_3$ reaction conditions.

c. Type 3 adduct, designated as $H_M(4-B)$, shows a free base-like spectrum in which band III is present, in contrast with that of H_2 TFPP. The spectrum is also red-shifted relative to H_2 TFPP. The species derived from AgTFPP features a band I which is more intense than bands II and III, Figure 4. Type 3 species may be prepared when M(2-B) is demetallated in TFA or, an acetic acid-nitric acid (catalytic, 5 drops) solution of MTFPP is refluxed for \sim 6 hours.

The splitting of the exo β -pyrrolic protons in the ¹H-NMR spectra of the newly-formed TFPP adducts provides evidence for the functionalization of β -pyrrolic double bonds. The extent of substitution is not clear in all cases; however, resolution of nine or ten bonds in a few instances reveal that up to two or three β -pyrrolic substituents may be present, Figure 5a and b.

In the FAB mass spectra of these adducts, observation of peaks at m/z 975 (M⁺, H₂TFPP), 993 (M⁺, H₂TFPP + H₂O), 1006 (M⁺, H₂TFPP + NOH), 1020 (M⁺, H₂TFPP + NO₂), 1038 (M⁺, H₂TFPP + HNO₃), as well as peaks alluding to higher order addition of these substituents and their metal derivatives shed more lights on the nature and extent of these substitution reactions.

Cu(II) or Ni (II) Adducts

CuTFPP in HOAC-HNO3 produced one major green fraction, which was chromatographed on a silica gel plate with dichloromethane-hexane (95:5) and collected as the least polar band. The absorption maxima of this Cu

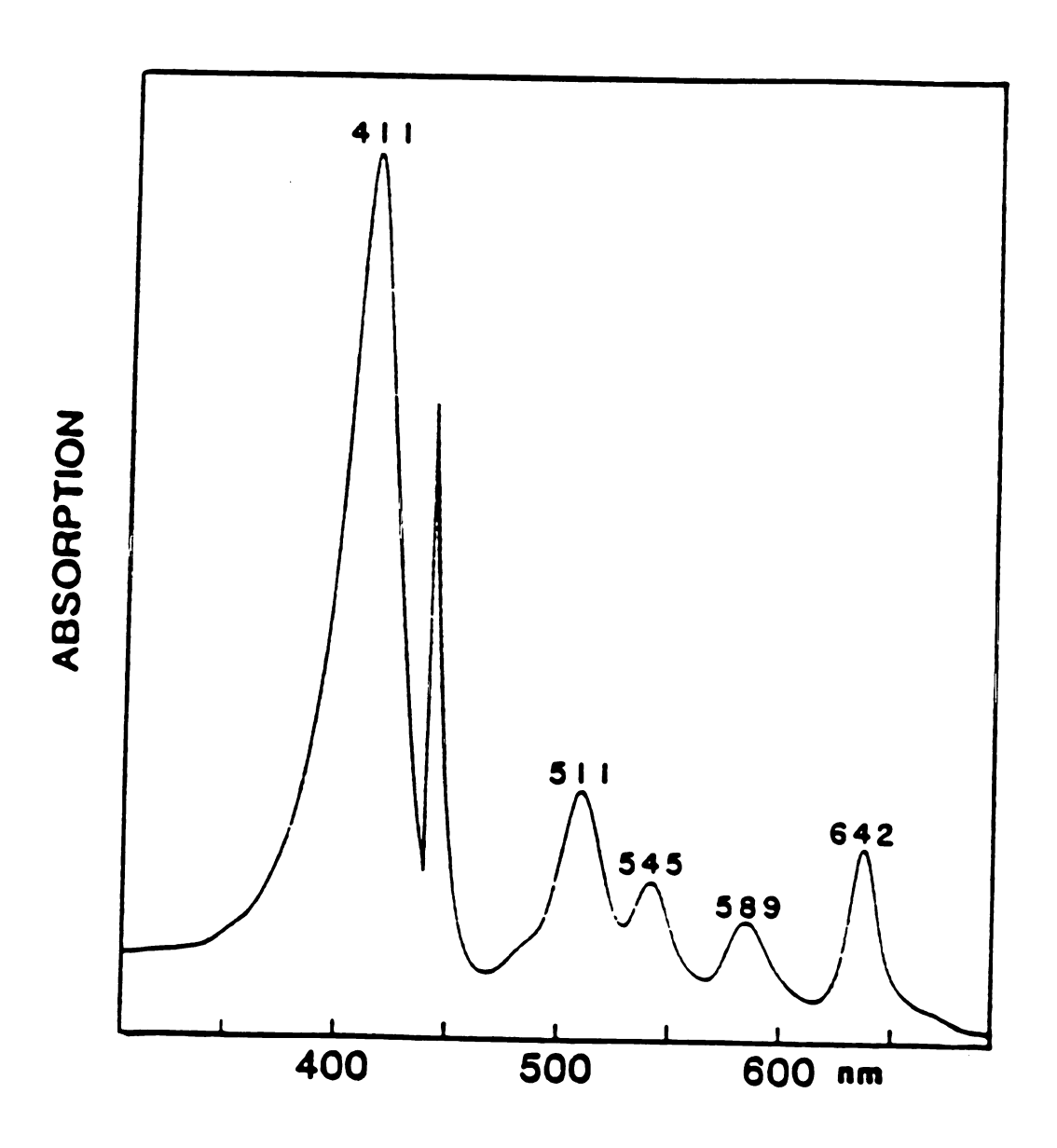


Figure 4. Absorption spectrum of $H_{Ag}(4-B)$ in CH_2Cl_2 .

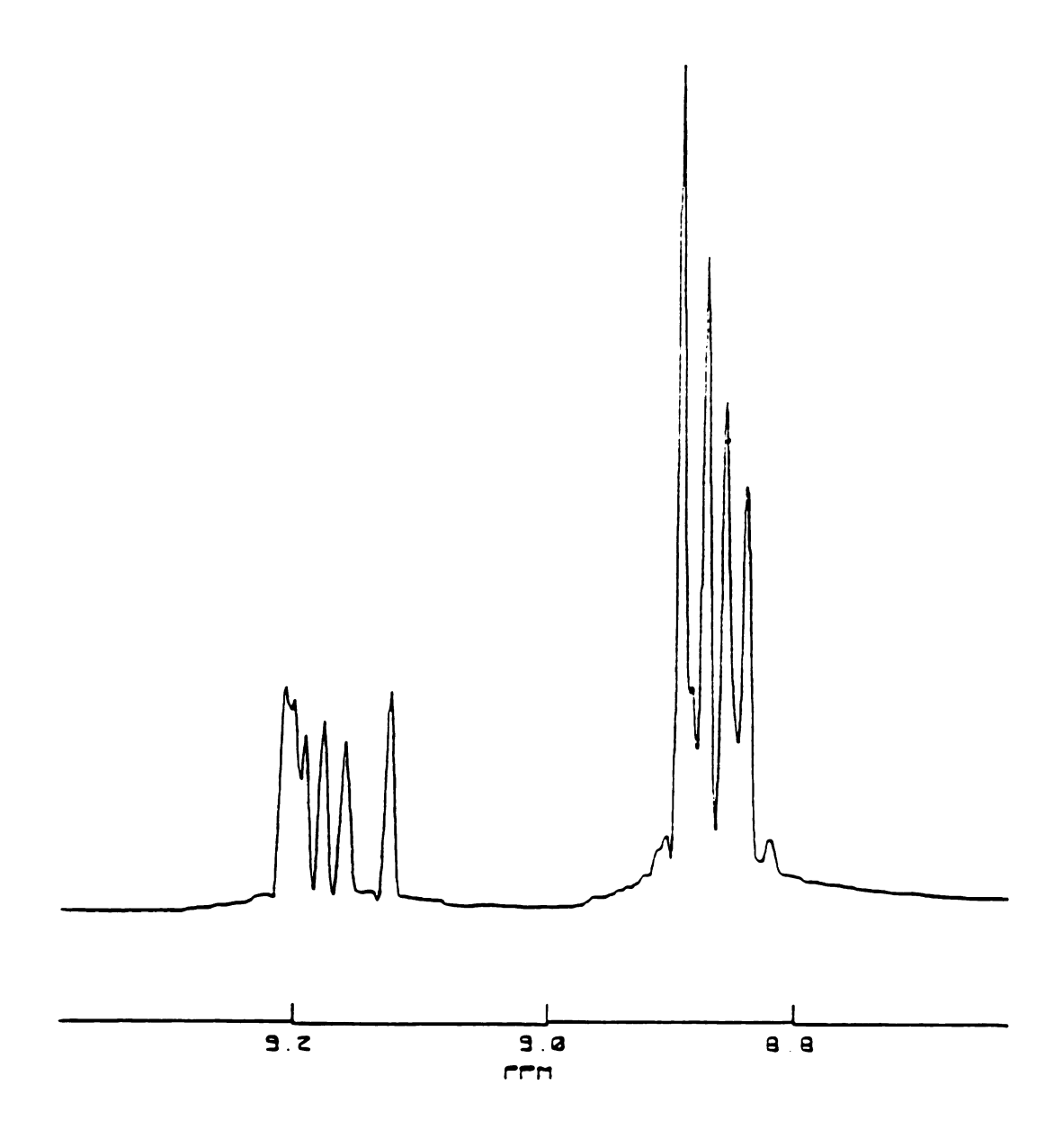


Figure 5a. Expanded β -pyrrolic region of ¹H-NMR spectrum of Zn(2-B), fraction 2, in CDCl₃.

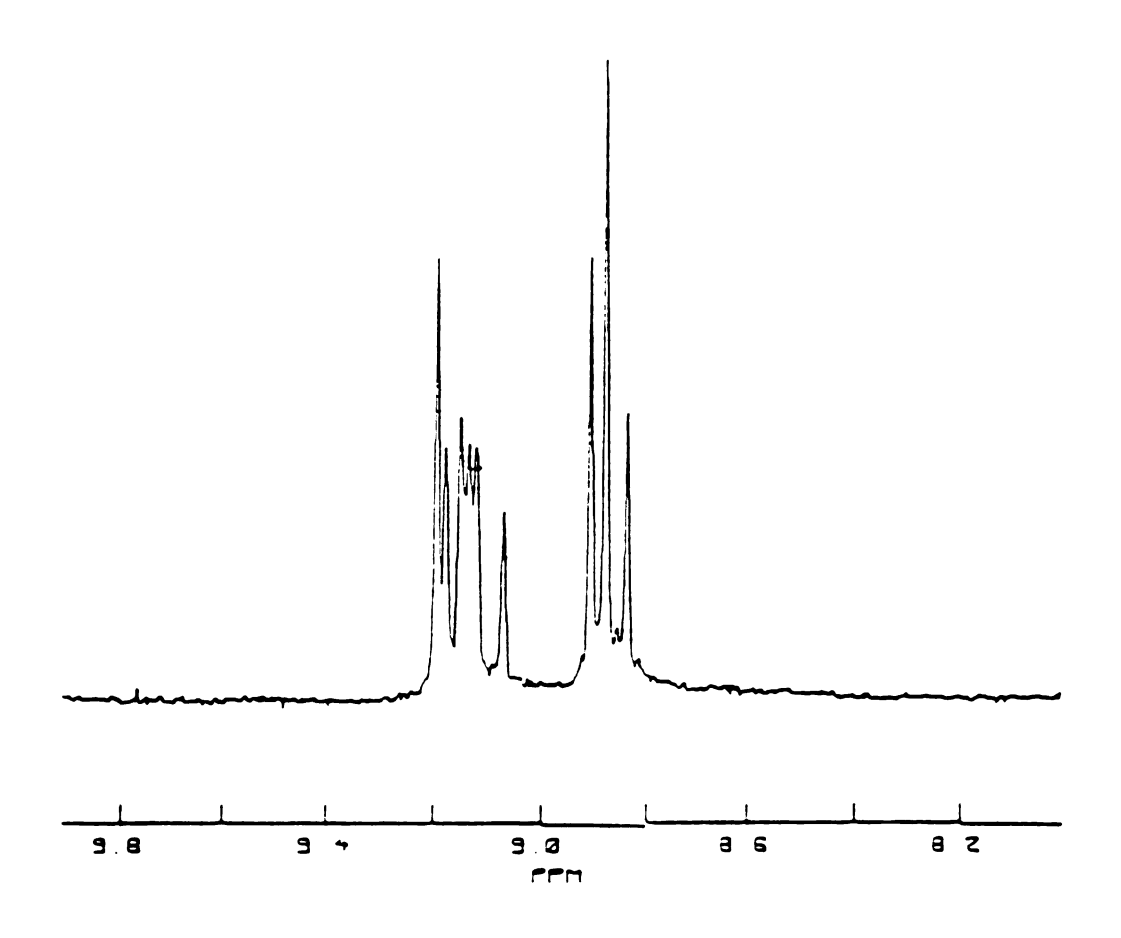


Figure 5b. Expanded β -pyrrolic region of ¹H-NMR spectrum of Zn(2-B), fraction 4, in CDCl₃.

(2-B) species, it demetallated derivative as well as those of CuTPP and its β -nitro substituted analogs are given in Table 5. This table shows a systematic wavelength-shifts caused by the introduction of β -nitro group in TPP is reproduced in the TFPP adducts. More importantly, a FAB-MS peak at m/z 1081 (M+, CuTFPP+NO₂) confirms the assignment.

Table 5. Absorption Maxima (Nm) of TFPP and TPP adducts in CH₂Cl₂.

Compound	Soret	Visible Bands
CuTFPP	408	533, 571
Cu(2-B)	416	543, 589
CuTPP	414	539
β-NO ₂ -CuTPP	422	551
H ₂ TFPP	412	506, 583, 655
$H_{Cu}^{-}(4-B)$	419	518, 590, 646
H ₂ TPP	417	514, 548, 592, 647
β-NO ₂ -H ₂ TPP	425	528, 561, 602, 664

NiTFPP reactivity is also analogous to that of Cu complex. One major fraction was obtained under the same condition described earlier for the copper derivative. Ni (2-B) species features absorption maxima at 423, 540, and 592 nm and a FAB-MS peak at m/z 1076 (M⁺, NiTFPP + NO₂). Demetallation of Ni (2-B) in TFA resulted in the formation of $H_{Ni}(4-B)$ with absorption maxima at 424, 520, 595 and 650 nm. This spectrum, with the exception of band I, is red-shifted relative to H_2 TFPP, analogous to that observed in H_{Cu} (4-B).

Ag(II) Adducts

Demetallation of the reaction products of $H_2TFPP + AgNO_3/HOAC$ in TFA followed by chromatography on alumina resulted in the separation of five green fractions. The absorption maxima and FAB-MS data are given in Table 6.

Table 6. Absorption Maxima and FAB-Ms Data on AgTFPP Adducts.

Elution No.	λ _{max} (nm)	m/z
1	422, 550, 595	1097 (M+,AgTFPP+H ₂ O)
2	428, 562, 604	1038 (M+,H ₂ TFPP+HNO ₃)
3	419, 515, 556, 594, 657	1038 (M ⁺ ,H ₂ TFPP+HNO ₃) 993 (M ⁺ ,H ₂ TFPP+H ₂ O)
4	422, 516, 555, 594, 649	1038 (M+,H ₂ TFPP+HNO ₃)
5	418, 510, 552, 595, 644	993 (M+,H ₂ TFPP+H ₂ O)

As it appears from the MS data in Table 6, addition of H₂O and HNO₃ moieties across the double bond and formation of chlorin-type structures is evident. Although these fractions have been purified on alumina column, they seem to be partially contaminated by one another. This is especially true for fraction three in which there seems to be equal amounts of water and nitric acid adducts present. If we rule out the possibility of functional group transformation, hydrolysis, tautomerism¹⁵.....during the acquisition of FAB-MS, then HPLC techniques may be required to further purify these fractions.

Zn (II) Adducts

Reaction of ZnTFPP with HOAC/HNO3 resulted in the separation of five major and a few minor fractions on silica plate after chromatography with dichloromethane-hexane (5%) as eluant. Table 7 summarizes absorption maxima and preliminary FAB-MS and ¹H-NMR data for the major bands. The proton NMR spectra of the Zn adducts, exhibit a more defined picture of β-proton splittings than other derivatives and may be utilized as the subject of further investigation. The prominent MS peaks of the fractions 1 and 2 indicate a higher order of substitution with Zn complexes than the previous systems. The m/z at 1128 in fraction 1 corresponds to the addition of two nitro groups and m/z at 1173 in fraction 2 corresponds to the substitution of three nitro groups in the ZnTFPP complex.

Table 7. Absorption Maxima (nm), FAB-MS m/z and 1 H-NMR β -proton Multiplicity Number (MN) of ZnTFPP Adducts.

Elution No.	λ's (nm) max	m/z	Ηβ ΜΝ
1	436, 566, 613	1128 (M+)	2 (8.77 and 8.81 ppm)
2	435, 565, 610	1172 (M+) 1128 (M+-NO ₂)	9 or 10
3	440, 572, 620		3 (8.,82, 8.86, 8.88 ppm)
4	439, 570-, 608		9
5	436, 573, 619		multiple

Discussion

The original reaction condition used by Gouterman and coworkers, i.e., $H_2TFPP+AgNO_3/HOAC$ was intended to find a more effective method for silver ion insertion into H_2TFPP . This is because the AgOAC/HOAC method also gives poor yield. Indeed, the AgNO₃/HOAC condition facilitates the insertion of silver ion and metallation is quantitative in < 1 hour; however, the reaction condition immediately proceeds to form the green adducts. The FAB-MS obtained on a sample which also refluxed for 3/4 hour already indicates the presence of addition products across C_bC_b double bond, Scheme 1. It is possible to speculate that the electron-deficient TFPP system triggers a

$$M^{+}=993$$
 $M^{+}=1007$
 $M^{+}=1020$
 $M^{+}=1038$

Scheme 1

metal-catalyzed addition reaction to occur. Of the structures suggested, the M^+ = 993 and 1038 peaks are more prominent in this sample than the others, Figure 6 a and b.

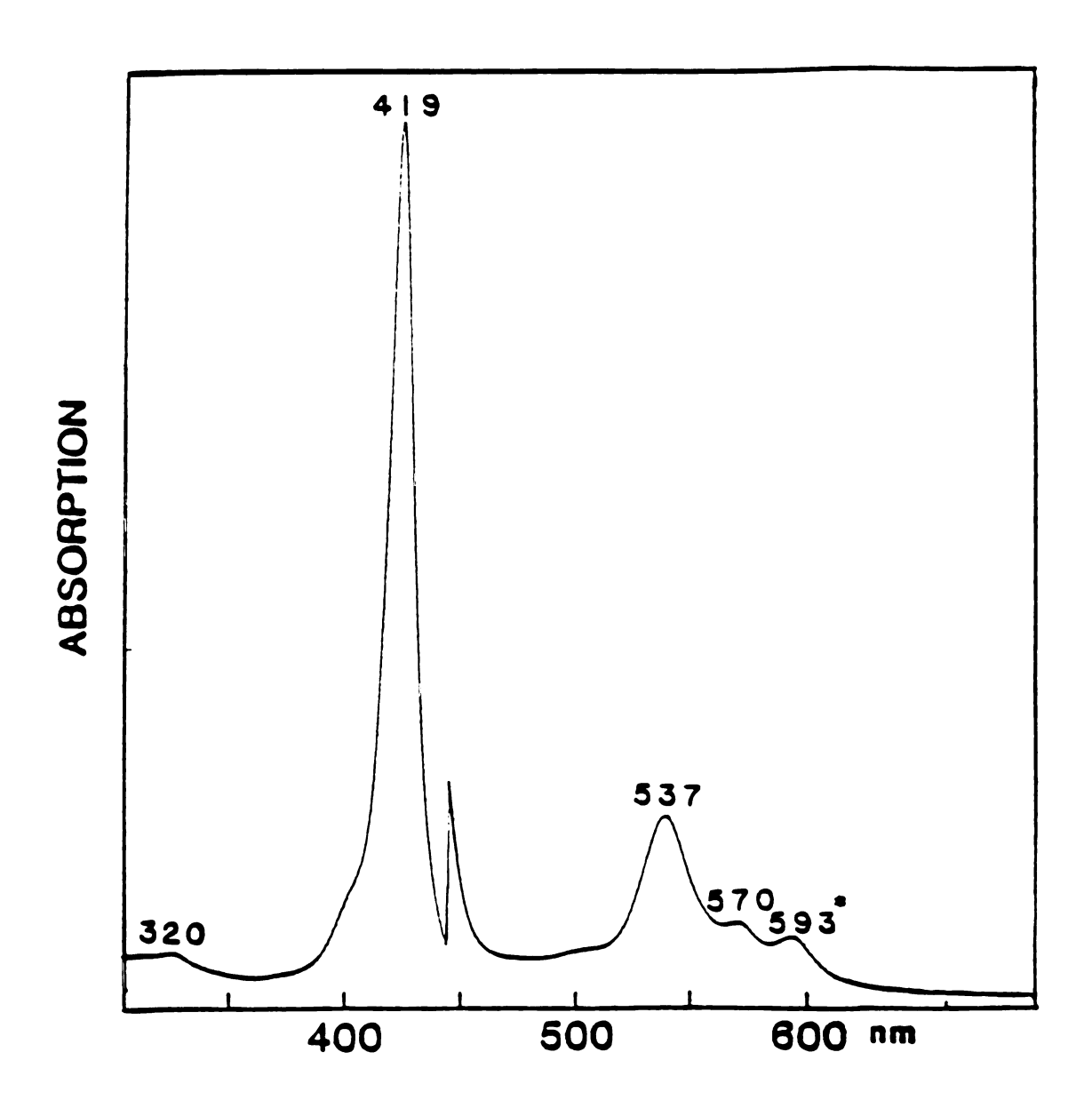


Figure 6a. *The 593 nm band is due to the β -pyrrolic adducts. *Gouterman reports AgTFPP $\lambda_{\max}^{'S}$ at 416, 536 and 570 nm in ϕ CH3.



Figure 6b: Partial FAB mass spectrum of AgTRPP prepared by AgNO3/HOAC method in < 1 hour. The m/z at 1081 (M⁺,AgTPP) is not shown.

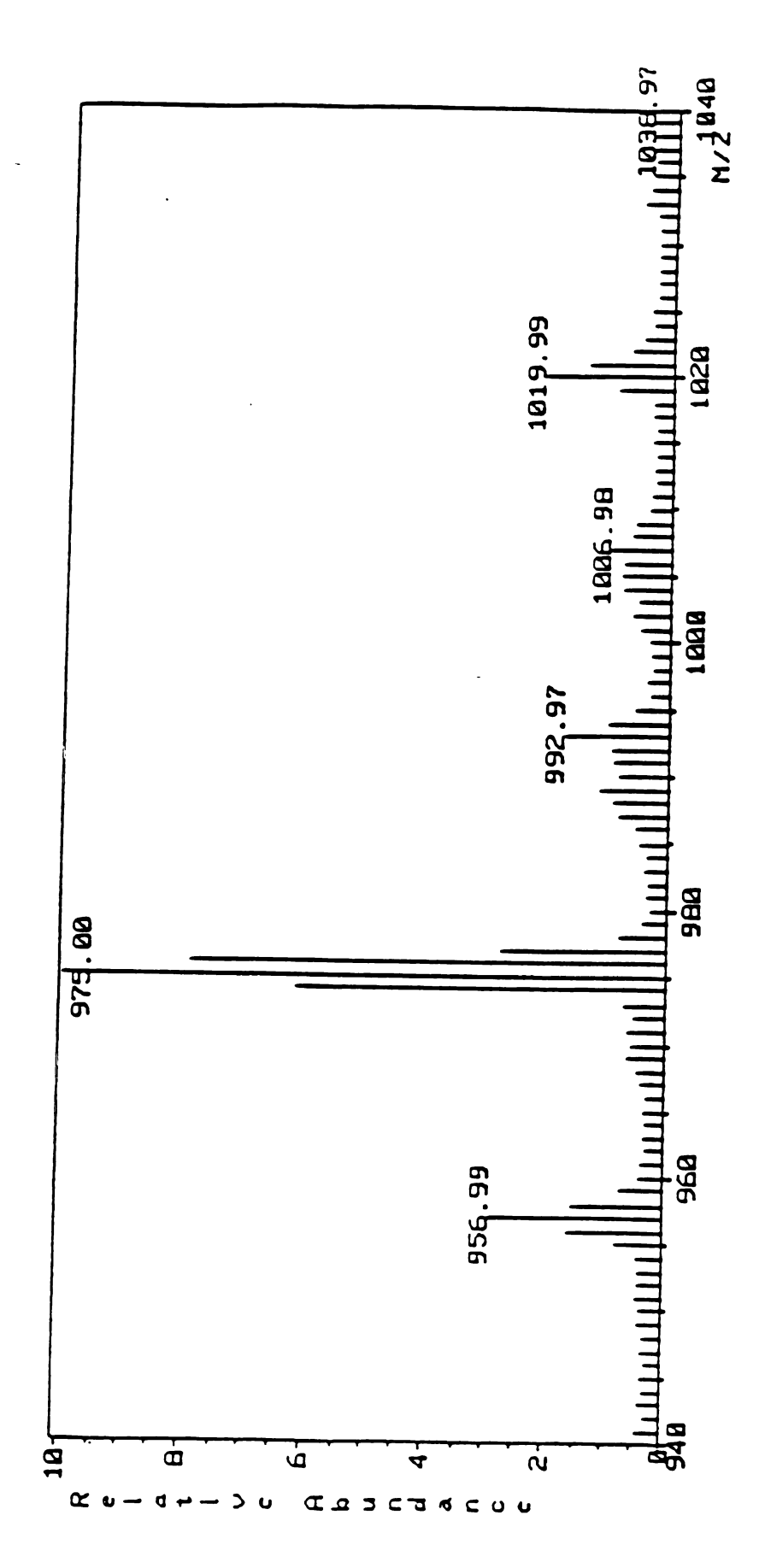


Figure 6b: Partial FAB mass spectrum of AgTPPP prepared by AgNO3/HOAC method in < 1 hour. The m/z at 1081 (M⁺,AgTPP) is not shown.

To test whether this reaction is unique to the TFPP system, samples of AgTPP and AgTFPP were treated with HOAC/HNO3 side-by-side. After refluxing for ~ 4 hours, AgTPP remained intact whereas AgTFPP produced the expected green products.

The electronegativity of the central metal may play a significant role in the regiospecificity of addition, product selection and the extent of substitution reaction. For example, Zn (II), Mg (II) and Cd (II) release electron density to the porphyrin, thus making it more nucleophilic. This is perhaps why higher order of substitution was observed with ZnTFPP. Ni (II), Cu (II) and Fe (II), on the other hand, withdraw electron density from the porphyrin ligand and, as a result, induce more electrophilic character in the ring.

The mechanism of aromatic nitration has been the subject of much discussion in recent years. However, it is generally accepted that aromatic cation radicals are considered as plausible intermediates in the mechanism for aromatic nitration. A number of nitrating reagents have been applied to the porphyrin system in the past decade, including Tl(NO₃)₃ or Ce^{IV}(NO₃)₆ (NH₂)₂, MO₂/CH₂Cl₂ or φH, Mo₂ I₂ I₂/CH₃OH+NaNO₂, Reaction of NO₂ with a MP+· of a_{1U} symmetry would lead to specific β-substitution, as was recently documented by Catalano and coworkers for the nitration of Ni (II), Cu (II) and pd (II) complexes of TPP. The mechanism of TFPP β-pyrrolic substitution reactions however is expected to be more complex owing to the involvement of the electron-deficient character of the TFPP system as a key factor, formation of both hydration and nitration products resulting in chlorin and β-derivatized porphyrin structures and possible participation of metals in the catalysis of these reactions (e.g., Ag¹¹). As was suggested earlier, it is tempting to

conclude that the metal complexes of the TFPP system are $pro^{-2}A_{1U}$ cationic radical state. On the other hand, it may be that by virtue of steric protection of meso carbons, the substitution reactions are forced to occur at the β -pyrrolic position despite the fact that the MTFPP+• may still be of ${}^2A_{2U}$ state. Thus, an ENDOR measurement on $Co^{III}TFPP+•2ClO_4^-$ would be informative to determine its ground state as ${}^2A_{1U}$ or ${}^2A_{2U}$.

As it stands, this project is yet to be explored in several dimensions. A few suggestions are as follows:

- 1. ENDOR Measurements. This study would reveal that β-substitution reactions of the TFPP complexes are directed by virtue of 1) the ²A_{1U} electronic ground state of MTFPP+, 2) steric protection of the meso carbons by fluorine atoms which force β-pyrrolic substitution reactions to take place or 3) the electronic distribution of the TFPP complexes is such that the c_bc_b double bonds reactivity approximates an isolated simple alkene in which addition across the double bond proceeds easily. This would then make it possible to test the reactivity of this system for other classical electrophilic substitution reactions such as deuteration, halogenation, formylation and acetylation.
- 2. High-field NMR spectroscopy, including decoupling and NOE difference measurements would be invaluable to sort out the β-pyrrolic protons in these newly-formed adducts. Moreover, the ¹⁹F NMR of these adducts would offer an independent means of characterizing the substitution reactions of the β-pyrrolic positions as well as the conformation of the porphyrin ring. It has already been shown that in the ¹⁹F spectrum of InTFPPCI, the spin-spin coupling patterns observed for the ortho and

- meta fluorines of H₂TFPP are doubled indicating the nonequivalence of the two sides of the phenyl ring. The signals for the para fluorine, however, remained the same.⁸
- 3. Purification by HPLC Techniques: It has already been demonstrated by Crossley and coworkers that methyl-nitro- and dinitro-adducts of the TPP may only be purified satisfactorily by HPLC methods.²¹ This is especially true for the AgTFPP adducts in which addition products from H₂O, HNO₃ coexist in one fraction purified by plate chromatography.

REFERENCES

- 1. Chang, C. K.; Ebina, F., Private Communication.
- 2. Cavaliero, J. A. S.; Evans, B.; Smith, K. In "Porphyrin Chemistry Advances," Longo, F. R., Ed., Ann Arbor Science: Ann Arbor, 1979, Chapter 26, 335.
- 3. Evans, B.; Smith, K. M.; Cavaleiro, J. A. S. J.C.S. Perkin 1, 1978, 768.
- 4. Ostovic, D.; Knoblar, C. B.; Bruice, T. C., J. Am. Chem. Soc. 1987, 109, 3444.
- 5. Chang, C. K.; Ebina, F. J. Chem. Soc. Chem. Comm. 1981, 778.
- 6. (a) Stone, A.; Fleischer, E. B., J. Am. Chem. Soc. 1968, 90, 2735.
 - (b) Ogoshi, H.; Watanabe, E.; Yoshida, Z., Tetrahedron 1973, 29, 3241.
- 7. Spellane, P. J.; Gouterman, M.; Antipas, A.; Kim, S.; Liu, Y. C., Inorg. Chem. 1980, 386.
- 8. Kim, J. B.; Leonard, J. J.; Longo, F. R., J. Am. Chem. Soc. 1972, 94, 3987.
- 9. Longo, F. R.; Finarelli, M. G.; Kim, J. B., J. Heterocycl. Chem. **1969**, <u>6</u>, 927.
- 10. Kadish, K.; Davis, D. G.; Fuhrhop, J. H., Angew. Chem. Int. Ed. 1972, 11, 1014.
- 11. Whitten, D. G.; Baker, E. W.; Corwin, A. H., J. Org. Chem. 1963, 28, 2363.
- 12. Fajer, J.; Davis, M. S. In "The Porphyrins," Dolphin, D., Ed., Academic press: New York, 1979, Vol. IV, 197.
- 13. Catalano, M. M.; Crossley, M. J.; Harding, M. M.; King, L. G., J. Chem. Soc. Chem. Comm. 1984, 1535.
- 14. Gouterman, M. Private Communication.

- 15. Crossley, M. J.; Harding, M. M.; Sternhell, S., J. Org. Chem. 1988, 53, 1132.
- 16. (a) Politzer, P.; Jayasuriya, K.; Sjoberg, P.; Laurence, P. R., J. Am. Chem. Soc. **1985**, 107, 1174.
 - (b) Ali, M.; Ridd, J. H., J. Chem. Soc., Perkin Trans. 2, 1986, 327.
- 17. Schmitt, R. J.; Buttrill Jr., S. E.; Ross, D. S., J. Am. Chem. Soc. 1984, 106, 926.
- 18. Barnett, G. H.; Smith, K. M., J. Chem. Soc. Chem. Comm. 1974, 772.
- 19. Bonnett, R.; Stephenson, G. F., J. Org. Chem. 1965, 30, 2791.
- 20. Cavaleiro, J. A. S.; Neves, M. G. P. M. S., J. Chem. Soc., Perkin Trans. 2, 1986, 575.
- 21. Crossley, M. J.; Harding, M. M.; Sternhall, S., J. Am. Chem. Soc., submitted.

CHAPTER VI

METAL-AXIAL LIGAND VIBRATIONS IN METALLOPORPHYRINS, THEIR Π-CATION RADICALS AND OTHER RELATED SYSTEMS

A PRELIMINARY VIBRATIONAL STUDY IN THE LOW-FREQUENCY REGION (<1,000 cm⁻¹)

In hemoproteins, their synthetic analogs and other related systems such as vitamin B_{12} , modulation of metal-axial ligand stretching frequency, $\upsilon(M\text{-}L)$, occurs as a function of macrocycle steric and electronic effects. The frequency of this vibration is closely related to the nature of the M-L bond and can provide additional information regarding the interactions between the ring (cis-effect) and the extraplanar ligand (trans-effect) transmitted through the central metal. Alternatively, this frequency can be used as a probe for the metal coordination number, macrocyclic deformation and regiospecific changes in peripheral substitution. Recent RR comparisons of the $\upsilon(V=O)$ in various hemoprotein model compounds support this notion. Additionally, several isolated reports of $\upsilon(Fe-Cl)$ and $\upsilon(FeOFe)$ values measured by IR for a series of ferric chloride and μ -oxo dimer complexes have shown that these frequencies differ as a function of the steric and electronic effects of a porphyrin peripheral substituents, Table 1.3

Table 1. Stretching Frequencies (cm $^{-1}$) of (Fe-Cl) and (FeOFE) Vibrations in Several Different Ferric Porphyrin (P) Complexes.

(P)	υ(Fe-Cl)	^{ပ္} (FeOFe)	Refs
Deut-DME	330	842	3a
TTP*	355	860	3b
T(MeO) ₃ PP	378	865	3c
OEP	357	870	3d
TPP	365	876	3c
Proto-DME		880	3a
Meso-DME		885	3a
Acdeut-DME		886	3a
TPC		867	3e

^{*}meso-Tetra(p-Tolyl)porphyrin

We have now begun to investigate the effect of porphyrin cation radical formation on the RR metal-axial ligand stretching frequencies of a series of ferric and cobaltic OEP radicals. This frequency may then be used to determine metal coordination number in the oxidized porphyrin species. Metal coordination may, in turn, affect ring stereochemistry and out-of-plane deformations may influence vibrations below 1,000 cm⁻¹. The frequency changes associated with M-L bonds (where M = Fe, Co and L = F, Cl, Br and I) in PM^{III}-L/P+·M^{III}-L system, although of lesser biological relevance than the PFe=O/P+·Fe=O system, is helpful in evaluating the RR data that are becoming available on the v(Fe=O) of ferryl porphyrins.^{3,4} Moreover, the M-L bond sensitivity to the steric and electronic effects of porphyrin structure as well as the effect of oxidized porphyrin on the metal-ligand CT transitions are of interest.

A recent study by Halpern and coworkers on vitamin B_{12} model compounds suggest that the high degree of conformational flexibility of the

corrin ring serves an essential role in the chemistry of vitamin B_{12} as a reversible "free-radical carrier".⁵ For this reason, the more rigid and planar porphyrin ligand does not occur in this coenzyme. In connection with this study, we present here the infrared $\upsilon(\text{Co-C})$ of a series of alkyl-cobaltic porphyrins of the type R-Co^{III}OEP (where R = Me, Et, i-Pr and t-Bu). These stretching frequencies should reflect the changes in porphyrin ring conformation as the size of the alkyl groups increase.

EXPERIMENTAL

⁵⁶FeOEPX, ⁵⁴FeOEPX, CoOEPX and R-CoOEP were prepared according to the published methods.⁶⁻⁹ One-electron oxidation products of the ferric and cobaltic porphyrins were obtained as described in Chapters II and III.

Infrared spectra of R-CoOEP species were examined as KBR disks by using a Perkin-Elmer 599 IR spectrophotometer. Laser emission at 363.8 and at 406.7 and 413.1 nm were provided by a Coherent Innova 100 Argon and Innova 90 Krypton ion lasers, respectively. Raman spectra were measured with a Spex 1877-B Triplemate and EG & G OMA III electronics.

Results & Discussion

Figure 1 shows the optical spectra of CoOEPX species. As described in Chapter II, the characteristic electronic absorption spectra of five-coordinate cobaltic porphyrins are quite distinct from those of six-coordinate derivatives. A salient feature observed in this figure is the appearance of a shoulder on the high-energy side of the band at ~ 550 nm which intensifies in the order Cl <Br<I. This may partially be due to the more in-plane cobalt ion along this series (i.e., decreasing $E_{\rm N}/r_{\rm i} \equiv {\rm electronegativity/atomic\ radius})$ approaching

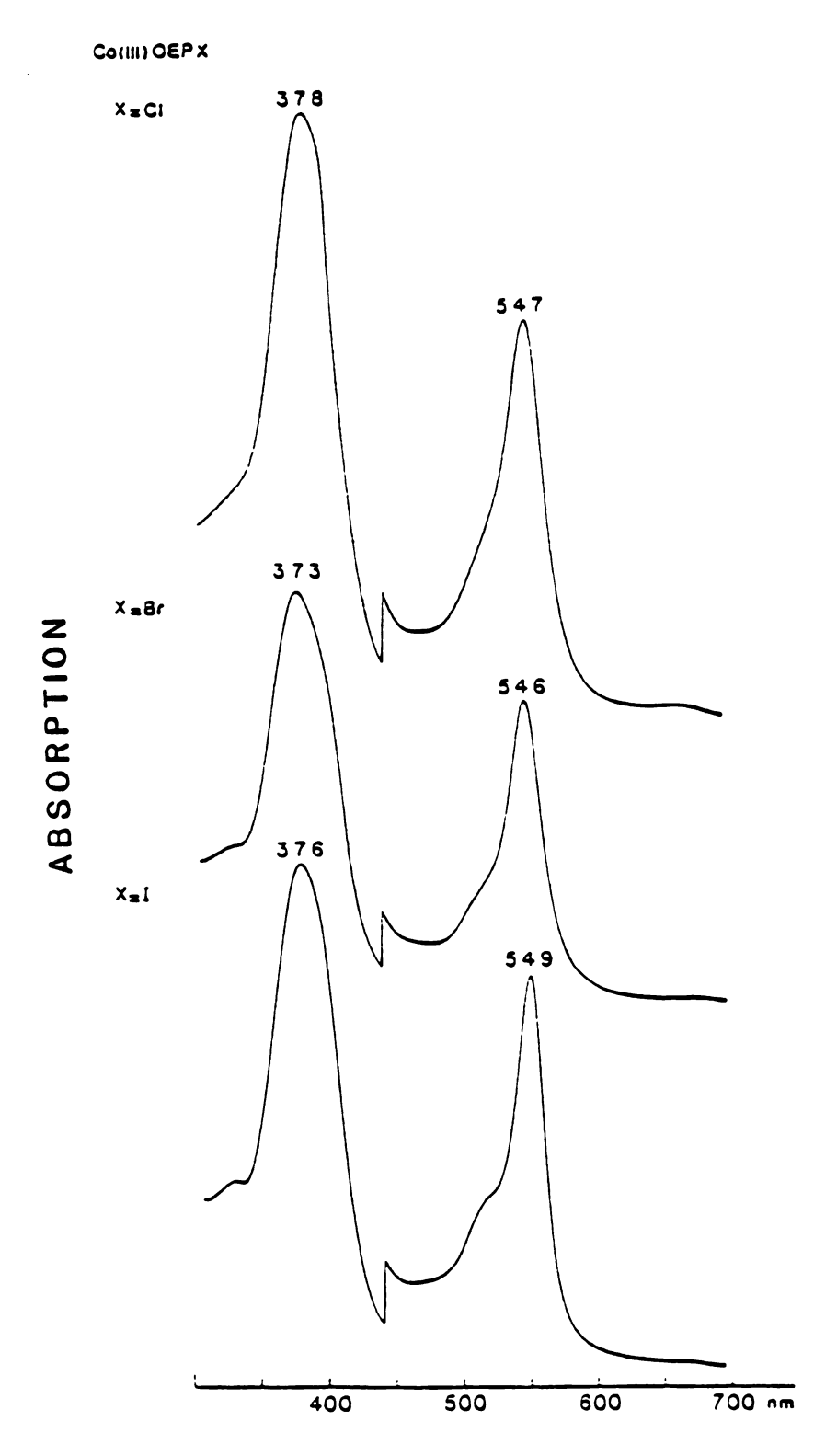


Figure 1. UV-vis spectra of CoOEPX in CH₂Cl₂.

those of CoOEP and Co^{III}(L)₂OEPX which display active β bands². The spectra of Co^{III}OEP+·2X- for X = ClO₄ and Br are shown in Chapter II. When FeCl₃ is used as the oxidant, a cation radical spectrum is obtained, Figure 2, in which the near-uv band at 634 nm lies in energy between those of X = Br at 670 nm and X = ClO₄ at ~ 620 nm. The overall spectral contour resembles more closely that of the X = ClO₄ adduct; however, the shoulders on the high-energy side of the Soret band are a characteristic of X = Br spectrum. It is more likely that X = FeCl₄ in this preparation because Setsune and coworkers obtained a different spectrum when Cl₂ was used as the oxidant.¹⁰

Figure 3 displays the optical spectra of ferric halide OEP complexes. The fluoro complex features a shoulder at ~ 350 nm which is absent in other derivatives. For X = F and Cl, the visible region contains three distinct absorptions; however, these bands are somewhat broadened out for X = Br and I. The spectra of $Fe^{III}OEP+\cdot 2X^-$ show almost no sensitivity to the nature of the counterion, in contrast with the neutral FeOEPX species as well as $Co^{III}OEP+\cdot 2X^-$ complexes. A representative spectrum is shown in Figure 4.

The RR spectra of CoOEPX, Figure 5, obtained at 363.8 nm are identical except for a feature in the low frequency region at ~ 370 cm⁻¹ that changes systematically with X in the order of increasing energy: I<Br<Cl. It is likely that this feature is derived predominantly from in-plane vibration involving the Co-N with possible contribution from the Co-X stretching motion, for the following reasons:

1. The terminal MX stretching bonds have been shown to appear in the regions of 750 - 500 cm⁻¹ for MF, 400 - 200 cm⁻¹ for MCl, 300 - 200 cm⁻¹ for MBr and 200 - 100 cm⁻¹ for MI. 18a

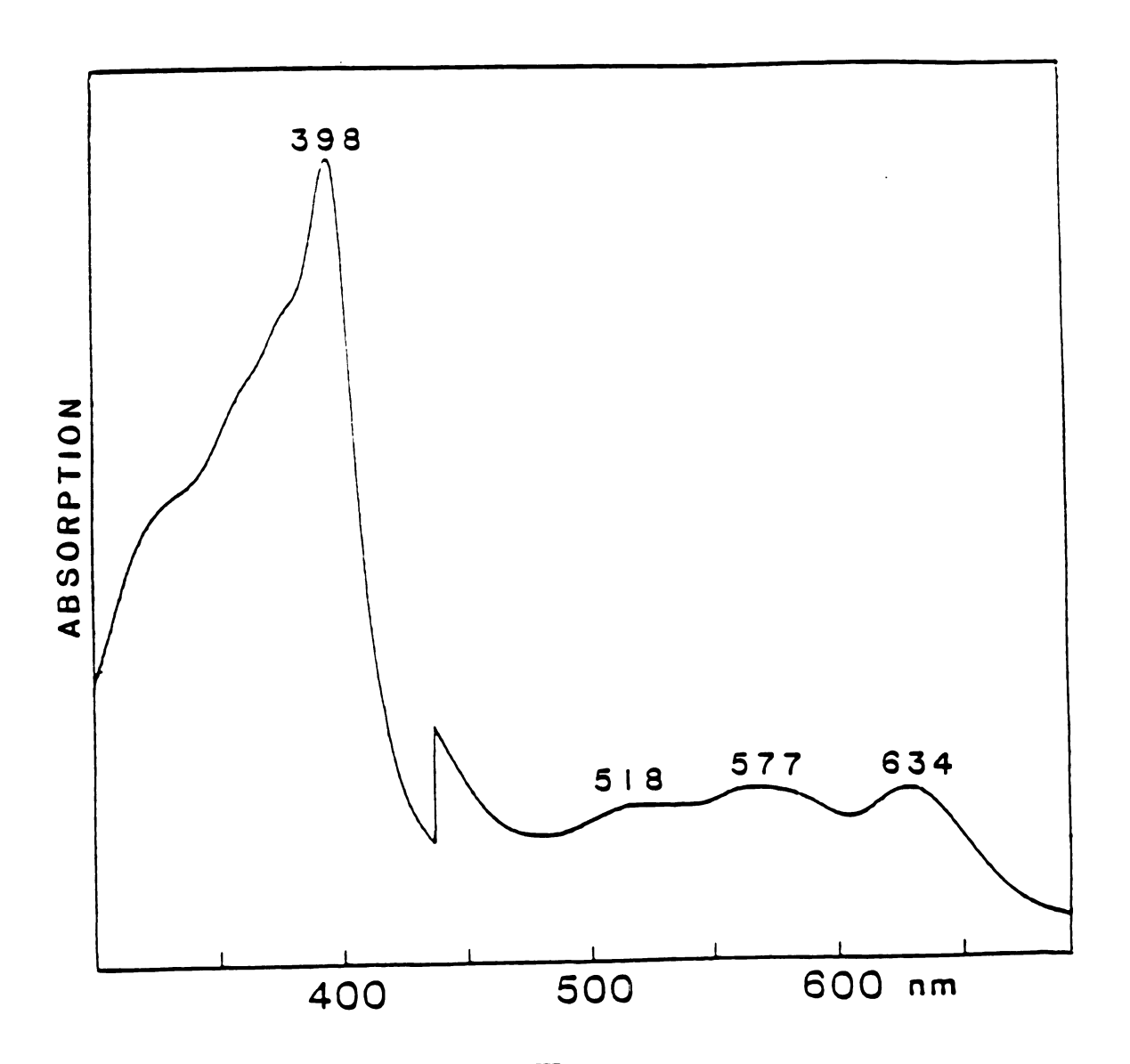
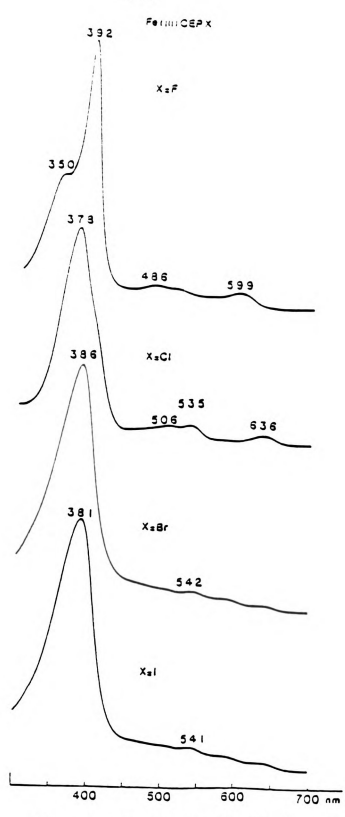


Figure 2. Absorption spectrum of Co^{III}OEP+·2X⁻ (where X = FeCl₄⁻ or Cl⁻) in CH₂Cl₂.





ABSORPTION

Figure 3. UV-vis spectra of FeOEPX in CH₂Cl₂.

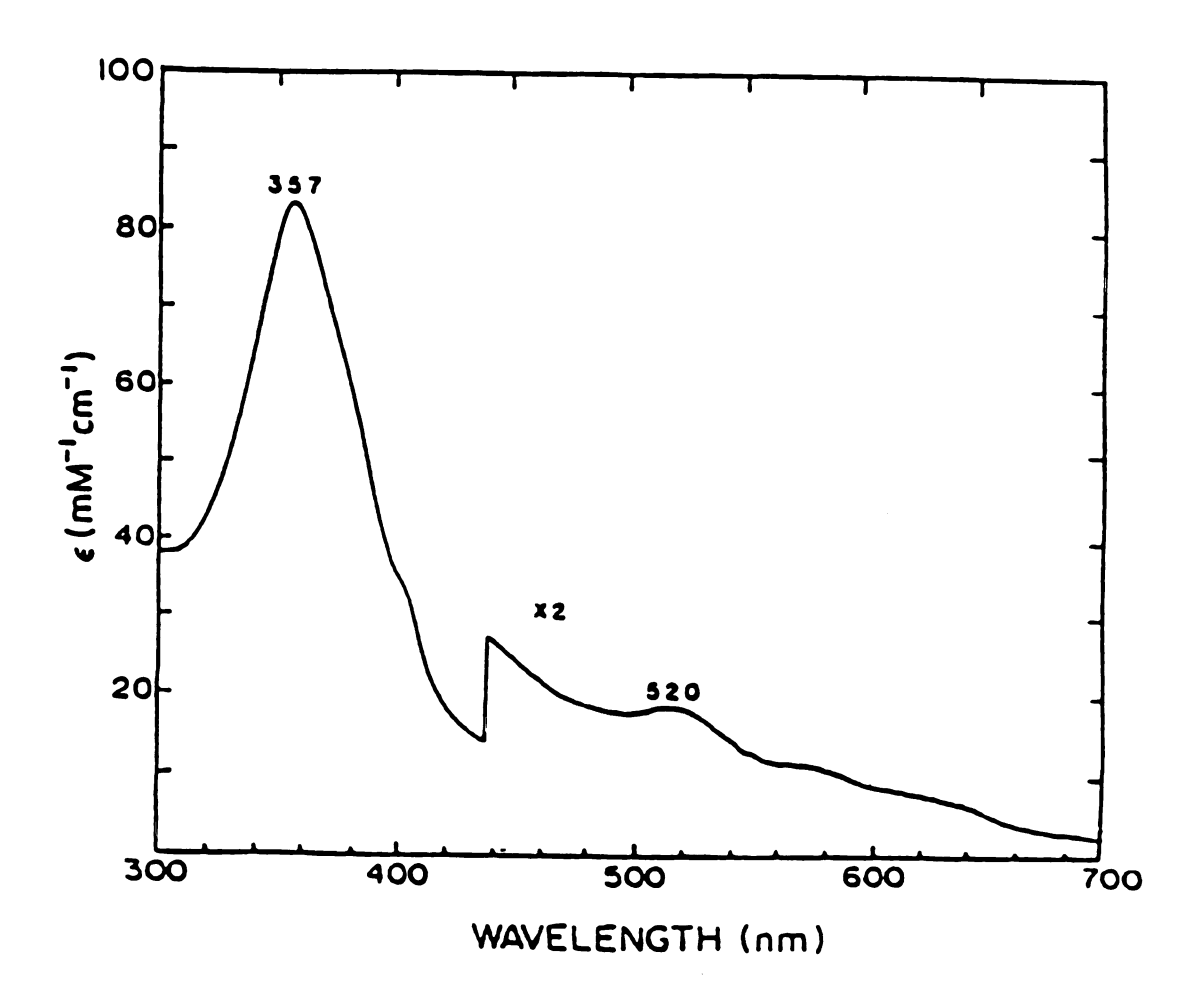


Figure 4. Absorption spectrum of Fe^{III}OEP+·(Cl⁻)(SbCl₆⁻) in CH₂Cl₂.

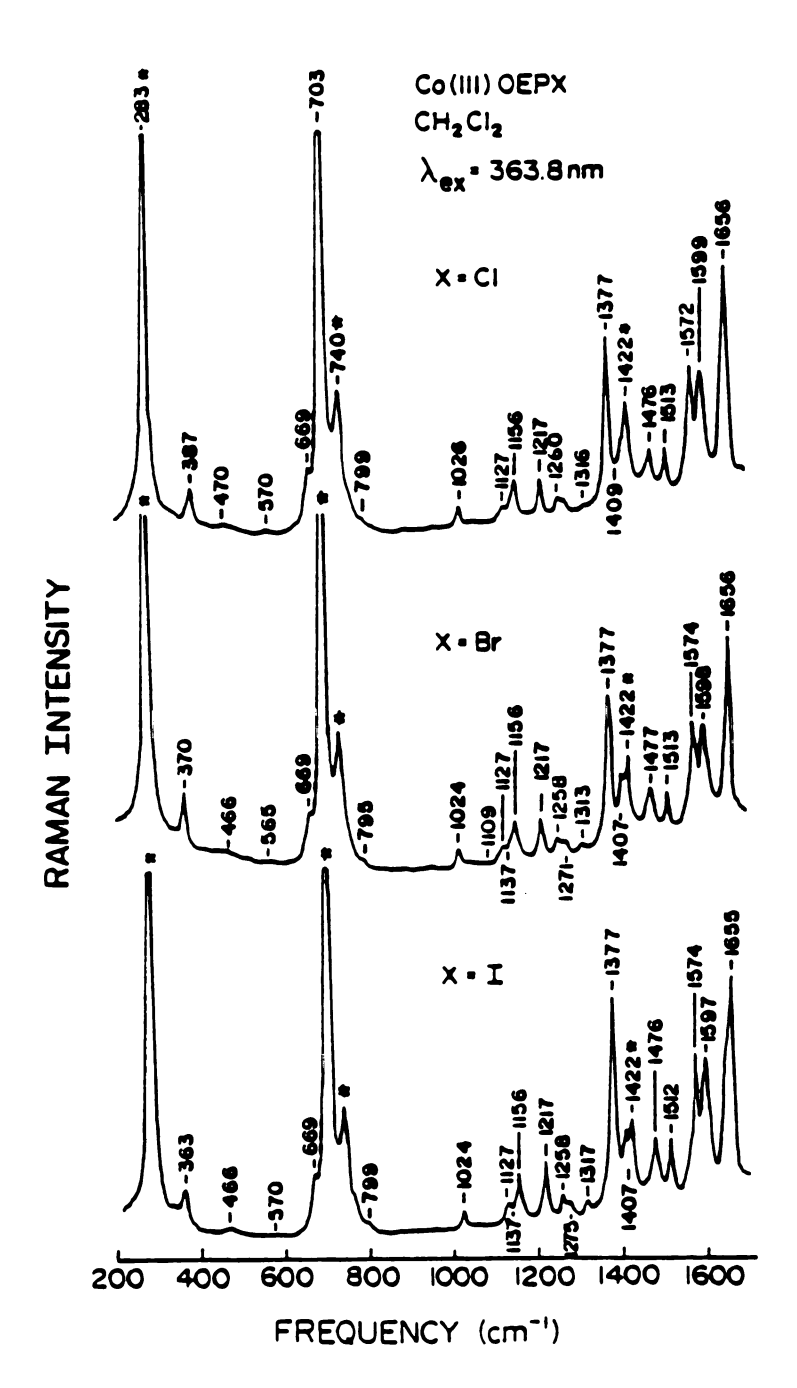


Figure 5. RR spectra of CoOEPX . The solvent bands at 1422, 703 and 283 $\,\mathrm{cm}^{-1}$ are labeled with an asterisk.

- 2. According to Clark and Williams, the v(MBr)/v(MCl) and v(MI)/v(MCl) ratios are 0.77 0.74 and 0.65, respectively. ^{18b}
- 3. Nakagawa and Shimanouchi have obtained the infrared spectra of [Co(NH₃)₅X]²- and trans-[Co(NH₃)₄X₂]⁺- type complexes.^{18c} Table 2 lists the observed frequencies and band assignments obtained by these workers.
- 4. These workers also obtained the following force constants (mdyn/Å) for Co-N and Co-X bonds: K(Co-N), 1.05; K(Co-F), 0.99; K(Co-Cl), 0.91; K(Co-Br), 1.03; and K(Co-I), 0.62.^{18d}
- 5. In general, the infrared intensity of $\upsilon(MX)$ decreases in the order $\upsilon(MF)>\upsilon(MCl)>\upsilon(MBr)>\upsilon(MI)$, whereas the opposite order prevails for the Raman intensity. ^{18c}

Basically, there is very limited information available on the vibrational characteristics of five-coordinate cobaltic porphyrin complexes in the literature. Beside the fact that 59 Co natural abundance is nearly 100% and halide isotopic substitution is extremely difficult, Gouterman and Zerner have shown that the cobaltic CT transitions are mostly of (π,d_Z^2) and (d_π,d_Z^2) character 11,12 , in contrast with the ferric halide species in which $X \to M$ CT transition in the near-UV region (i.e., 350 - 370 nm) is predominant. Thus, the RR spectra of Co^{15} N-OEPX, Co-X derivatives of porphyrins other than OEP and IR studies of these systems will be necessary to assign this mode positively.

Figure 6 depicts that FeOEPX Raman Spectra, excited at 363.8 nm in CH₂Cl₂, are also identical, however they do exhibit strong differences in the relative RR band intensities owing to the differences in the near-UV electronic transitions. The most striking difference is observed in the relative

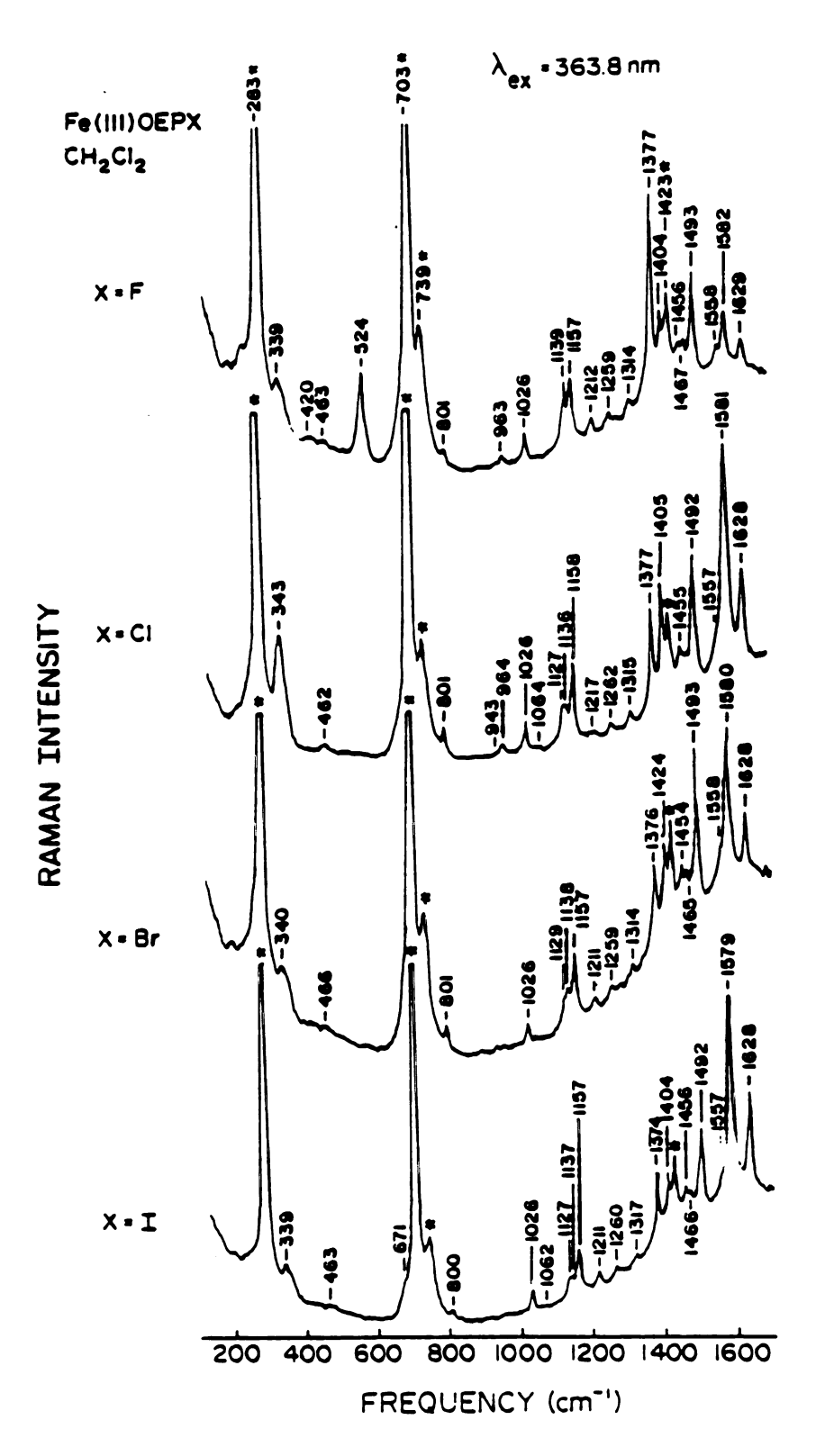


Figure 6. RR spectra of FeOEPX.

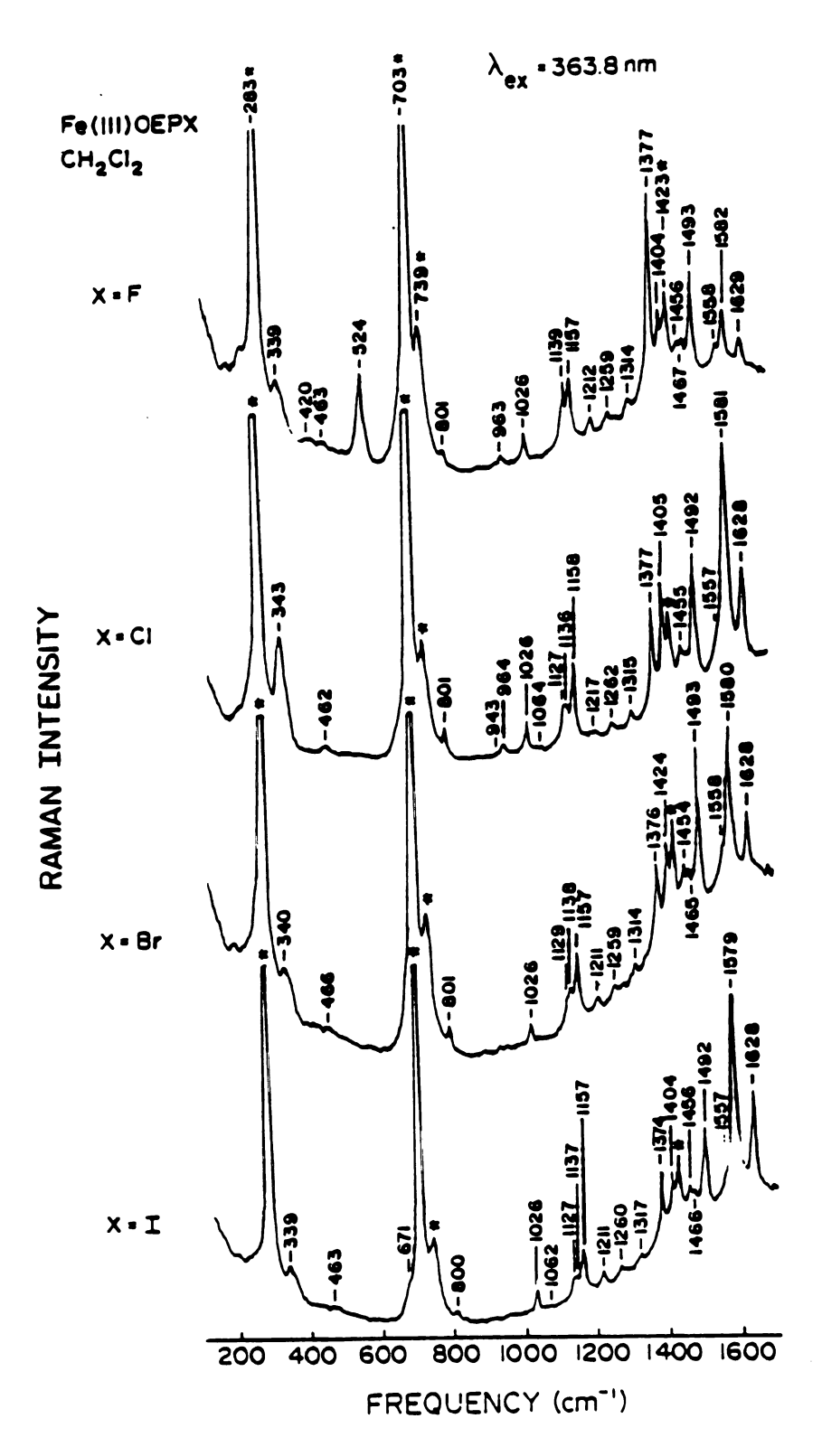


Figure 6. RR spectra of FeOEPX.

intensities of high and low frequency modes. A prominent feature is observed at 574 cm⁻¹ in the fluoro adduct which is absent in all other derivatives. 54/56Fe frequency shifts (3 cm⁻¹) in CH₂Cl₂, Figure 7a, confirms the 574 cm⁻¹ band assignment as Fe-F stretching vibration. This is possibly in contradiction to the previous assignment of ν (Fe-F) at 606 cm⁻¹ in THF by Kitagawa and Kincaid. 14,15 The discrepancy, on the other hand, may arise from solvent effects, which are currently under investigation.

Interestingly, the well-studied v(Fe-Cl) at ~ 360 cm^{-13d} is not observed with excitation at 363.8 nm and in CH₂Cl₂, Figure 6. Figures 7b and 8, however, reveal the presence of this mode at 360 cm⁻¹ with excitation at 406.7 and 413.1 nm in ϕ H. The v(Fe-F), on the other hand, is not enhanced under this condition or it is obscured by the ϕ H peak at 606 cm⁻¹, Figure 8. These observations lead to the notion that v(Fe-X) are not only CT enhanced, as demonstrated by Hendrickson et al. 13, but solvents may shift both these electronic transitions and the metal-ligand stretching frequency.

The FeOEPBr spectrum features a mode at 274 cm⁻¹, Figure 8, which is close to the reported value for v(Fe-Br) at 270 cm⁻¹⁶. Although there are other porphyrin vibrations in this region, as shown by the presence of a split mode at 245 and 270 cm⁻¹ in the spectra of other derivatives, the single 274 cm⁻¹ band of the bromo adduct most likely reflects the v(Fe-Br) as well. ^{54}Fe substitution should confirm this assignment. The feature at 245 cm⁻¹ in FeOEPI spectrum may not be due to v(Fe-I) reported at 246 cm⁻¹⁶ owing to the presence of a similar mode at 246 cm⁻¹ in the spectrum of the chloro derivative, Figure 8. The stretching force constants in the ferric halide complexes differ in the order K(Fe-F) > K(Fe-CI) > K(Fe-Br), as reported by

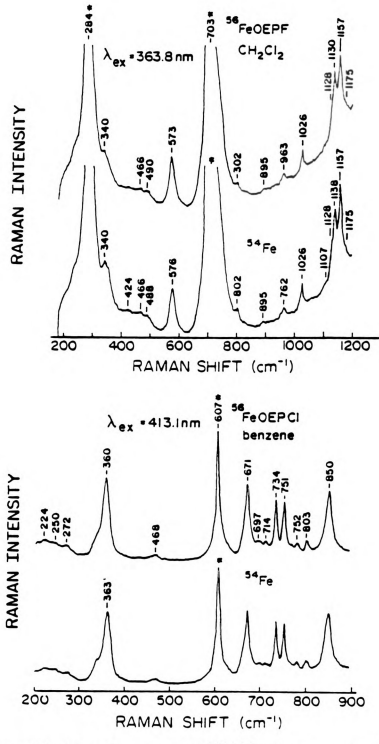


Figure 7. (a) RR spectra of 54/56 FeOEPF ; (b) RR spectra of 54/56 FeOEPC1 .

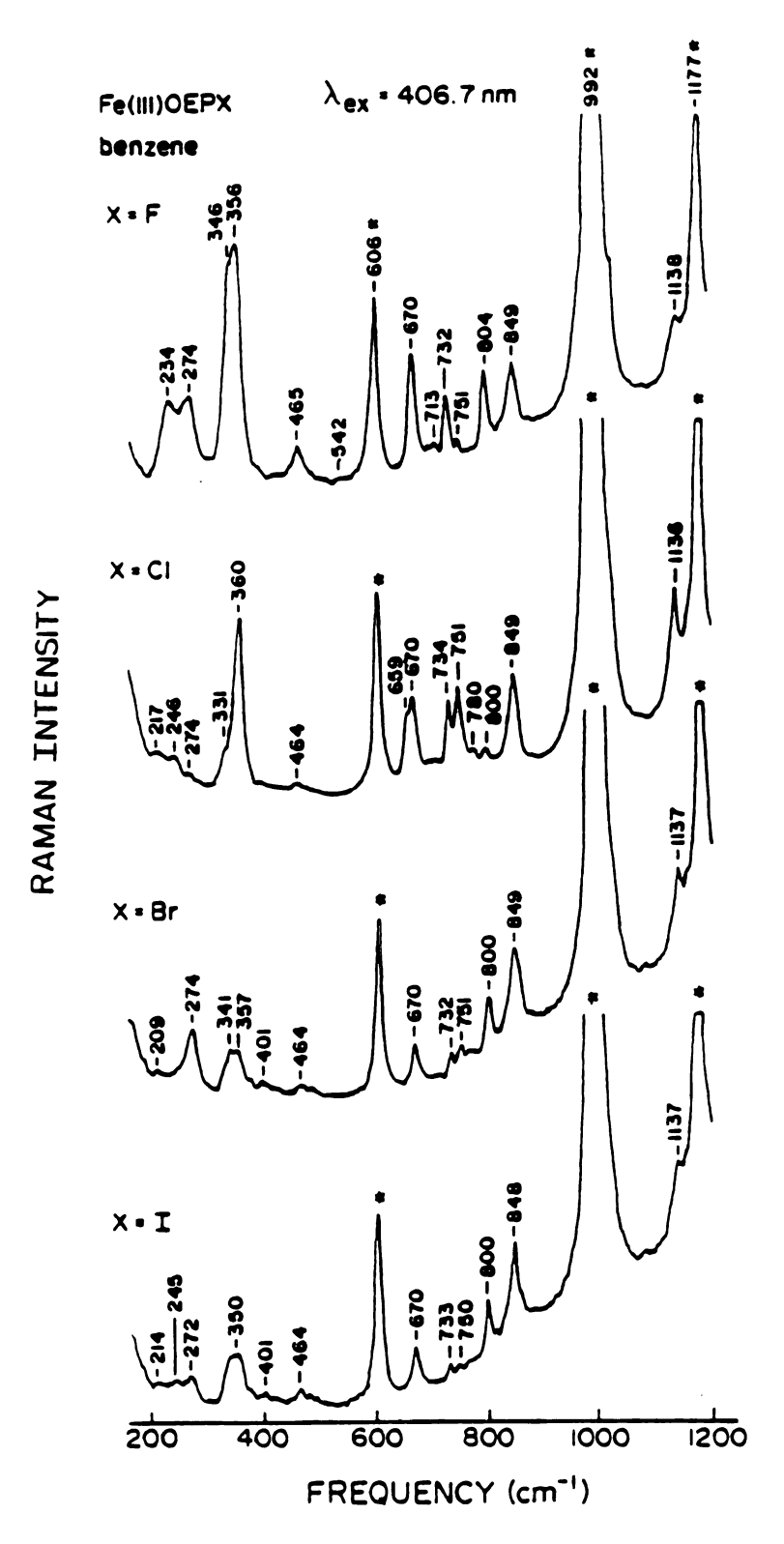


Figure 8. RR spectra of FeOEPX . The solvent bands are marked with an asterisk.

Kitagawa et al. 14 Meso-deuteration, $^{54/56}$ Fe, as well as 15 N-OEP shifts will be utilized to make definite assignments.

We have not yet observed the v(M-X) in the oxidized species. It is possible, however, that $L\to M$ CT transitions are red-shifted or more likely vanished in the π -cation radicals. Since there are no differences in the absorption spectra of ferric porphyrin radicals, Figure 4, as there are in the corresponding neutral species, Figure 3, the CT transitions, based on uv-vis features, are expected not to be present or to be of very low probability. On the other hand, the cobaltic porphyrin radical for X = Br reveals a feature at ~ 160 cm⁻¹ with 676.4 nm RR excitation (not shown) which we believe to be a mode involving metal and the bromide ligand. This mode is also observed in the spectrum excited at 406.7 nm (not shown), but not at 363.8 nm, Figure 9.

The optical spectra of cobaltic-alkyl complexes differ substantially from those of six-coordinate $Co(ROH)_2OEPX$ and five-coordinate CoOEPX: the absorption maxima of the Soret, β and α bands hardly shifts relative to those of CoOEP and remain at 390, 520 and 552 nm, respectively. The characteristic optical feature, however, is the nearly equal intensity of the α and β bands.⁹

CoOEPR (where R = Me, Et, i-Pr and t-Bu) displays an infrared mode at 343, 344, 339 and 343 cm⁻¹, respectively, analogous to that observed in methylcobalamine at 348 cm⁻¹. The latter absorption was shown to be due to the υ (Co-C) by the slow disappearance of this band when the sample (KBr pallet) was irradiated with tungsten light: the photolysis product, hydroxocobalamine does not absorb at this frequency. The absence of any significant changes in the υ (Co-C) of these complexes may be the result of offsetting effects. The increase in the steric bulk of the alkyl chain, which tends to decrease the bond frequency by virtue of mass effect, is compensated

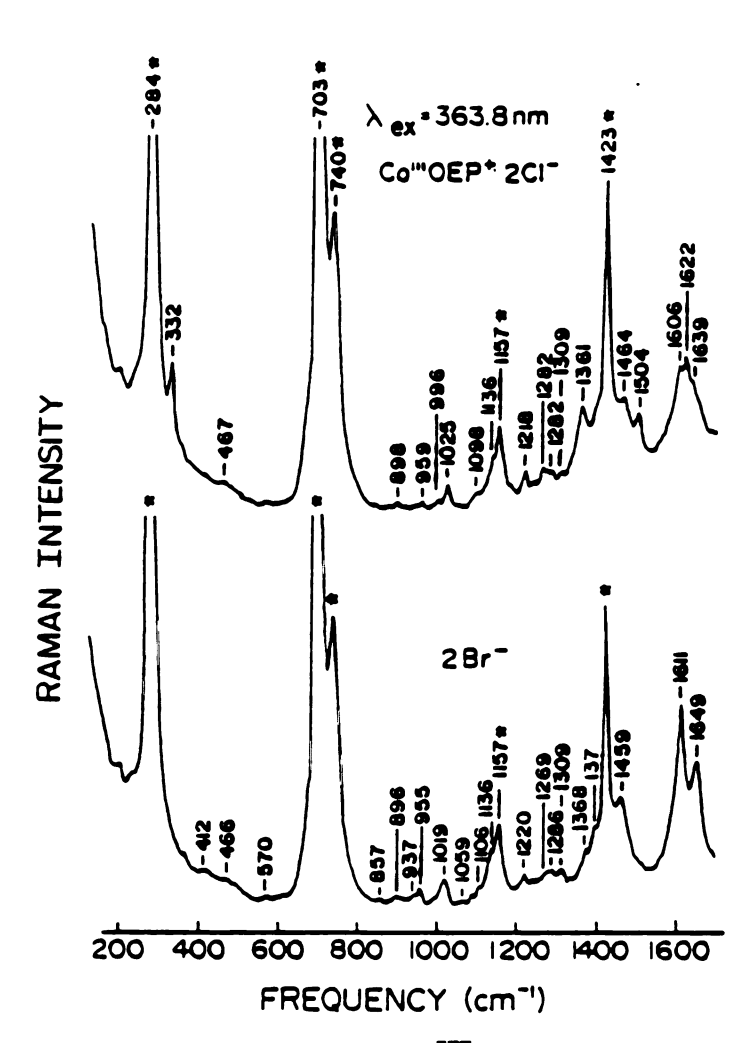


Figure 9. RR spectra of $Co^{III}OEP+\cdot 2X^-$: (a) $X^- = FeCl_4^- \sim Cl^-$; (b) $X^- = Br^-$.

by the greater electron-releasing ability of the more substituted alkyl group, which increases the force constant, bond order and bond frequency of the Co-C bond. Further confirmation of this mode requires isotopic substitution of the alkyl chain as well as preparation of Co-R derivatives of other porphyrins. Besides, a more complete investigation of $\upsilon(\text{CoC})$ measurement should also include other macrocyclic ligands such as chlorins and corrins to develop a better understanding of the use of the corrin ring in vitamin B_{12} prosthetic group, as a means of modulation of the Co-C bond strength.

REFERENCES

- 1. Buchler, J. W.; Kokisch, W.; Smith, P. D., Struct. Bonding 1978, 34, 79.
- 2. Su, Y. O.; Czernuszerwics, R. S.; Miller, L. A.; Spiro, T. G., J. Am. Chem. Soc., **1988**, <u>110</u>, 4150.
- 3. (a) O'Keefe, D. H.; Barlow, C. H.; Smythe, G. A.; Fuchsman, W. H.; Moss, T. H.; Lilienthal, H. R.; Caughy, W. S., Bioinorg. Chem., 1975, 5, 125.
 - (b) Lueken, H.; Buchler, J. W.; Lay, K. L.; Z. Naturforsh, 1976, 31b, 1596.
 - (c) Vaska, L.; Amundsen, a. R.; Brady, R.; Flynn, B. R.; Nakai, H., Finn. Chem. Lett., 1974, 66.
 - (d) Ogoshi, H.; Watanabe, E.; Yoshida, Z.; Kincaid, J.; Nakamoto, K., J. Am. Chem. Soc., 1973, 95, 2845.
 - (e) Strauss, S. H.; Pawlik, M. J.; Skowyra, J.; Kennedy, J. R.; Anderson, O. P.; Spartalian, K.; Dyne, J. L., Inorg. Chem. 1987, 26, 724.
- 4. Hashimoto, S.; Tatsuno, Y.; Kitagawa, T., J. Am. Chem. Soc., 1987, 109, 8096.
- 5. Geno, M. K.; Halpern, J., J. Am. Chem. Soc., 1987, 109, 1238.
- 6. Ogoshi, H.; Watanabe, E.; Yoshida, Z.; Kincaid, J.; Nakamoto, K., J. Am. Chem. Soc., 1973, 95, 2845.
- 7. Choi, S.; Spiro, T. G.; J. Am. Chem. Soc., 1983, <u>105</u>, 3683.
- 8. Datta-Gupta, N.; Bardos, T. J., J. Pharm. Sci. 1968, <u>57</u>, 300.
- 9. Ogoshi, H.; Watanabe, E. I.; Kokatsu, N.; Yoshida, Z. I., Bull. Chem. Soc. Jpn., **1976**, <u>49</u>, 2529.
- 10. Setsune, J. I.; Ikeda, M.; Kishimoto, Y.; Kitao, T.; J. Am. Chem. Soc., 1986, 108, 1309.
- 11. (a) Tait, C. D.; Holten, D.; Gouterman, M., J. Am. Chem. Soc., 1984, 106, 6653.
 - (b) Tait, C. D.; Holten, D.; gouterman, M., Chem. Phys. Lett., 1983, 100, 268.

- 12. Edwards, W. D.; Zerner, M. C., Can. J. Chem., 1985, 63, 1763.
- 13. Hendrickson, D. N.; Kinnaird, M. G.; Suslick, K. S., J. Am. Chem. Soc., 1987, 109, 1243.
- 14. Kitagawa, T.; Abe, M.; Kyogoku, Y.; Ogoshi, H.; Watanabe, E.; Yoshida, Z., J. Phys. Chem., 1976, 80, 1181.
- 15. Kincaid, J.; Nakamoto, K., Spectros. Lett., **1976**, <u>9</u>, 19.
- 16. Oertling, W. A.; Salehi, A.; Chung, Y. C.; Leroi, G. E.; Chang, C. K.; Babcock, G. T., J. Phys. Chem., <u>91</u>, 5887.
- 17. Hogenkamp, H. P. C.; Rush, J. E.; Swenson, C. A., J. Biol. Chem., **1965**, <u>240</u>, 3641.
- 18. (a) Nakamoto, K., In "Infrared and Raman Spectra of Inorganic Coordination Compounds", Nakamoto, K., Ed., John Wiley & Sons: New York, 1986, 324.
 - (b) Clark, R. J.; Williams, C. S., Inorg. Chem., 1965, 4, 350.
 - (c) Nakagawa, I.; Shimanouchi, T., Spectrochim. Acta, 1966, 22, 759.
 - (d) Shimanouchi, T.; Nakagawa, I.; Inorg. Chem., 1964, 3, 1805.
 - (e) Ref. 18a, p. 379.

MICHIGAN STATE UNIV. LIBRARIES
31293007815792